Biocatalytic (De)carboxylation of Phenolic Compounds: Fundamentals and Applications

Vom Promotionsausschuss der
Technischen Universität Hamburg-Harburg

Zur Erlangung des akademisches Grades
Doktor der Naturwissenschaften (Dr. rer. nat.)

genehmigte Dissertation

von
Lorenzo Pesci

aus
Rom

2017

Betreuer: Prof. Dr. Andreas Liese

1. Gutachter: Prof. Andreas Liese

2. Gutachter: Prof. Andrew Torda

Datum der mündlichen Prüfung: 12.01.2017

Abstract

Carbon dioxide is a pivotal compound in the biotic world of metabolism and in the abiotic world of chemical synthesis. These two worlds can merge, to some extent, when biological catalysts for (de)carboxylations are used to accelerate chemical conversions for industrial applications. A particular set of lyases which display this type of activity on phenolic starting materials belong to microbial degradation pathways. Such enzymes are hydroxybenzoic acid and phenolic acid (de)carboxylases, which catalyze reversible carboxylations and can be differentiated according to their regio-selectivity based on which the carboxylic group is added and removed: *ortho* and *para*, for phenolic compounds, and *beta*, for hydroxycinnamic acids. Because carbon dioxide and its hydrated form, bicarbonate, have considerably low standard Gibbs free energies, the equilibrium of the reactions often lie strongly on the decarboxylation side in physiological conditions. In this work, two *ortho*-(de)carboxylases and one *beta*-(de)carboxylase were studied in the reaction directions relevant for application. For *ortho*-selectivity, dihydroxybenzoic acid (de)carboxylases –from *Rhizobium* sp. and *Aspergillus oryzae*– were studied in the synthesis –"up-hill"– direction, which yields salicylic acids from phenols. This reaction resembles the abiotic Kolbe-Schmitt synthesis, which is conducted at elevated temperatures and pressures. Therefore, the establishment of an "enzymatic counterpart" for large scale production is highly desirable in order to achieve efficient CO_2 utilization for chemical synthesis. Fundamental studies on kinetics and thermodynamics revealed the reactions bottlenecks, allowed the proposition and verification of a catalytic mechanism and gave new insights on the biocatalysts' substrate spectra. The development of an amine-coupled method to use carbon dioxide –instead of bicarbonate, the effective co-substrate usually accepted by these biocatalysts– reveled interesting properties of ammonium ions in determining approximately five-fold increases in reaction rates and approximately two-fold equilibrium conversions for the carboxylation of catechol. Moreover, the analyses of strategies to overcome the thermodynamic equilibrium are critically discussed and demonstrate how the system may have a realistic future only on the laboratory scale. *Beta*-(de)carboxylases catalyze the reversible (de)carboxylation on the C–C double bonds of abundant and naturally occurring *para*-hydroxycinnamic acids yielding *para*-hydroxystyrenes, which are normally obtained by using multistep synthesis, toxic reagents and high temperatures. Therefore, these enzymes represent a

promising tool for the deoxygenation of biomass-derived feedstocks. In the present work, a phenolic acid (de)carboxylase from *Mycobacterium colombiense* was studied as biocatalyst for the decarboxylation of ferulic acid, yielding 4-vinylguaiacol, an Food and Drug Administration-approved flavoring agent. Kinetic studies revealed the occurrence of strong product inhibition, which was then tackled by performing the biotransformation in two liquid-phase systems. The optimized reaction conditions using hexane as the organic phase were demonstrated also in gram scale, affording the target product in 75% isolated yield. A reactor concept including the integrated product separation is also presented and discussed. In order to further exploit this biocatalytic reaction for applications, a sequential Pd-catalyzed hydrogenation step was carried out in the organic layer, affording 4-ethylguaiacol, another industrially relevant flavoring agent. In gram scale, the whole reaction sequence afforded the final product in 70% isolated yield. Both biotransformation and chemo-enzymatic sequence were evaluated using the E-factor as a measurement of their environmental impact; a comparison with existing synthetic paths shows how the strategies developed in this work are promising "green" methods in view of large scale applications.

Kurzfassung

Kohlenstoffdioxid dient als Schlüsselkomponente im biotischen Stoffwechsel sowie in der abiotischen, chemischen Synthese. Mit einigen Ausnahmen können beide Bereiche zusammengeführt werden, indem im Hinblick auf industrielle Anwendungen Biokatalysatoren für (De)Carboxylierungs-Reaktionen zur Beschleunigung von chemischen Reaktionen eingesetzt werden. Einige Lyasen, die bezüglich phenolischer Ausgangsstoffe diese katalytische Aktivität aufweisen, sind an mikrobiellen Abbauprozessen beteiligt. Die Hydroxybenzoesäure- und Phenolsäure-(De)Carboxylasen katalysieren reversible Carboxylierungs-Reaktionen und werden anhand ihrer Regioselektivität bezüglich der Addition oder Abspaltung einer Carboxylgruppe differenziert: *ortho* und *para* für phenolische Komponenten und *beta* für Hydroxyzimtsäuren. Aufgrund der geringen freien Standard Gibbs-Energien von Kohlenstoffdioxid und seiner hydrierten Form als Hydrogencarbonat liegt das Gleichgewicht der Reaktionen unter physiologischen Bedingungen häufig deutlich auf der Seite der Decarboxylierung. In dieser Arbeit wurden zwei *ortho*-(De)Carboxylasen und eine *beta*-(De)Carboxylase untersucht, wobei für die Richtung der Reaktion die Relevanz für industrielle Anwendungen im Fokus stand. Bezüglich der *ortho*-spezifischen Selektivität wurden Dihydroxybenzoesäure-(De)Carboxylasen von *Rhizobium* sp. und *Aspergillus oryzae* in die sogenannte Syntheserichtung („up-hill“) untersucht, wodurch Salizylsäuren als Produkt ausgehend von Phenol gewonnen werden. Diese Reaktion ähnelt der abiotischen Kolbe-Schmitt Synthese, die unter erhöhten Temperaturen und Drücken durchgeführt wird. Daher ist es wünschenswert, ein alternatives Konzept unter Einsatz von Enzymen (“enzymatic counterpart“) im großen Maßstab zu etablieren, um eine effiziente CO_2-Nutzung zu ermöglichen. Durch detaillierte Studien der Kinetik und Thermodynamik wurden Einschränkungen der Reaktionen aufgezeigt, der katalytische Mechanismus beschrieben und verifiziert, sowie neue Einblicke in das Substratspektrum der Biokatalysatoren gewonnen. Die Entwicklung einer Amin gekoppelten Methode zur Nutzung von Kohlenstoffdioxid (anstatt von Bicarbonat, welches das effektive Cosubstrat der betrachteten Biokatalysatoren ist) zeigte einerseits erhöhte Reaktionsgeschwindigkeiten des Ammonium-Ions (ca. 5-fach) und andererseits höhere Gleichgewichts-Umsätze (ca. doppelt so hoch) für die Carboxylierung von Catechol. Darüber hinaus wurden Strategien zur Verschiebung des thermodynamischen Gleichgewichts diskutiert und ein Lösungsansatz für den zukünftigen Einsatz des

Systems im Labormaßstab vorgestellt. *Beta*-(De)Carboxylasen katalysieren hingegen die reversible (De)Carboxylierung einer C–C-Doppelbindung natürlich vorkommender (und reichlich vorhandener) *para*-Hydroxyzimtsäuren. Als Produkt werden in diesen Reaktionen *para*-Hydroxystyrole erhalten, die in einem mehrstufigen chemischen Prozess unter Einsatz von toxischen Reagenzien bei hohen Temperaturen synthetisiert werden. Daher stellt die Anwendung der genannten Enzyme eine vielversprechende Möglichkeit zur Deoxygenierung aus Biomasse basierten Rohstoffen dar. In der vorliegenden Arbeit wurde zur Decarboxylierung von Ferulasäure eine Phenolsäure-(De)Carboxylase aus *Mycobacterium colombiense* untersucht, um den von der Food and Drug Administration genehmigten Aromastoff 4-Vinylguaiakol als Produkt zu gewinnen. In kinetischen Studien konnte eine starke Produktinhibierung beobachtet werden, welche durch die Überführung der Biotransformation in ein Zwei-Phasensystem umgangen werden konnte. Unter optimierten Reaktionsbedingungen mit Hexan als organischer Phase wurde das Zielprodukt mit einer isolierten Ausbeute von 75% im Gramm-Maßstab gewonnen. Zudem wurde ein Reaktorkonzept mit integrierte Produktabtrennung präsentiert und diskutiert. Um die biokatalytische Reaktion im Hinblick auf Anwendungen zu untersuchen, wurde eine sequentielle, Pd-katalysierte Hydrogenierung in der organischen Phase durchgeführt. Dadurch wurde 4-Ethylguaiakol als weiterer industriell relevanter Aromastoff mit einer isolierten Ausbeute von 70% im Gramm-Maßstab synthetisiert. Sowohl die Biotransformation, als auch die chemo-enzymatische Sequenz wurden auf Basis des E-Faktors als Maß für den Umwelteinfluss bewertet. Ein Vergleich mit bereits existierenden synthetischen Ansätzen zeigt die vielversprechende Entwicklung der vorgestellten Reaktionen als „grüne“ Methoden für Anwendungen im großen Maßstab.

Contents

List of Used Abbreviations and Symbols

Abbreviations

2,3-DHBA	2,3-dihydroxybenzoic acid
Rsp_DHBD	2,6-dihydroxybenzoic acid (de)carboxylase from *Rhizobium* sp.
Ao_DHBD	2,3-dihydroxybenzoic acid (de)carboxylase from *Aspergillus oryzae*
McPAD	phenolic acid (de)carboxylase from *Mycobacterium colombiense*
IPTG	isopropyl-β-D-thiogalactopyranoside
CFE	cell-free extract
KP_i	potassium phosphate
4MeOSA	4-methoxysalicylic acids
LFER	linear free energy relationship
KS	Kolbe-Schmitt
TFA	trifluoroacetic acid
TE	triethylamine
FTIR	fourier transform infrared spectroscopy
2LPS	two-liquid phase system
DCM	dichloromethane
TBACl	tetrabutyl ammonium chloride
GlC	glycerol carbonate
Gl	glycerol
FA	ferulic acid
4VG	4-vinylguaiacol
4EG	4-ethylguaiacol

Symbols

[A]	M	molar concentration of A
t	min	time
$\tau_{1/2}$	min	half-life time
MW	Da	molecular weight
H^{cp}	M atm^{-1}	Henry's law solubility constant defined via concentration
OD	-	optical density
K_M	M	Michaelis-Menten constant
K_i	M	inhibition constant
K_a	M^{-1} s^{-1}	specificity constant
K_{eq}	-	equilibrium constant
V_{max}	µmol min^{-1} mg^{-1}	maximum reaction rate
k_{cat}	s^{-1}	turnover frequency

k_d	min^{-1}	deactivation constant
σ	-	electronic constant
π	-	hydrophobicity constant
logP	-	logarithmic octanol/water partition coefficient
K_P	-	partition coefficient
ε	-	dielectric constant
δ	-	solubility parameter
X	%	conversion
Y	%	yield

1 Introduction

Between the 1950s and the 1980s the chemical industry had an enormous expansion period in terms of size and product differentiation, while at the same time producing hazardous stoichiometric waste, pollution and using fossil fuel-derived feedstocks (*i.e.*, ethylene, propylene, methanol, benzene, etc.) (Murmann 2002). The positive image of the industrial facilities, which were producing goods like dyes and polymers (*e.g.*, polyesters), began to change between the 1960s and the 1980s due to disastrous incidents which ,more or less directly, influenced such a foundation of modern developed countries. Worth mentioning are the Bhopal disaster (Union Carbide plant) of 1984, where 3000 people were killed after 40 tons of methyl isocyanate leaked from pipelines, and the fire at a Sandoz chemical facility in Switzerland, which caused heavy pollution of the Rhine river (Murmann 2002). During this time period, the public opinion regarded chemistry as something harmful and polluting. Even though economics, politics, public opinion as well as science and technology may seem quite unrelated, they are strongly dependent on each other. This appears quite clear from the "revolution" that we have been observing in the chemical industry for almost 30 years. In fact, this negative perception ,which is ideological as well as practical, likely contributed to the definition of the "green chemistry" concept in 1993 by the Office of Pollution Prevention and Toxics (OPPT) in the USA. The key foundations of this concept were formulated in 1998 by the Environmental Protection Agency (EPA) jointly with the American Chemical Society through the publication of the *12 Principles of Green Chemistry* (Centi & Perathoner 2003). Its goal was to set the basis for, and stress the importance of designing a more sustainable chemical industry. This includes the production of less waste, the design of simpler and safer processes and the avoidance of the use of fossil fuels, which are projected to be depleted by the year 2100 (Höök & Tang 2013). In the following years, rapid expansions of so called "green chemistry and greener methods" have been appearing in scientific literature as well as in industrial reports and marketing campaigns. Green chemistry should be viewed strictly as a social concept rather than as a new chemical discipline; in fact, there is no pivotal change in the chemistry itself, but rather a long-term consideration of the chemical reactions which will eventually develop into industrial processes. In this sense, green chemistry should be interpreted as the spontaneous evolution of the creative human art of research and

development. Improved chemical processes in a "green chemistry" perspective already began developing well before the *12 Principles* were published. For example, the synthesis of maleic anhydride using butane instead of benzene as starting material, led to several advantages in terms of safety and waste prevention (Bergman & Frisch 1966; Centi & Perathoner 2003; Dmuchovsky *et al.* 1965) (Scheme 1.1).

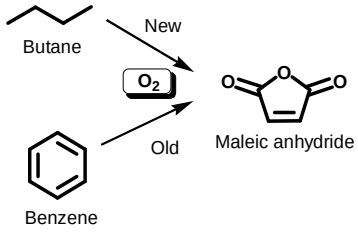

Scheme 1.1: New and old oxidation routes to maleic anhydride.

Therefore, green chemistry is rather a modern chemistry concept included in the more global sustainability strategy, which itself is deeply related to many aspects of society, such as economics, politics and public opinion. Science and technology – when properly used – build the basis for both environmental and economic sustainability. For example, in the case of maleic anhydride, the butane route was developed because a new vanadium catalyst with unprecedented activity, vanadyl pyrophosphate $(VO)_2(P_2O_7)$, was discovered (Guliants *et al.* 1996). Involving a catalyst is not arbitrary because catalysis is the "driver" that promotes the elimination of stoichiometric reactions, allowing simpler processes that produce less waste. Biocatalysis and (white) biotechnology theoretically enhance these benefits as the biocatalysts are natural molecules. After the understanding of the chemical entity, structure, scope and mechanism of enzymes achieved in the 1960s, their applications have been implemented in many companies for the production of bulk, fine and pharma chemicals (Liese *et al.* 2006). In general, the use of enzymes as catalysts satisfies at least 7 of the 12 principles of green chemistry (see Table 1, where the principles which are satisfied by biocatalysis are highlighted in bold), including the use of renewable feedstocks such as syngas, (hemi)cellulose and lignin derivatives (Willke *et al.* 2006).

Table 1: Green chemistry principles and biocatalysis.

Green chemistry principles	Biocatalysis
1. Waste prevention	-
2. Atom economy	-
3. Less hazardous reactions	Enzymes do not represent significant hazard for the human health and the environment
4. Design safer chemicals	-
5. Safer solvents/auxiliaries	The preferred solvent for enzymes is water and co-factors are in many cases not toxic
6. Energy efficiency	Enzymes usually do not require intense energy inputs (*e.g.*, ambient temperature)
7. Use renewable feedstocks	Biocatalysts are mostly active on their natural substrates
8. Reduce derivatization	The high selectivity ensures the avoidance of derivatization steps
9. Design for biodegradation	-
10. Catalysis	Enzymes are biological catalysts
11. Real time analysis	-
12. Safer chemistry	The conditions in which enzymes show their activity usually allows easy and safe processes

This last argument is particularly important because chemical catalysts are less likely to show the same tremendous selectivity towards oxygenated feedstocks as enzymes. In this context, carboxylic acids are an important class of compounds widespread throughout nature. Therefore, enzymatic selectivity for this functional group is of considerable importance to the design of catalytic routes for applications. To further understand this point, carbon dioxide, the molecule most related to carboxylic acids, will be discussed in detail from different points of view.

1.1 Biological, Industrial and Environmental Importance of Carbon Dioxide

Carbon dioxide is a molecule of key importance for living beings, as well for industry, for the environment, and society in general. It is therefore relevant to discuss the role that CO_2 plays in these different contexts beginning with its molecular and reactivity properties. Carbon dioxide is a linear molecule having carbon with an oxidation state of +4 and containing two dipole moments that, because of their geometric arrangement, globally result in a non-polar molecule. Being a combustion product, its thermodynamic stability in terms of ΔG_f^0 ≈ –390 kJ mol^{-1}, is very high (Lide 1994). With respect to its chemical reactivity, the partially positive charge on the C atom is greater than the negative charges on the oxygen atoms. As a result, CO_2 acts mainly as an electrophile (Aresta 2006). In water, carbon dioxide has a solubility of 32 mM at 25°C and 760 mmHg total pressure (Lide 1994) and undergoes a series of equilibria, particularly important for living systems, forming bicarbonates and carbonates. When gaseous CO_2 comes into contact with water, an equilibrium is established and dissolved CO_2 slowly reacts with water forming H_2CO_3 (pK_{a1} = 6.37). The concentration of carbonic acid is directly correlated with the CO_2 partial pressure pCO_2 through Henry's law, for which $H^{cp} = [H_2CO_3]/pCO_2$ (H^{cp} ≈ 3 x 10^{-2} M atm^{-1} at 25°C (Lide 1994)). Carbonic acid is in equilibrium with HCO_3^- (pK_{a2} = 10.25) and CO_3^{2-}. As protons are involved in the equilibria, the relative concentration of the species at equilibrium is highly dependent on pH. Bicarbonate, unlike carbon dioxide, is a base and nucleophile and has an even higher thermodynamic stability (ΔG_f^0 ≈ –600 kJ mol^{-1}). Carbon dioxide can be subjected to *i)* redox transformations (*e.g.*, reduction to methanol, carbon monoxide or formate), or *ii)* redox neutral transformations (*e.g.*, carboxylation/decarboxylation ((de)carboxylation), esterification, amidation,etc.). A carboxylation reaction can be described as an insertion of CO_2 in the C–H bond (pK_a ≈ 50 in alkanes), requiring a heterolytic cleavage and carbanion formation (Scheme 1.1.1):

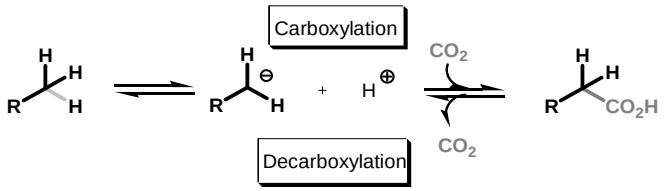

Scheme 1.1.1: General (de)carboxylation mechanism.

The reverse reaction can be easily deduced for decarboxylations. These features already point out the limitations of (de)carboxylation reactions: a thermodynamic issue for carboxylation with the low free energy of the starting material and, conversely, a kinetic issue for decarboxylation through stabilization of the carbanion. For example, even though the carboxylation of methane has a negative ΔH_f^0 (≈ –16.6 kJ mol^{-1}) the Gibbs free energy difference –at 298 K– is ≈ + 70 kJ mol^{-1} (Aresta 2006). Notwithstanding these difficulties, different strategies are applied –either by nature or man– to "handle" both reaction directions efficiently.

1.1.1 A Biochemical Perspective of (De)carboxylation Reactions

Carbon dioxide, a central component of the carbon cycle, is the simplest inorganic C1 unit which is fixed by photosynthetic organisms while forming central metabolites and which is released during respiration by aerobic organisms. Carboxylation/decarboxylation reactions (here indicated as (de)carboxylations) are key transformations in these fluxes and are catalyzed *in vivo* by (de)carboxylases (EC 4.1.x.x). Scheme 1.1.2 represents some examples of these biological transformations:

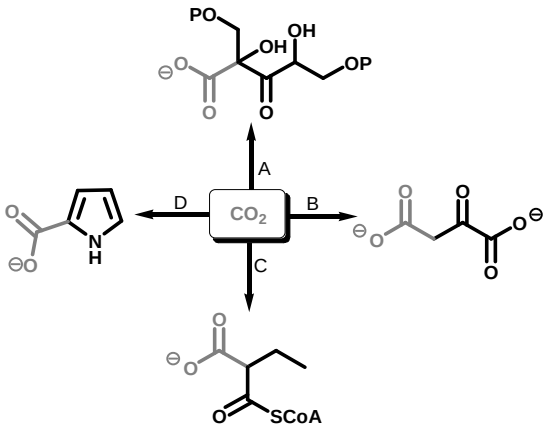

Scheme 1.1.2: Examples of metabolic reactions involving CO_2; P = PO_3^{2-}; A: carboxylation of ribulose by RubisCO; B: (de)carboxylation of pyruvate; C: (de)carboxylation of crotonyl-CoA by crotonyl-CoA carboxylase/reductase; D: (de)carboxylation of pyrrole by pyrrole-2-carboxylate carboxylase.

Many enzyme-catalyzed reactions are reversible. Therefore, if a reaction is catalyzed exclusively in one direction it will be explicitly declared in this text. Otherwise, any enzymatic reaction described can be thought as a reversible (de)carboxylation. The –irreversible– carboxylation of ribulose in route (A) is responsible for the biggest

carbon dioxide turnover on earth, whereby 100 Gt of CO_2/year are converted (Aresta 2006). This reaction is performed inside the Calvin-Benson-Bassahm cycle by *D*-ribulose-1,5-bisphosphate carboxylase/oxygenase (RubisCO) in photosynthetic organisms, yielding two units of *D*-3-phosphoglycerate after cleavage of the β-ketoacid (Scheme 1.1.2A). The term "oxygenase" signifies that RubisCO can accept molecular oxygen as electrophile as well, generating 2-phosphoglycolate as a "by-product". The importance of this reaction is demonstrated by the fact that RubisCO is the most abundant enzyme on earth (≈ 5 Kg RubsiCO/person) (Erb 2011). Route (B) describes the carboxylation of pyruvate via an anaplerotic reaction yielding oxaloacetate, an intermediate of the tricarboxylic acid cycle (TCA-cycle). Pyruvate/oxaloacetate interconversion is quite important; in fact, it can be performed in both directions by different enzymes (*e.g.*, pyruvate carboxylase, oxaloacetate decarboxylase and phosphoenolpyruvate carboxylase). (De)carboxylases are key to the reductive TCA-cycle; in the carboxylation of α-oxoglutarate by isocitrate dehydrogenase, for example, isocitrate is yielded after reduction. Route (C) constitutes a recently discovered (de)carboxylation which occurs in anaerobic autotrophs. This reaction is catalyzed by crotonyl-CoA carboxylase/reductase and, starting from crotonyl-CoA, produces ethylmalonyl-CoA by reductive carboxylation using reduced nicotinamide cofactors (Erb *et al.* 2009). The last route presented here is (D), where pyrrole undergoes a carboxylation reaction catalyzed by pyrrole-2-carboxylate carboxylase. This type of catalytic activity was initially discovered by studying degradation pathways of anaerobic microbial consortia (Knoll & Winter 1989) and then extended to other microorganisms and substrates (Wieser *et al.* 1998). The enzymatic carboxylation of electron-rich aromatics will be discussed in more detail in section 1.2. An interesting question now arises: how can nature establish efficient (de)carboxylation reactions? Considering carboxylation, it was pointed out in the previous section that fundamental constraints are the considerable thermodynamic stability of CO_2 –as HCO_3^-– and the requirement for heterolytic C—H bond cleavage. With respect to decarboxylation, the release of a neutral – dissolved – gas molecule is without doubt a significant entropic boost, but how can the resulting carbanion be stabilized? Unsurprisingly, satisfactory explanations arise from the fundamentals of enzyme catalysis and metabolic networking.

Let us start this discussion with carboxylation, which presents both kinetic and thermodynamic constraints. To counteract the low starting material free energy,

metabolic pathways are energetically designed to build globally exergonic processes. In this particular case, strategies are designed to make use of:

i) Light, which is the primary energy source for photosynthesis and therefore the main contributor to the ribulose's carboxylation energy balance;

ii) Redox equivalents (*e.g.*, NADPH for isocitrate dehydrogenase);

iii) ATP hydrolysis (*e.g.*, pyruvate carboxylase).

Kinetics issues are being solved by activation of the substrates in the catalytic pockets. Regarding the "main" substrate, activation is realized by formation of enolates or enaminates, which can be obtained in different ways (Table 1.1.1).

Table 1.1.1: Electrophilic and nucleophilic activation in enzymatic (de)carboxylations; A = general acid; M^{n+}= metal cation.

Nucleophile	Electrophile
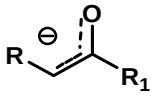	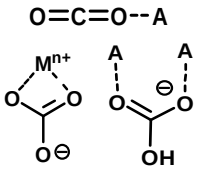
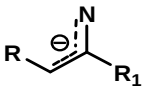	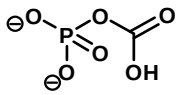
	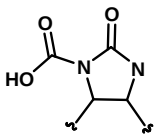

The routes (A) to (D) are representative of the four most common strategies (Schada von Borzyskowski, L. *et al.* 2013). In (A) and (B) it can be easily recognized that the C−H bonds are in α to a carbonyl group, which dramatically enhances their acidity ($pK_a \approx 19$) due to carbanion stabilization in the enol(ate) form. Additional stabilization comes from the ionic interactions with divalent cations, often part of the active site (*e.g.*, RubisCO). Similarly, dephosphorylation is another strategy to activate the nucleophile with enolates as substrates (*e.g.*, phosphoenolpyruvate carboxylase). The same strategy cannot be applied in route (C) because the precursor crotonyl-CoA contains a double bond in α position to the thioester; the activation in this case is realized by reduction of the double bond by a nicotinamide cofactor and formation of the enolate. In route (4), deprotonation of pyrrole yields an enaminate reactive intermediate as a nucleophile. With respect to the co-substrate, the scenario is more complex and considerations have to be done about: *i)* the

CO_2/HCO_3^- equilibrium, *ii)* binding to the enzyme, and *iii)* electrophilic activation (Table 1.1.1). The majority of the enzymes use carbon dioxide as substrate, even though at physiological pH $[HCO_3^-] > [CO_2]$ ($pK_{a1} \approx 6$). For example, at pH 8.0, the molar concentration of HCO_3^- is about 50 times that of CO_2. Astonishingly, this pH value is found in chloroplasts and RubisCO uses carbon dioxide. The fact that enzymes prefer to use CO_2 is not surprising, because it is the most reactive. On the other hand, bicarbonate has more possibilities to realize hydrogen bonds and ionic interactions due to its negative charge (O´Leary 1992). These observations indicate that a fine trade-off between reactivity and binding versatility occurs in enzymatic carboxylations. In general, CO_2 activation is realized by hydrogen bonding to the oxygen atoms, formation of carboxyphosphate labile intermediates (*e.g.*, phosphoenolpyruvate carboxylase), or covalent bonding to biotin via biotin-dependent enzymes, resulting in an increased CO_2 concentration at the active site. HCO_3^- activation can be realized by hydrogen bonding or ionic interactions to metal centers (Schada von Borzyskowski, L. *et al.* 2013). With respect to decarboxylations, the limitation has mainly kinetic characteristics because the carbanion has to be stabilized. In this case, the formation of enolates/enaminates is also efficient, and their stability can be enhanced by the formation of ionic interactions with metal centers or by formation of Schiff bases (*e.g.*, pyridoxal 5´-phosphate dependent decarboxylases and thiamine pyrophosphate dependent decarboxylase) (O´Leary 1992). Moreover, the hydrophobicity in the proximity of the carboxylic group binding site may facilitate CO_2 departure (Frank *et al.* 2012).

1.1.2 Carbon Dioxide in the Environment

Before the industrial point of view can be adequately discussed, a background of the environmental impacts of CO_2 must be introduced since awareness of these impacts contributed, in part, to the current development of chemical reactions and technologies based on carbon dioxide utilization. CO_2 is one of the main greenhouse gasses and its accumulation in the atmosphere increased dramatically during the flourishing industrialization period between 18th and 20th centuries (45% increase to 407 ppm from the pre-industrial period through 2016 (NOAA Research 2016)). In 2014, when total emissions amounted to 6.87 million metric tons of CO_2 equivalents, industrial activities were responsible for a significant share of the emissions (21%), after transportation (26%) and electricity (30%) (EPA 2016). A relatively old albeit detailed report by the OECD (Organization for Economic Co-operation and

Development) of 2001 shows that of the 16% CO_2 emissions coming from industrial processing, 4% can be ascribed to the chemical and petrochemical industries (OECD 2001). It is the responsibility of joint agreements between different nations – such as the 2015 United Nations climate change conference – to counteract emissions and the use of fossil fuels for human activities such as chemical production and transportation. Biomass-derived feedstocks are resources which theoretically are "emissions-proof", even though logistical factors such as harvesting and transportation need careful evaluation when calculating global emissions contributions. The use of natural feedstocks and the capture, storage, and utilization of CO_2 are currently "hot" topics that the chemical industry, jointly with political legislation, should address efficiently.

1.1.3 An Industrial Perspective of (De)carboxylation Reactions

From the industrial point of view, carboxylation and decarboxylation reactions are also quite important in view of the challenges of modern chemistry. In general, the two reaction directions are discussed here separately because, unlike typical enzyme-catalyzed reactions, chemical reactions are designed to be irreversible. In view of CO_2 and renewable feedstocks utilization in the chemical industry, three key points can be stressed:

1) carboxylation reactions represent very successful chemistries both historically and practically, as different methods are still applied today;

2) modern carboxylation methodologies could significantly contribute to the decrease of CO_2 gas by incorporation into useful products;

3) decarboxylation reactions are thermodynamically favorable reactions and this could allow for the design of "deoxygenations" of biomass-derived carboxylic acids to obtain valuable products.

Regarding the first point, Scheme 1.1.3 summarizes the industrial redox-neutral routes which make use of CO_2:

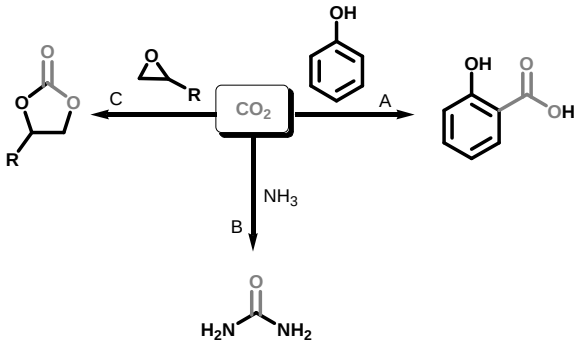

Scheme 1.1.3: Industrially applied carboxylation reactions. A: Kolbe-Schmitt synthesis of salicylic acid; B: urea synthesis from ammonia; C: synthesis of cyclic carbonates.

(A) is the Kolbe-Schmitt synthesis of salicylic acid and (B) is the urea synthesis starting from ammonia –both developed at the end of the 19th century–, while (C) is the synthesis of carbonates starting from a substituted epoxide. These three processes are able to use ≈ 200 Mt/year of carbon dioxide overall, which, even though it may seem an enormous amount, is minimal when compared to the few Gt/year that should be removed annually to achieve a significant balance (Aresta 2006). Notwithstanding the relatively long history of industrial chemistry, it is worth noticing that only a few processes have shown success in large-scale applications. The reasoning with thermodynamics in the previous section can explain this lack of efficient methods. Chemical carboxylations make use of similar strategies as nature to increase the efficiency, hence using *i)* high energy co-substrates (*e.g.*, Grignard reagents, epoxides (route (C)), or hydrogen), *ii)* providing energy through an external source such as light or electricity, and/or *iii)* pushing/changing the thermodynamic equilibrium by varying reaction conditions in terms of pressure/temperature (routes (A), (B)). These established methods require intense energy inputs. Therefore it would be interesting to know the CO_2 input/output ratio, but such data is often not available. Recent studies based on life-cycle assessment indicate that even though the utilization of CO_2 (*e.g.*, for dimethylcarbonate synthesis) does show significant results in terms of emissions reduction, carbon capture and storage (CCS) technologies generally show superior results. Such differences in performance depend also on the synthesis of the starting material and on the process conditions (Cuéllar-Franca & Azapagic 2015). In general, it is of current interest to develop new routes which would make use of carbon dioxide without a high energy demand. Catalysis offers a great potential in this context, as demonstrated by the recent discoveries in transition metal-catalyzed carboxylation reactions. Scheme 1.1.4 reports an overview of the catalytic strategies to afford C–H

carboxylations. C−metal and C−boron reagents can also be carboxylated, however, substrates need to be synthesized beforehand.

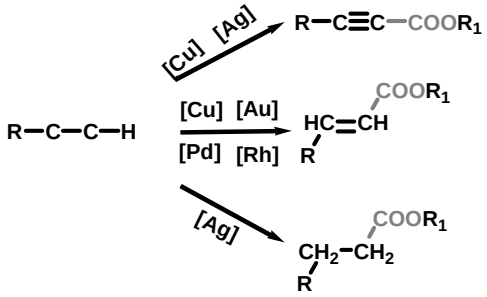

Scheme 1.1.4: Metal-catalyzed carboxylation reactions using CO_2; metallic species in brackets represent the key metal contained in the catalyst. R_1 = H, organic residue (Yu *et al.* 2015).

The reactions proceed by the formation of a highly nucleophilic carbon-metal bond which undergoes carbon dioxide insertion. A collection of different catalysts have been disclosed in the literature, allowing the access to many different carboxylic acids – and ester derivatives – in yields averaging ≥ 50% through the activation of C−H bonds in different hybridization states (Yu *et al.* 2015). However, for industrial applications, efforts must still be made, especially to increase catalytic activity and allow milder reaction conditions – in most cases employed temperatures are between 60–100°C –. Though biocatalytic carboxylation reactions are quite appealing from the biotechnological point of view, no industrial processes are presently making use of carboxylases. Apart from the reaction-related issues, carboxylases often show low turnover frequencies[1] (*e.g.*, RubisCO presents, on average, 5 s^{-1} (Glueck *et al.* 2010)), narrow substrate scope and dependency on external co-factors.

The high oxygen content of modern feedstocks requires so-called "deoxygenation" strategies. These would allow, for example, the production of fuel components and molecular frameworks typical of fossil-fuel chemicals (*e.g.*, glucose to ethanol, or lignin to BTX (Benzene-Toluene-Xylene)). Decarboxylation is one of the possibilities to reduce the oxygen content from renewable resources. Key derivatives include fatty acids, levulinic acid, aromatic acids, and aminoacids. Scheme 1.1.5 depicts some promising transformations in this view (Dawes *et al.* 2015).

[1] Turnover frequency is defined as the number of substrate molecules which are converted by a single active site of an enzyme per time unit.

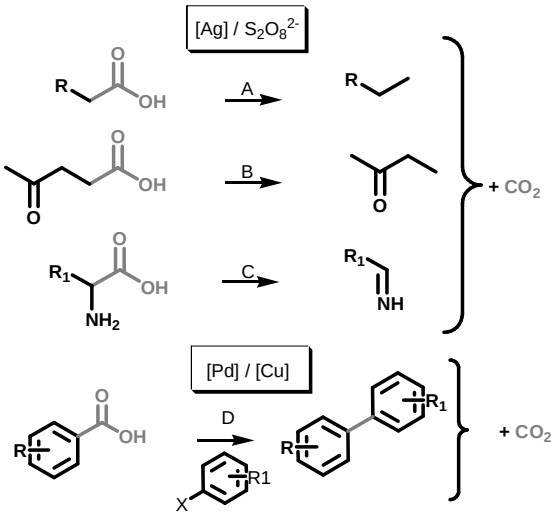

Scheme 1.1.5: Decarboxylation of biomass-derived carboxylic acids using metal-catalysis; in routes A,B,C: R = fatty acid chain; R_1 = organic residue; in route D: R,R_1 = H or organic substituent.

Fatty acids are used on an industrial scale to produce bio-diesel by trans-esterification from tryacylglycerols, however, alternative fuels can also be obtained by decarboxylation. Ag(II)-based catalytic systems are promising in this sense, especially for their versatility because they can aid the decarboxylation of fatty acids, levulinic acid (yielding 2-butanone) and amino acids (yielding imines/aldehydes) (see A,B,C in Scheme 1.1.5). Another route to long-chain alkanes is the electrochemical decarboxylative coupling of fatty acids (Kolbe reaction). Aromatic acids (*e.g.*, benzoic, vanillic, and anisic acids) can be subjected to decarboxylation via Ag(I)-based catalysts. An emerging field is the use of biomass-derived aromatic scaffolds to realize decarboxylative cross-coupling reactions through Pd/Cu catalysis (D, in Scheme 1.1.5); such protocols are also employed on industrial scale to access biaryl systems for agrochemicals (Rodríguez & Goossen 2011). On the side of white biotechnology, biocatalytic decarboxylations constitute one of the – oldest – examples of enzymatic application in the industry (Scheme 1.1.6).

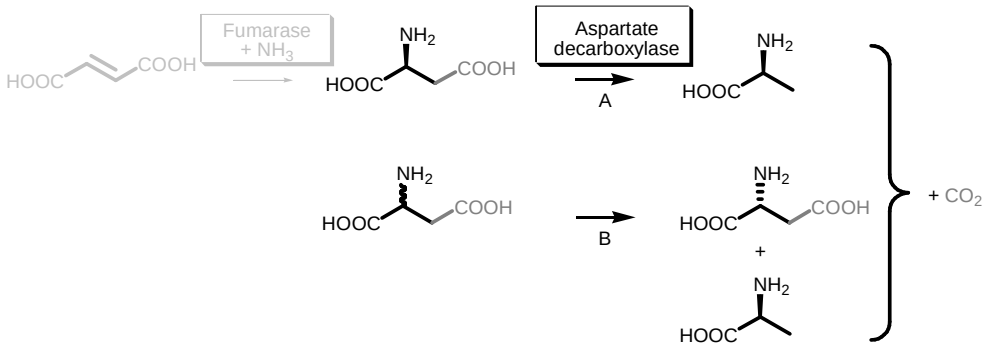

Scheme 1.1.6: Industrially applied biocatalytic decarboxylation reactions.

For example, aspartate β-decarboxylase from *Pseudomonas dacunhae* has been employed since 1965 for alanine production from aspartate or in a two-step process from fumarate (A) (Liese *et al.* 2006). The same enzyme can also be used for the racemic resolution of *D,L*-aspartate to obtain *L*-alanine and *D*-aspartate, an intermediate for the synthesis of Apoxycillin (B) (Liese *et al.* 2006).

In the next section, (de)carboxylations involving phenolic compounds will be described and discussed in further detail, as they are the main topic of this work.

1.2 The Case of Aromatics

As previously noted, a very fortunate carboxylation reaction which was discovered more than 100 years ago, which is still in use today, is the Kolbe-Schmitt synthesis of salicylic acids from a phenolate salt (Schmitt 1885). This aromatic carboxylation was demonstrated to occur via electrophilic aromatic substitution, where *ortho* and *para* positions of the aromatic ring are activated as nucleophiles. The selectivity is highly dependent on the size of the counter cation of the phenolate (*ortho* for Na^+ and *para* for the larger K^+) (Markovic *et al.* 2002). Scheme 1.2.1 depicts some general reaction conditions for phenol carboxylation, even though they vary strongly depending on the substituents, which also influence yield and regio-selectivity.

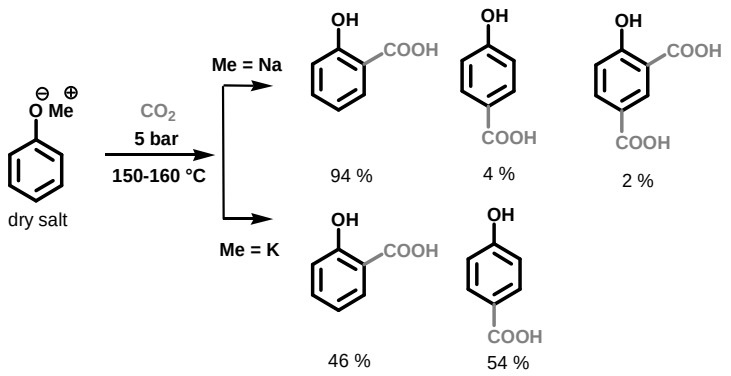

Scheme 1.2.1: Kolbe-Schmitt synthesis and influence of alkali-metal on the selectivity. Percentages refer to an overall yield in acids of ≈ 80% (Lindsey A & Jeskey H 1957).

The method is quite general and a plethora of different phenolic compounds have been carboxylated. Yields average 60% under temperature and pressure values of 100–200°C and 5–100 bar, respectively (Lindsey A & Jeskey H 1957). Electron deficient phenols require temperatures of up to 250°C and pressures of 1200 bar (Ritzer & Sundermann 2000). More reactive diphenols, such as catechols, can also be carboxylated in aqueous carbonate solutions. Aromatic hydroxycarboxylic acids are used for various industrial purposes as disinfectants, preservatives, emulsifiers, and as starting materials to produce dyes and drugs, the most important of which being acetylsalicilyc acid (Aspirin®) (Ritzer & Sundermann 2000). The search for milder and more selective methods is of current interest, as demonstrated by recent studies on the use of "reactive" bicarbonate-containing ionic liquids (Stark *et al.* 2009), of transition-metal catalyzed protocols (Wang & Gevorgyan 2015), alternative energy sources –like microwaves– and flow operation modes (Krtschil *et al.* 2009). On the other hand, microbial metabolic pathways offer an interesting set of (de)carboxylases for this purpose. Aromatic and phenolic compounds are, in fact, widespread xenobiotics present in water and soil that microorganisms manage to degrade efficiently. Apart from the well-studied aerobic degradation pathways occurring by ring oxidation, anaerobic degradations of phenolic compounds were found to proceed via non-oxidative carboxylation, providing an increased solubility of the metabolite and the establishment of a useful functional group for further metabolic reactions (Ding *et al.* 2008). Moreover, enzymes belonging to aerobic bacteria known to degrade phenolic and heteroaromatic acids using non-oxidative decarboxylation, were described for their ability to catalyze the carboxylation reactions as well (Schada von Borzyskowski, L. *et al.* 2013). As most members of this diverse group of enzymes were demonstrated to be able to catalyze reactions in both directions, they will be

addressed as (de)carboxylases. Figure 1.2.1 summarizes the key scaffolds that are subjected to (de)carboxylations:

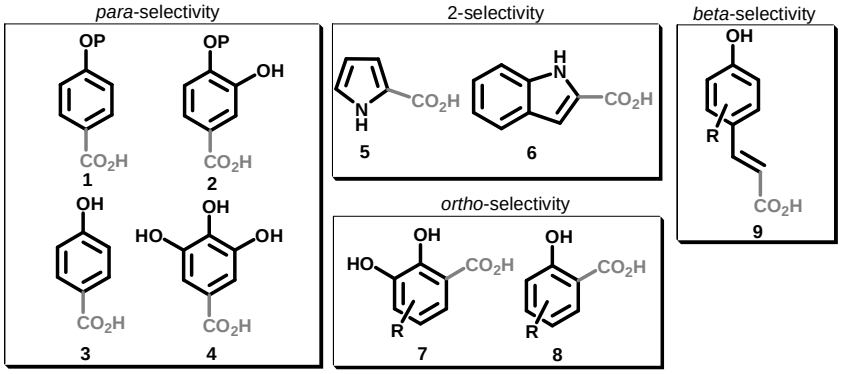

Figure 1.2.1: Phenolic and heteroaromatic substrates for (de)carboxylases; P = PO_3^{2-}.

For simple phenolics, in line with the mechanism of electrophilic aromatic substitutions observed in the Kolbe-Schmitt reaction, two selectivities were found: *ortho* and *para* carboxylation. For *para*-selectivity, **1** and **2** are substrates for anaerobic bacteria (*e.g.*, iron-reducing, denitrifying, sulfate reducing, etc.). The most characterized enzymes is the phenylphosphate carboxylase from *Thauera aromatica*, a denitrifying bacterium (Ding *et al.* 2008). The carboxylation does not occur directly on phenol but on the phosphorylated derivative –whose formation is catalyzed by phenylphosphate synthase–. The carboxylation of phenylphosphate has been also applied *in vitro* with 90% conversion using CO_2 as a substrate (Aresta *et al.* 1998). However, drawbacks include the preparation of the substrate via phenol phosphorylation and the oxygen sensitivity of the (Mn^{2+}–dependent) biocatalyst. It is reported that the free phenol **3** can be (de)carboxylated only by fermenting anaerobes, such as *Sedimentibacter hydroxybenzoicum* (Schmeling & Fuchs 2009). However, it is interesting to see that in the literature 4-hydroxybenzoic acid (de)carboxylase coming from *Chlamydophila pneumoniae* (facultative anaerobe) it is also able to catalyze the direct *para*-carboxylation of phenol, albeit with low conversion (Liu *et al.* 2007). Gallic acid **4** decarboxylation by a decarboxylase contained in *Pantoea agglomerans* was also reported; no reverse carboxylation activity of pyrogallol could be found for this system (Zeida *et al.* 1998). Heteroaromatics **5** and **6** are subject to (de)carboxylation by pyrrole-carboxylate carboxylase and indole-carboxylate carboxylase; the most characterized enzymes come from *Bacillus megaterium* and *Arthrobacter nicotianae* (Wieser *et al.* 1998; Yoshida *et al.* 2002). The substrate specificity of these enzymes is quite high; for example, between a collection of substrate screened, indole-3-carboxylate (de)carboxylase could act only on indole, 3-methylindole and quinoxaline. *Ortho*-selectivity (**7**, **8**) is displayed by benzoic acid and salicylic acid (de)carboxylases; here, the most characterized biocatalysts come from the microbes *Rhizobium* sp.,

Pandoraea sp. and from *Aspergillus* sp. (Iwasaki *et al.* 2007; Kamath & Vaidyanathan 1990; Matsui *et al.* 2006). 2,6 and 2,3-dihydroxybenzoic acid (de)carboxylases were shown to have a remarkable substrate scope, which is supported by their function in biodegradation and resulting metabolic flexibility (Wuensch *et al.* 2014). The β-(de)carboxylation (on scaffold **9**) has been recently demonstrated in the carboxylation direction using phenolic acid (de)carboxylases coming from the genera *Mycobacterium*, *Bacillus* and *Lactobacillus* (Wuensch *et al.* 2015). In view of practical applications, advantages common to the whole group of aromatic non-oxidative (de)carboxylases are their exclusive regio-selectivity and the absence of external cofactor dependencies. However, the biocatalytic *ortho*-carboxylation appears to be more promising because of broader substrate scopes and oxygen stability ((de)carboxylases belonging to anaerobe microorganisms are in fact oxygen sensitive). With the exception of phenylphosphate carboxylase, carboxylations generally run, due to thermodynamics, with about 300–fold molar excess of bicarbonates in order to achieve conversions averaging 10–40% (Wuensch *et al.* 2014). Not only is β-(de)carboxylation already extremely interesting for carboxylation from a fundamental perspective because no chemical catalysts are known to realize the same transformation, it also constitutes a promising catalytic route to produce styrenes from hydroxycinnamic acids, an abundant class of aromatic compounds present in lignin-based biomass.

1.3 Aim of the Thesis

The design of more efficient, cleaner and safer transformations is a target of modern industrial chemistry, driven by both economic and environmental sustainability and desired globally by society. Carboxylation and decarboxylation reactions are a class of transformations which are of key importance, allowing: *i)* the use of carbon dioxide to produce useful chemicals and *ii)* the "deoxygenation" of renewable, biological feedstocks, achieving the production of chemical scaffolds and products ordinarily produced in the oil refinery stream. Nature offers a series of catalysts which are able to work selectively in very practical operational conditions. The design of a (bio)catalytic process requires the interconnection between the fundamental understanding of an enzyme's performance and suitable reaction engineering strategies. Moreover, a careful and realistic comparison with existing technologies is also important to evaluate the application scope. In this work, 2,6- and 2,3-dihydroxybenzoic acid decarboxylases from *Rhizobium* sp. and *Aspergillus*

oryzae are investigated for their ability to catalyze the *ortho*-carboxylation of phenolics. In particular, the objectives of the work are the following:

- Elucidation of enzyme kinetics and reaction thermodynamics towards a model system to identify intrinsic limitations;
- Study of the substrate scope to understand the influence of phenolic substituents on the biotransformation outcomes;
- Understand the feasibility of substituting the co-substrate bicarbonate with gaseous CO_2;
- Reaction engineering studies to overcome the thermodynamic barrier.

Additionally, the phenolic acid decarboxylase from *Mycobacterium colombiense* is evaluated as a hydroxycynnamic acids decarboxylation catalyst to produce value-added products. The objectives of the work are the following:

- Characterization of enzyme kinetics using a model system with particular attention to elucidating product inhibition;
- Establishment of a two-phase system to realize a gram-scale decarboxylation protocol;
- Establishment of a chemoenzymatic decarboxylation/hydrogenation reaction sequence in order to produce the fragrance compound 4-ethylguaiacol from ferulic acid.

For both reaction systems, the plasmid vectors containing the enzymes sequences were received from Prof. Kurt Faber and Dr. Silvia Glueck from the University of Graz.

2 *ortho*-Carboxylation of Phenols

Note: Topics in section 2.1 and 2.1.1 are also included in:

L. Pesci, S. Glueck, P. Gurikov, I. Smirnova, K. Faber and A. Liese, Biocatalytic carboxylation of phenol derivatives: kinetics and thermodynamics of the biological Kolbe-Schmitt synthesis. FEBS Journal, 282 (2015), 1334-1345.

Topics in section 2.1.3 are also included in:

L. Pesci, S. Kara, A. Liese, Evaluation of the substrate scope of benzoic acid (de)carboxylases according to chemical and biochemical parameters. ChemBioChem, (2016), doi: 10.1002/cbic.201600333.

2.1 Fundamental Studies on Benzoic Acid (De)carboxylases

Ortho-hydroxybenzoic acids (salicylic acids) are produced via the Kolbe-Schmitt reaction, which requires harsh pressure and temperature conditions and often shows regio-selectivity problems, making isomer separation necessary (Lindsey A & Jeskey H 1957). The biocatalytic "counterpart" is catalyzed by benzoic acid (de)carboxylases acting in the carboxylation direction. In this section of the thesis, fundamental features of the enzymes 2,6-dihydroxybenzoic acid (de)carboxylase from *Rhizobium* sp. and 2,3-dihydroxybenzoic acid (de)carboxylase from *Aspergillus oryzae* are investigated. The acquired fundamental knowledge is discussed within the context of the quest for reaction engineering strategies to overcome the identified limitations, aiming to finding out the feasibility of processes based on this system. Unless otherwise stated, the model system shown in Scheme 2.1 was used:

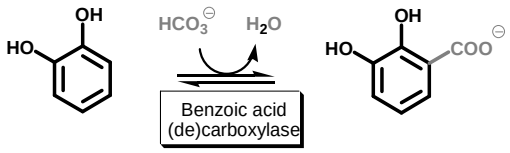

Scheme 2.1: Model system chosen: carboxylation of 1,2–dihydroxybenzene (catechol) to 2,3–dihydroxybenzoic acid (2,3–DHBA).

The carboxylation of 1,2–dihydroxybenzene (catechol) yields 2,3-dihydroxybenzoic acid (2,3-DHBA) as the sole carboxylation product with a yield of 30% using an approximately 300-fold molar excess of $KHCO_3$, which is needed to upset the equilibrium. In brief, this study encompasses: *i)* a general enzyme characterization of activity and stability, *ii)* a detailed kinetic and thermodynamic study, including the analysis of structure-activity relationships, and *iii)* the evaluation of CO_2 as a carboxylation co-substrate.

2.1.1 Reaction Medium and Enzyme Characterization

This part of the study was conducted using 2,6-dihydroxybenzoic acid (de)carboxylase from *Rhizobium* sp. (Rsp_DHBD) as biocatalyst. Rsp_DHBD is a Zn^{2+}-dependent enzyme consisting of a homo-tetramer (4 x 37.5 kDa). This was chosen because the (de)carboxylase's gene, located in the plasmid vector pET21a+ –between the restriction sites HindIII and XhoI–, which was received from the cooperation partners at the University of Graz (Prof. Faber, Dr. Glueck) contains a 6-histidine tag; this allows for a quick and easy purification approach. Chemically competent *E. coli* cells BL21(DE3) were transformed and the enzyme was expressed using a standard protocol with IPTG as an inducer. Details about cells transformation, growth and expression can be found in the experimental section. Regarding the analytical methods to measure activity, UV-based continuous assays could not be used quantitatively because of competitive absorption of catechol and 2,3-DHBA in the wavelength range of 250-280 nm. Therefore, an HPLC/UV-based discontinuous method was developed (Figures A1 and A2). The carboxylation activity of *ortho*-(de)carboxylases is dependent on the addition of bicarbonate in an adequate molar excess as co-substrate in order to detect significant conversions. Such an excess is necessary to drive substrate conversion according to the Le Chatelier effect. Previous publications on similar systems report the use of 0.1 M potassium phosphate (KP_i) buffers to counteract pH increases following the addition of bicarbonate (Kirimura *et al.* 2010; Wieser *et al.* 1998; Wuensch *et al.* 2012). Aiming to find a more effective and simpler reaction medium, we compared the influence of different aqueous solutions on reaction rate and equilibrium conversion. The same reaction rates, as well as conversions, were observed by performing reactions in 2 M $KHCO_3$, 2 M $KHCO_3$ in KP_i buffer 0.1 M pH 5.5 and 2 M $KHCO_3/K_2CO_3$ buffer. The results in terms of reaction rates are shown in Figure 2.1.1:

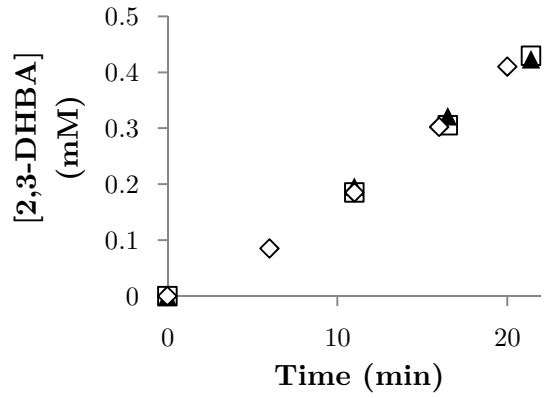

Figure 2.1.1: Initial reaction rates for catechol carboxylation in different reaction media; white squares: 2 M *KHCO₃*; black triangles: 2 M *KHCO₃*/KP_i buffer; white diamonds: 2 M *KHCO₃*/*K₂CO₃* buffer. Reactions conditions: 10 mM catechol, 4 mg mL^{-1} cell-free extract (CFE) at 30°C and 500 rpm.

In all cases, equilibrium conversions were determined to be 26-28%. These results indicate that the biotransformations can be easily performed in an unbuffered bicarbonate solution, as the phosphate ions do not exhibit an appreciable effect. Moreover, the buffer is not necessary to maintain the pH because, considering the equilibrium constants for dissociation and hydrolysis of bicarbonate (K_a = 1.3 x 10^{-4} at 25°C), it can be easily calculated that the pH would be 8.3 regardless of the salt concentration. Moreover, since bicarbonate is added in large excess, no pH shift is to be expected as a consequence of carboxylate formation. Catechols are subject to oxidation to form quinones, which undergo polymerization reactions (Schweigert *et al.* 2001). This transformation is biologically important for the synthesis of melanin, which starts from the – enzymatic – oxidation of tyrosine to the *ortho*-quinone derivative. The occurrence of this side-reaction in our conditions was evaluated by following reaction progresses in open and closed reaction vessels. After around three hours of reaction time, using 10 mM catechol concentration and 4 mg mL^{-1} crude extract, the product concentration reached a constant value of approximately 2.6 mM although catechol continued to be consumed. The progress curves indicate that catechol is oxidized through contact with the air, yielding the reactive *o*-quinone, which in turn polymerizes. This polymerization is qualitatively observable by the color change of the solution from light brown to black (Figures 2.1.2(A) and A3). The same phenomenon was observed with purified Rsp_DHBD, which excludes the undesired action of oxidases – such as Cu-dependent monooxygenases – present in the crude extract. In order to circumvent the competing chemical oxidation, several conditions – addition of sodium sulfite, solution degassing, protection from light –

were tested and the addition of stoichiometric amounts of ascorbic acid was found to be an effective tool to suppress the chemical formation of quinone by autoxidation (Figure 2.1.2(B) and Scheme 2.1.1).

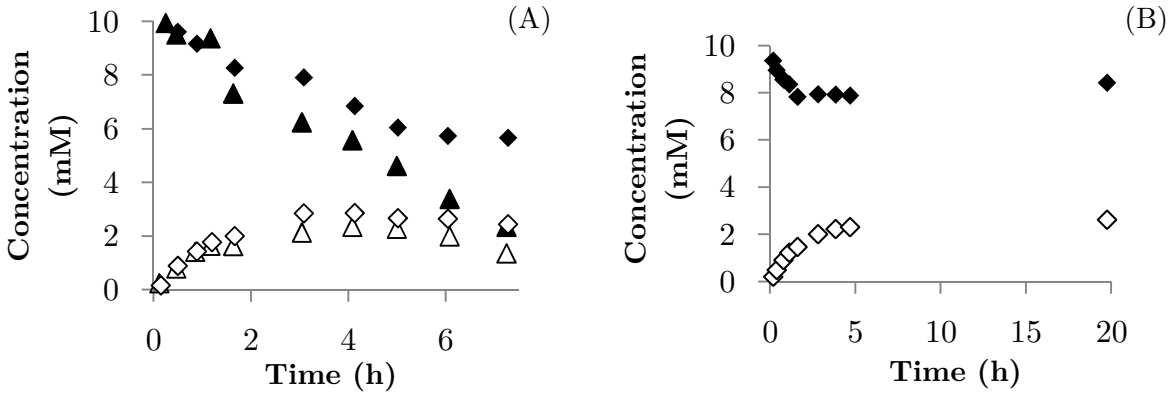

Figure 2.1.2: Filled symbols represent catechol, open symbols represent 2,3-DHBA; A: reaction progress with open (black and white triangles) and closed (black and white diamonds) reaction vessels; B: Reaction progress in the presence of 10 mM ascorbic acid. Reactions conditions: 10 mM catechol, 2 M *$KHCO_3$*, 4 mg mL^{-1} CFE, at 30°C and 500 rpm.

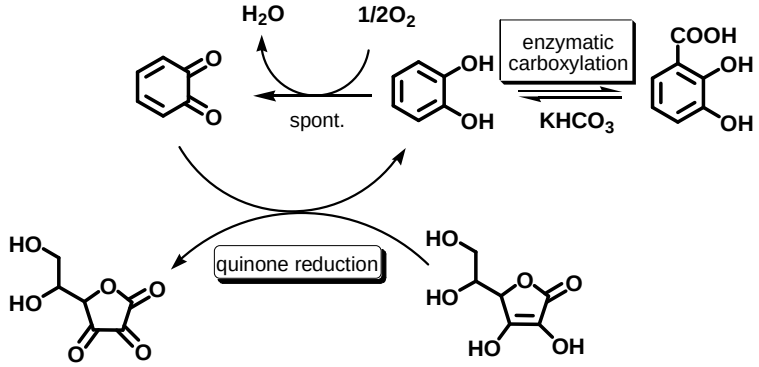

Scheme 2.1.1: Biocatalytic carboxylation of catechol and prevention of non-enzymatic catechol oxidation by chemical reduction.

Knowing the behavior of the biotransformation with respect to pH and temperature is important in evaluating its influence on enzyme activity/stability and on the equilibrium conversion. Previous studies on the same enzyme showed that the equilibrium conversion was maximum between pH 7.5-8.5 and decreased dramatically at pH 6.5 (Wuensch *et al.* 2013b). As the concentration of the co-substrate depends on pH, it is quite difficult to determine the catalytic effects because of differing ionization of the amino acids residues and the rate dependency on concentration. Figure 2.1.3 shows the dependency of the molar fraction of the three carbonate species on pH.

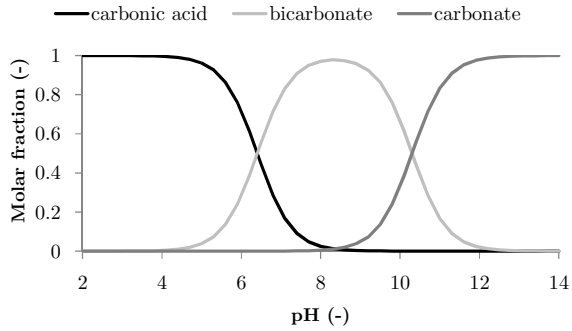

Figure 2.1.3: Dependency of the carbonate species molar fractions on pH.

At pH 6.5, for example, $[HCO_3^-]$ is ≈ 50% of that at pH 8.0. After performing reactions at different pH values, it is not surprising to observe the highest substrate conversion and reaction rate at pH 8.0, where the HCO_3^- species has the highest concentration (Figure A4). When the pH is greater than 8.0, CO_3^{2-} is the major species at equilibrium, resulting in a lower reaction rate and conversion. The activity with respect to the temperature profile shows a behavior typical of enzyme catalysis: a progressive increase in a lower temperature range (20-50°C), followed by a steep decrease after a certain threshold (60°C) (Figure 2.1.4).

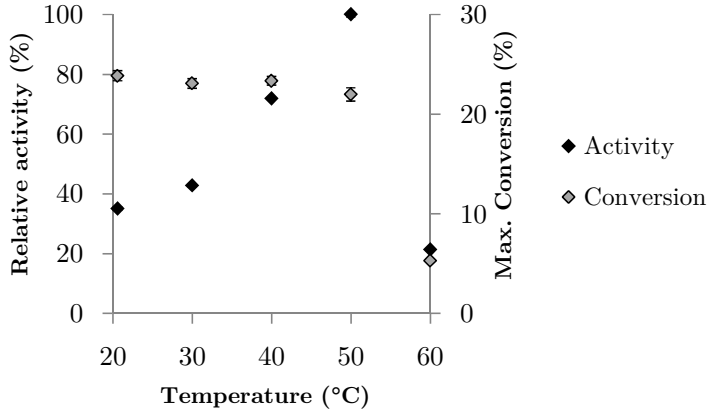

Figure 2.1.4: Influence of reaction temperature on activity and maximum conversion on Rsp_DHBD-catalyzed catechol carboxylation. Reaction conditions: 80 mM catechol, 80 mM ascorbic acid, 2 mg mL^{-1} CFE in 2 M $KHCO_3$, at different temperatures and 500 rpm.

The decrease in conversion at 60°C is reasonably attributable to enzyme deactivation. Comparable results were reported for similar systems both in terms of activity (Kirimura *et al.* 2010; Yoshida *et al.* 2004b) and maximum conversion (Wuensch *et al.* 2013b). When studying an enzymatic reaction, the activity of the

catalyst has to be investigated hand-in-hand with its stability under the operational conditions, so that the biochemical effects such as enzyme deactivation can be discerned from chemical effects. For this reason, the temperature stability of Rsp_DHBD was tested by incubating the enzyme at different temperatures. Figure 2.1.5 shows the results.

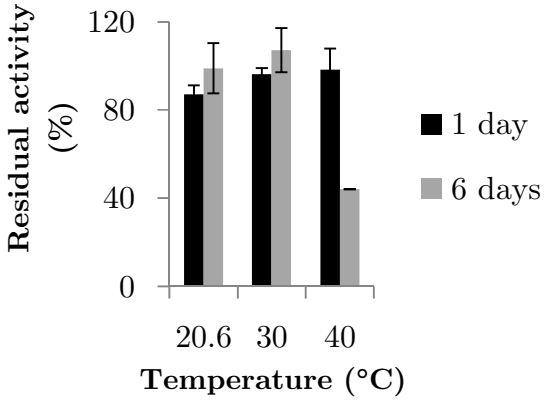

Figure 2.1.5: Stability of Rsp_DHBD at three different temperatures after one and six days. Reaction conditions: 80 mM catechol, 80 mM ascorbic acid, 2 mg mL^{-1} CFE in 2 M $KHCO_3$, at different temperatures and 500 rpm.

The enzyme can be considered quite heat resistant, especially if compared with other (de)carboxylases (Liu_2007). Another 2,6-DHBD from the related microorganism *Agrobacterium tumefaciens* has been previously addressed as "thermophilic" (Yoshida *et al.* 2004a). Due to the almost complete stability over six days, 30°C was chosen for further studies. The stability was also tested under the storage conditions – as crude extract at 4°C, Figure A5 –, which was also satisfactory ($\tau_{1/2}$= 3.4 months).

In conclusion:

- The enzyme 2,6-dihydroxybenzoic acid (de)carboxylase from *Rhizobium* sp. (Rsp_DHBD) was expressed in *E. coli* as bacterial host and its general properties were described;
- The use of ascorbic acid for the carboxylation of catechol was demonstrated to be necessary to counteract spontaneous oxidation in the reaction conditions employed;

- The enzyme showed to possess a typical temperature profile, while regarding pH it is difficult to separate the effects due to a different ionization of the amino acids and the concentration profile of the co-substrate.

2.1.2 Kinetics and Thermodynamics

Enzyme kinetics and reaction thermodynamics are fundamentally important for understanding how enzymes work and technically important for elucidating bottlenecks of possible processes (Vasic Racki *et al.* 2003). In the case of benzoic acid (de)carboxylases, it is quite clear that the thermodynamic equilibrium is one of the main, if not the most important, issues. However the quantitative determination of an enzyme's and reaction's features shines a light either on additional issues or on useful characteristics that can be exploited for application purposes. The fundamental data that are described in this chapter are discussed in terms of both chemical biology and biotechnology.

The enzymatic carboxylation is a condensation reaction followed by the elimination of water. However, from an enzyme kinetics viewpoint the reaction can be considered as a bi-uni reaction, since it is performed in aqueous media. Being a reversible reaction, the determination of the kinetic parameters requires the analysis of the forward (carboxylation) and reverse (decarboxylation) directions. Moreover, since two substrates are involved in enzyme binding and catalysis, the individual substrates have to be characterized separately. In order to calculate the enzyme's mass-specific activity, Rsp_DHBD was purified making use of the histidine tag at the C-terminus of the protein via Ni^{2+}-NTA affinity chromatography (Figure A6). The enzyme was purified with a yield of 13%[2]. With the forward kinetics, employing 0.2-0.3 mg mL^{-1} enzyme, it was possible to measure initial rates directly by taking samples in the first 20 min of reaction (zero order kinetics, ≤ 10% conversion, Figure A6). In order to evaluate the kinetics for only the phenolic substrate, [$KHCO_3$] was fixed at 2 M (as will be discussed soon in this section, this value corresponds to 2.3 times its K_M). Figure 2.1.6(A) shows the initial rates measurements for catechol.

[2] The yield refers to the mass of the (de)carboxylase with respect to the mass of the total proteins in the crude extract.

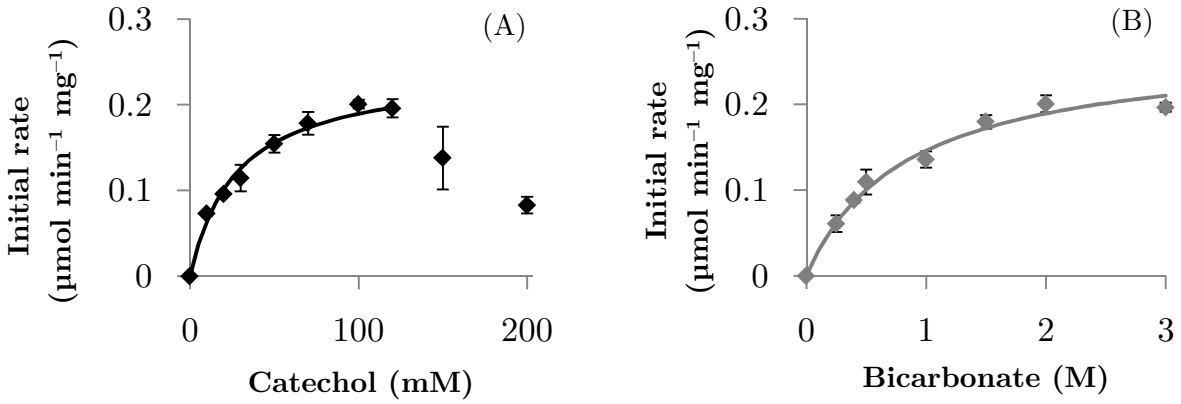

Figure 2.1.6: Initial rates measurements for catechol (A) and bicarbonate (B). Reaction conditions A: 0-200 mM catechol and an equimolar amount of ascorbic acid, 0.2-0.3 mg mL^{-1} Rsp_DHBD in 2 M $KHCO_3$,. Reaction conditions B: 100 mM catechol, 100 mM ascorbic acid, 0-3 M $KHCO_3$, 0.2-0.3 mg mL^{-1} Rsp_DHBD. Assays were performed at 30°C and 500 rpm. Non-linear fit (black and grey lines) were performed with Microsoft Excel by the least squares method.

The kinetic plot displays a hyperbolic shape between 0 and 120 mM, followed by a steep decrease beyond this value. In the case of excess substrate inhibition, a second catechol molecule would bind to the enzyme-substrate complex forming an inactive enzyme complex, resulting in initial rate decreases. However, the plot could not be fitted to the corresponding equation, indicating the occurrence of a different phenomenon. The range until 120 mM was fitted to Eq. 2.1.1, the double substrate Michalis-Menten equation, where due to the high concentration of the second substrate, the second term of the equation remains almost constant.

$$v_f = V_{max}^f \frac{[C]}{(K_{M,c} + [C])} \frac{[B]}{(K_{M,b} + [B])} \qquad \text{(Eq. 2.1.1)}$$

$[C]$ and $[B]$ are catechol and bicarbonate concentrations, respectively, while $K_{M,c}$ and $K_{M,b}$ are the respective affinity constants. A $K_{M,c}$ of 30 ± 3 mM and a V_{max}^f of 0.35 ± 0.01 µmol min^{-1} mg^{-1} were determined. A similar K_M value of 25.9 mM was reported towards 1,3-dihydroxybenzene for a 2,6-DHBD from *Agrobacterium tumefaciens* (Yoshida *et al.* 2004b).

Literature shows that maximum conversions for these non-oxidative (de)carboxylations are higher at relatively low substrate concentrations with specific values depending on the enzyme and substrate. For example, in the *ortho*-carboxylation of 5-methyl-1,3-dihydroxybenzene (orcinol) and 1,3-dihydroxybenzene (resorcinol), conversions decrease from 67 and 35% at substrate concentrations of 10–50 mM to 4 and 15% at substrate concentrations of ≈ 200 mM (Wuensch *et al.*

2013b; Wuensch *et al.* 2014). The same behavior was found in the *ortho*-carboxylation of *para*-aminophenol, yielding *para*-aminosalicylic acid, where the maximal conversion decreased from 70% at 10 mM to 20% at 200 mM using a salicylic acid (de)carboxylase (Ienaga *et al.* 2013). The same trend was observed with hetero-aromatics –pyrrole to pyrrole-2-carboxylate–(Wieser *et al.* 1998). An intrigiung example showing how enzyme and substrate are both critical factors is the case described by Matsui *et al.*, where, using 2,6-DHBD from *Pandoraea* sp. a constant conversion of 50% for resorcinol could be achieved at up to 3 M substrate concentration, while 0.3 M catechol showed only a conversion of 6% (Matsui *et al.* 2006). Although these findings are generally explained by substrate inhibition, our kinetic plot for catechol does not fit with this hypothesis. The drastic decrease in the reaction rate might be better explained by enzyme deactivation at elevated substrate concentrations. The irreversible decrease in activity in the system investigated in this work is also illustrated by the formation of protein aggregates almost immediately in the reaction solution when the purified enzyme is challenged with higher substrate concentrations (150-200 mM). To verify this hypothesis, we performed a deactivation test first developed by M. J. Selwyn in 1965 (Selwyn 1965). The test is based on the fact that, in the absence of enzyme deactivation, product formation is only a function of time and enzyme concentration if all the other parameters are kept constant. It follows that, when performing enzymatic reactions with different concentrations of enzyme and plotting product concentration versus time multiplied by enzyme concentration, the points must coincide in the same curve. If denaturation occurs, the enzyme amount itself becomes a function of time, and different curves are obtained. Figure 2.1.7 shows the results of the deactivation test at substrate concentrations of 30 and 200 mM. Reaction progress clearly shows that, at high substrate concentrations, the enzyme concentration no longer remains constant, because higher conversions were obtained with higher enzyme amounts. Figure A7 shows additional deactivation tests using catechol concentrations of 80 and 100 mM.

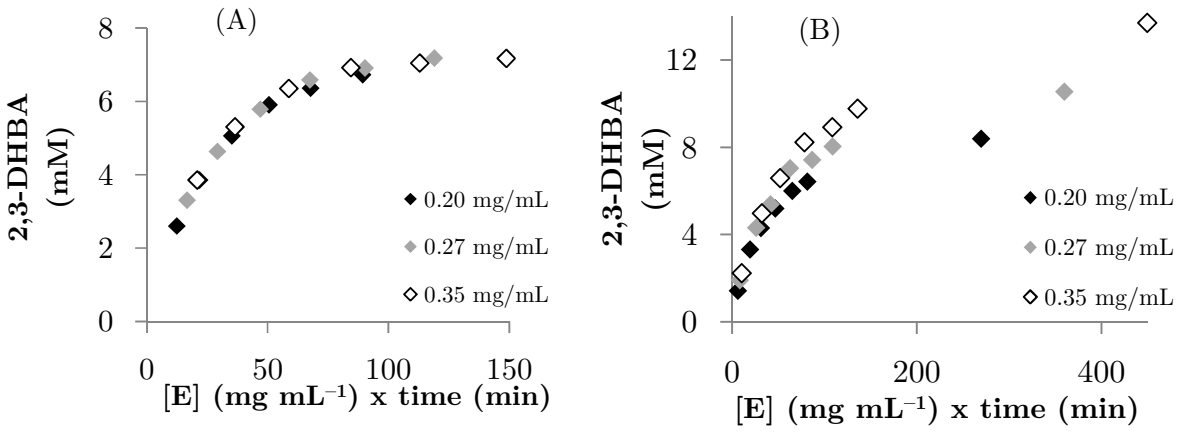

Figure 2.1.7: Deactivation assay using 30 mM (A) and 200 mM (B) catechol; black diamonds: 0.20 mg mL^{-1} CFE; grey diamonds: 0.27 mg mL^{-1} CFE; white diamonds: 0.35 mg mL^{-1} CFE; reaction conditions: 30 or 200 mM catechol, 30 or 200 mM ascorbic acid, Rsp_DHBD, in 2 M $KHCO_3$, at 30°C and 500 rpm. The time difference between the last two points is 15 h.

Recently, Ienaga *et al.* have shown that a constant equilibrium conversion of 70% could be obtained for a range of 10-200 mM *para*-aminosalicylic acid by performing two amino acids mutations in the active site of salicylic acid decarboxylase from *Trichosporon moniliiforme (Ienaga et al. 2013)*. This suggests that the deactivation involves interactions of the phenolic substrate in the catalytic cavity and that a few residues are strong determinants of the (de)carboxylase's stability. Specifically, the substitution involved exchanging Tyr^{64} and Phe^{195} –corresponding to Asn^{60} and Phe^{189} in Rsp_DHBD– with Thr and Tyr, respectively. This shows how key amino acid residues may be substituted, resulting in enhanced protein stabilization as a possible consequence of the introduction of additional OH groups through Thr^{64} and Tyr^{195}.

To assess the kinetic behavior with respect to bicarbonate, 100 mM of catechol was used as a saturating concentration, 3.39 times its K_M value, and the co-substrate concentration was varied from 0 to 3 M –approximately the solubility limit. Figure 2.1.6(B) shows the double-substrate Michaelis–Menten fit obtained while treating the first term of equation 2.1.1 as a constant. For each bicarbonate concentration, the ionic strength of the solution changes. However, from the typical rectangular hyperbola, it can be concluded that the enzyme is not significantly affected by different ionic strength values. A $K_{M,b}$ of 839 ± 4 mM can be calculated, which is extremely high for enzyme catalysis and may indicate that the carboxylation is not the natural function of the enzyme. Being a reversible reaction, the decrease in velocity due to product binding and conversion in the active site have to be considered in order to describe the entire carboxylation progress. The measurements of V_{max}^{r} and $K_{M,HA}$ for 2,3-DHBA were conducted at pH 8.0 using a

0.1 M KP_i buffer to counteract the pH decrease caused by the addition of the hydroxyacid. Unlike the carboxylation direction, the decarboxylation's initial rates could not be easily measured directly due to the higher specific activity; for this reason, reaction progress curves were realized by taking samples for the first 10-15 min of the reaction when employing 0.2-0.3 mg mL^{-1} enzyme. Using these conditions, the conversions were approximately quantitative and linear regressions were performed in the zero-order kinetics range (Figure A8). Figure 2.1.8 shows the kinetic plot. A $K_{M,HA}$ of 1.2 ± 0.3 mM and a V^r_{max} of 1 ± 0.1 µmol min^{-1} mg^{-1} were calculated by non-linear fit to Eq. 2.1.2.

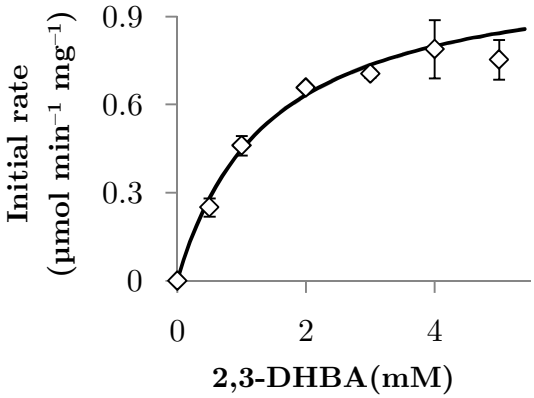

Figure 2.1.8: Initial rates measurements for 2,3–dihydroxbenzoic acid (2,3–DHBA). Reaction conditions: 0-5 mM 2,3-DHBA and an equimolar amount of ascorbic acid, 0.38 mg mL^{-1} Rsp_DHBD in 0.1 M KP_i buffer, pH 8.0. Non-linear fit (black line) was performed with Microsoft Excel by the least squares method.

$$v_r = V^r_{max} \frac{[HA]}{(K_{M,HA} + [HA])} \qquad \text{(Eq. 2.1.2)}$$

In the equation V^r_{max} is the maximum velocity in the reverse direction, $[HA]$ is the concentration of 2,3-DHBA and $K_{M,HA}$ its K_M value. Table 2.1.1 summarizes the enzyme's parameters.

Table 2.1.1: Catalytic parameters for the enzymatic (de)carboxylation of catechol/2,3-DHBA.

Carboxylation					
K_M (mM)		V^f_{max} (µmol min^{-1} mg^{-1})	k_{cat} (s^{-1})	K_a (mM^{-1} s^{-1})	
catechol ($K_{M,c}$)	bicarbonate ($K_{M,b}$)	$0.35 \pm 1.1\text{x}10^{-2}$	$0.12 \pm 3.0\text{x}10^{-3}$	catechol (K_a^c)	bicarbonate (K_a^b)
30 ± 3	839 ± 4			$4.2\text{x}10^{-3} \pm 6.5\text{x}10^{-4}$	$1.5\text{x}10^{-4} \pm 5.7\text{x}10^{-6}$

Decarboxylation			
K_M(mM) ($K_{M,HA}$)	V^r_{max} (µmol min^{-1} mg^{-1})	k_{cat} (s^{-1})	K_a^{HA} (mM^{-1} s^{-1})
1.2 ± 0.3	1 ± 0.1	0.52 ± 0.025	$0.44 \pm 9\text{x}10^{-2}$

As it can be seen, the enzyme is more effective in catalyzing the decarboxylation reaction. The lower V_{max} in the carboxylation direction can be easily interpreted as consequence of the thermodynamically challenging C—C bond formation, which would have the highest activation energy. It can also be seen that the K_M ratio between catechol and 2,3-DHBA is ≈ 30, which, in terms of initial rate, indicates a strong product inhibition. This was recognized as a common pattern in enzyme catalysis for energetically challenging reactions (Schmidt *et al.* 1983). Thinking in an evolutionary context, where enzymes "evolve" to maximize their catalytic efficiencies (k_{cat}), the constancy of the equilibrium constant for a reversible reaction can be satisfied only by the guarantee of strong affinities of the enzyme towards the product(s). A very useful mathematical visualization of this concept is provided by the Haldane equations (see Eq. 2.1.3).

Data on the thermodynamics of the reaction also need to be collected to provide a comprehensive picture. Long-term experiments were performed using relatively high amounts of (de)carboxylase – 0.5-1 mg mL^{-1}, ensuring the occurrence of steady-state concentrations after a few hours of reaction – and varying the concentration of the two substrates. A linear correlation of maximal conversion is expected by increasing the substrate (catechol) concentration at a fixed bicarbonate concentration. Strong product inhibition and/or enzyme deactivation may cause the establishment of steady-state concentrations not corresponding to the thermodynamic equilibrium, which would need longer time to be established. Conversely, increasing conversion is expected by increasing the bicarbonate

concentration while maintaining a fixed substrate concentration. The results are depicted in Figures 2.1.9 and 2.1.11 and are in accordance with previously reported trends for similar systems (Iwasaki *et al.* 2007; Kirimura *et al.* 2010; Wieser *et al.* 1998; Wuensch *et al.* 2013b).

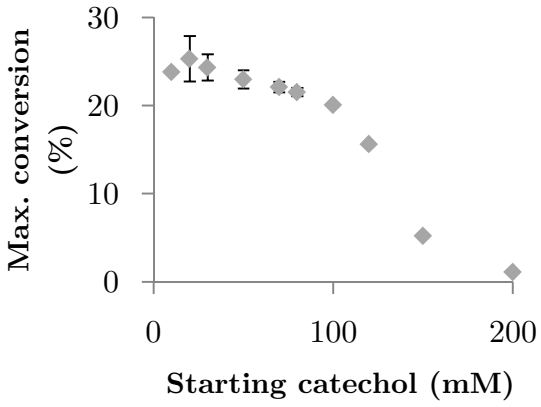

Figure 2.1.9: Maximum substrate conversion that can be achieved at different starting concentrations. Reaction conditions: 10-200 mM catechol and an equimolar amount of ascorbic acid, 0.5-1 mg mL^{-1} Rsp_DHBD in 2 M $KHCO_3$, at 30°C and 500 rpm.

Figure 2.1.9 shows that a constant maximal conversion of approximately 23% is obtained between 10 and 80 mM, where deactivation effects are negligible. In this range, it can be assumed that the maximal conversion corresponds to the equilibrium conversion. Beyond this threshold, the conversion decreases dramatically due to enzyme deactivation and the value therefore depends on the enzyme concentration. For the converse experiment, a fixed 10 mM concentration of catechol was used to measure the equilibrium displacement at increased amounts of bicarbonate. From the law of mass balance, the equilibrium constant for the reaction was calculated to be $1.6 \times 10^{-4} \pm 8.0 \times 10^{-6}$. From this, the difference in standard free energy at 30°C results to be: $\Delta G_r^0 = +5.2 \pm 0.03$ kcal mol^{-1}.

The information collected and described can be implemented in an overall kinetic model describing the biotransformation at any given time point. This allows verification of parameters' reliability and appreciation of their effects not only at the beginning, but during the course of the whole reaction. Moreover, a simple combination of the kinetic model with mass balance equations of different reactor configurations provides a valuable tool to describe and optimize a process. In order to suggest a kinetic model, it is helpful to look into the details of the biochemical mechanisms. The crystal structure of Rsp_DHBD was solved, contributing greatly to elucidating its catalytic strategy in both forward and reverse directions (Goto *et al.*

2006; Wuensch *et al.* 2014). The active site with the complexed substrate 2,6-dihydroxybenzoic acid is shown in Figure 2.1.10:

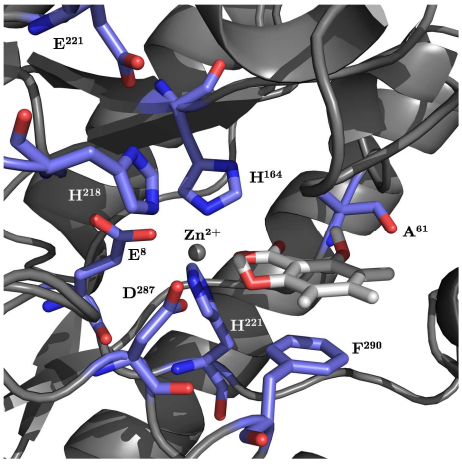

Figure 2.1.10: Active site of the Rsp_DHBD with the complexed 2,6-DHBA (source: PDB database, code: 2DVU). Visualization created using Pymol.

The divalent cation has trigonal bipyramidal geometry, where His^{164} and Asp^{287} act as axial ligands and His^{10}, Glu^{8} and a water molecule act as equatorial ligands. The native substrate 2,6-dihydroxybenzoic acid is stabilized by π-π interactions with Phe^{290} and by hydrogen bonds of the 2-OH group with Asp^{287} –also a Zn^{2+} ligand– and of the 6-OH group with a water molecule coordinating with Ser^{20} and Ala^{61}. This binding mode partially explains why the ligands 2,4-, 2,5- and 3,5-dihydroxybenzoates are not substrates. In fact, the phenolic groups in positions 3, 4, and 5 restrict the access in the active site due to the presence of Phe^{23}. However, it is not clear why the simpler 2-hydroxybenzoate (salicylate) cannot be accepted as a substrate. The (bio)chemical mechanism for carboxylation already has been proposed and it showed interesting common elements with the chemical Kolbe-Schmitt reaction. The comparison of the key steps are reported in Scheme 2.1.2:

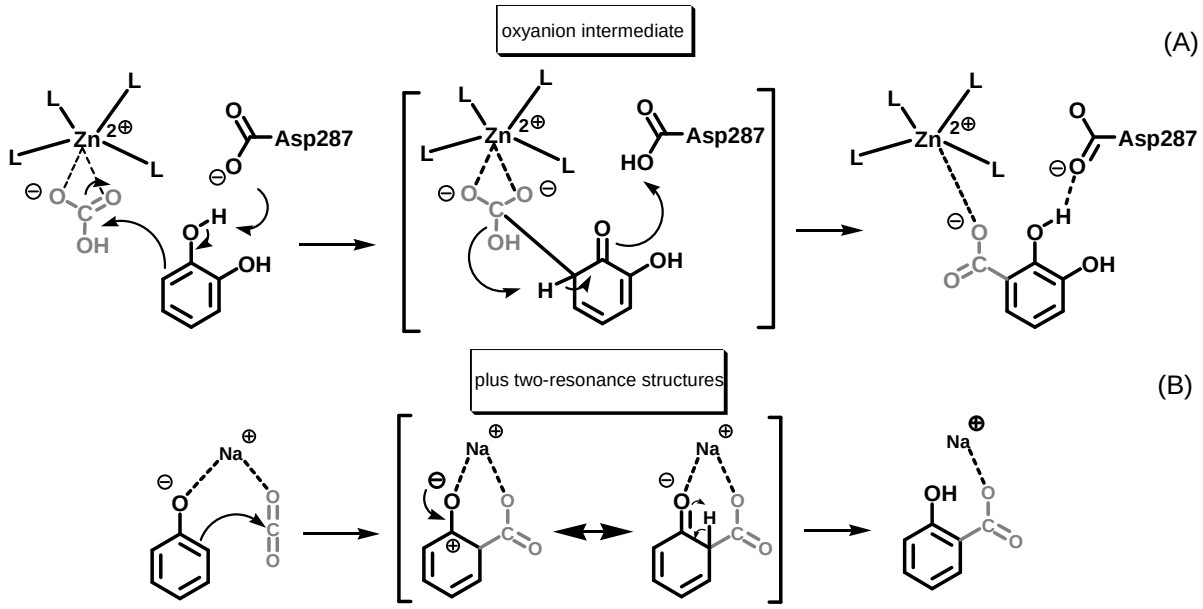

Scheme 2.1.2: Comparison of the key mechanistic step of the enzymatic (A) and chemical (B) Kolbe-Schmitt reaction.

The chemical counterpart can be described as a classical electrophilic aromatic substitution reaction (S_{NelAr}); the metal ion makes a complex with the two reactants, activating CO_2 for the nucleophilic attack, and resulting in the formation of a resonance stabilized intermediate which regains aromaticity by tautomerization. In the biochemical mechanism, Asp[287], –assisted by His[218] and Glu[221], which overall form a catalytic triad– acts as a general base and deprotonates the phenolic group, therefore increasing the electron density of the *ortho*-carbon. This exerts a nucleophilic attack on bicarbonate, forming what is postulated to be an oxyanion intermediate, which regains aromaticity by water elimination/tautomerization. The mechanism describes two distinct binding sites that are responsible for the interactions with the two substrates. Therefore, we suggested a random binding sequence, as opposed to an ordered one, which is more typical for co-factor dependent enzymes (Everse 1982; Gerhard & Schomburg 2013). Moreover, because of the low k_{cat} for this thermodynamically-challenged reaction, we assumed the catalytic step to be rate limiting with the other binding/unbinding events occurring in rapid equilibrium. Such a catalytic pathway would be a reversible random bi-uni mechanism (Karlheinz D. & Waldmann 2002) (Scheme 2.1.3 and Eq. 2.1.2):

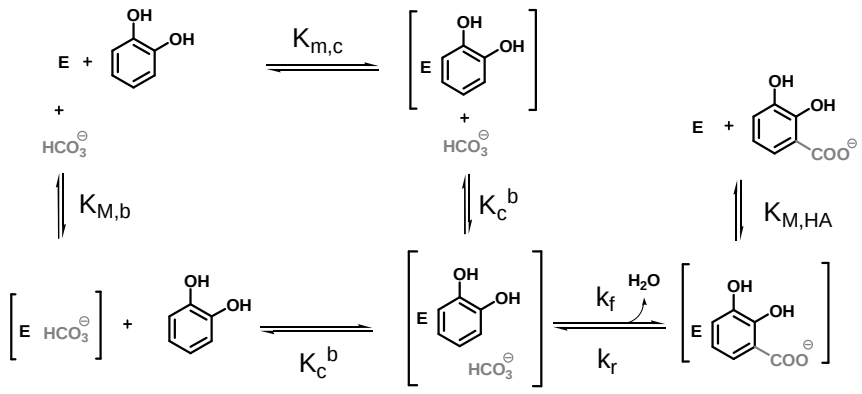

Scheme 2.1.3: Reversible random bi-uni mechanism proposed for enzymatic (de)carboxylation.

$$\frac{d[HA]}{dt} = [E]\,v = [E]\frac{\frac{V^f_{max}}{K_{M,c}K^b_c}[C][B] - \frac{V^r_{max}[HA]}{K_{M,HA}}}{1+\left(\frac{[C]}{K_{M,c}}\right)+\left(\frac{[B]}{K_{M,b}}\right)+\left(\frac{[HA]}{K_{M,HA}}\right)+\left(\frac{[C][B]}{K^b_c\,K_{M,c}}\right)} \qquad \text{(Eq. 2.1.2)}$$

In Eq. 2.1.2, the velocity for carboxylation decreases when the product concentration increases, which, to an extent, depends on its V^r_{max} and $K_{M,HA}$. The denominator takes into account all the adsorption events. The dissociation constant of the ternary complex K^b_c is the only unknown parameter, but it can be algebraically calculated using the Haldane equation, which correlates the catalytic parameters at equilibrium (Eq. 2.1.3).

$$K_{eq} = \frac{[HA]_{eq}}{[C]_{eq}[B]_{eq}} = \frac{V^f_{max}\;K_{M,HA}}{V^r_{max}\;K^b_c\;K_{M,c}} \qquad \text{(Eq. 2.1.3)}$$

This dissociation constant can be calculated as 87 mM. The complete kinetic model can be used to simulate the course of biotransformation, once the appropriate mass-balance is formulated. Eq. 2.1.2 corresponds to product formation in batch mode, where $[E]$ is the (de)carboxylase concentration. Figure 2.1.11 shows that the reaction progresss, as well as the equilibrium positions, can be modeled with good agreement. Therefore, the proposed model is a viable catalytic pathway for this biocatalytic carboxylation (see Figure A9 for additional comparisons).

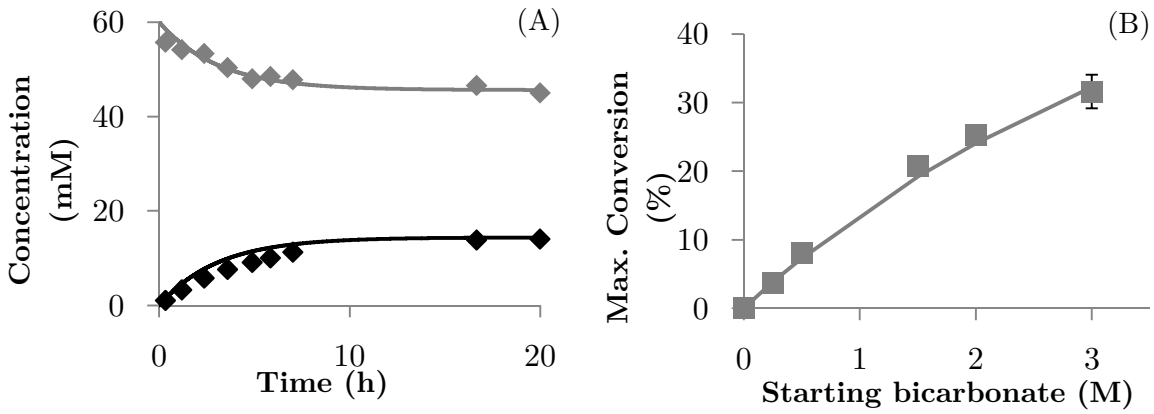

Figure 2.1.11: Comparison of experimental data (grey and black diamonds and grey squares) with numerical simulations of Eq. 2.1.2 (grey and black lines); A: Reaction conditions: 60 mM catechol, 60 mM ascorbic acid, 0.25 mg mL^{-1} Rsp_DHBD in 2 M *KHCO₃*, at 30°C and 500 rpm; B: Reaction conditions: 10 mM catechol, 10 mM ascorbic acid, 0.5–1 mg mL^{-1} Rsp_DHBD, in 0-3 M *KHCO₃*, at 30°C and 500 rpm.

Table 2.1.2 lists the limitations identified in view of practical applications of the system. The "bottlenecks" are divided according to the chemical or biochemical nature. Moreover, possible solutions which can come from reaction engineering, chemistry or biology are also provided, together with practical limitations that may arise from their implementation.

Table 2.1.2: Challenges for the biocatalytic *ortho*-carboxylation. "+": the challenge can be overcome;"–": the limitation cannot be overcome; "?": not enough data are available at this stage.

			Challenges for applicability				
			Reaction features	**Enzyme features**			
			Thermodynamic limitation	Low carboxylation activity	High K_M for HCO_3^-	Deactivation by substrate	**Practical limitations**
Solutions	**Chemistry**	High co-substrate concentrations	+	+	+	-	Complication of downstream processing, higher E factor, solubility limit
		Use of substrates with higher free energy	+	?	-	?	Restriction of the substrate scope
	Reaction Engineering	Continuous product extraction	+	-	-	-	Higher hydrophobicity of the substrate/ selectivity
		Continuous product adsorption	+	-	-	-	Selectivity between substrate and product
		Substrate feeding	-	-	-	+	Lower reaction rate/productivity
		Low substrate concentration	-	-	-	+	Lower reaction rate/productivity
		High biocatalyst loading	-	+	+	+	Enzyme cost, solubility limits
		Use of co-solvents	+	-	-	?	Complication of downstream, influence on enzyme activity
	Biology	Protein engineering, enzyme screening	-	+	+	+	Research intensive

From the table it appears clear that reaction engineering has a good potential to overcome each limitation identified (e.g., product removal in combination with substrate feeding), once proven the absence of additional limitations.

In conclusion:

- The kinetics of catechol carboxylation catalyzed by Rsp_DHBD was studied in the forward and in the reverse directions;
- The catalytic parameters are in accordance with the thermodynamics of the reaction, hence, a lower V_{max} and a higher K_M were determined for the carboxylation direction;
- Catechol causes enzyme deactivation at high (≈ 120 mM) concentrations;
- On the basis of the molecular mechanism, a reversible random bi-uni mechanism was proposed and validated through comparison of the experimental data with simulations.

2.1.3 Linear Free-Energy Relationships with the Substrate Scope

The understanding of the chemical-physical determinants of the substrate scope of a chemical reaction is a considerable step forward in achieving the understanding of its mechanisms and structural requirements. This holds true for enzymatic reactions as well, where such understanding may also lead to further rational planning of scope's expansion. As already shown in section 1.2, a diverse group of (de)carboxylases acting on phenolic nuclei is available. The substrate spectra of these enzymes vary significantly and can be extremely broad (*e.g.*, dihydroxybenzoic acid (de)carboxylases and phenolic acid (de)carboxylases (Wuensch *et al.* 2014; Wuensch *et al.* 2015) as well as extremely narrowed (*e.g.*, pyrrole-2-carboxylate (de)carboxylase (Wieser *et al.* 1998)). Reasons for this diversity is still not clear, although it is likely a consequence of the interconnection between chemical and biochemical determinants. Understanding an enzyme's substrate scope is, in fact, not an easy task, due to reasons such as the interactions of substrate molecules with non-homogeneous enzymes surfaces and their variety of functional groups, both inside and outside active sites (Langone 1991; Williams 2003).

Linear free energy relationships (LFERs) are easy-to-use, but difficult to interpret, tools correlating structural variations to changes in the equilibrium (K_{eq})

and rate (k) constants. They are based on the proportionality between the base-10 logarithms of equilibrium and rate constants, and the Gibbs free energy function and free energy of activation.[3] Two classes of LFERs can be distinguished (Williams 2003). Eq. 2.1.4 refers to the class I, where equilibrium constants and rate constants for the same process are compared:

$$\log k = a \log K_{eq} + b \qquad \text{(Eq. 2.1.4)}$$

Where a and b are two coefficients that depend on the reaction. The class II refers to reactions where the changes in equilibrium or rate constants are related to the changes for a similar reference process (*e.g.*, Eq. 2.1.5):

$$\log k = a \log k' + b \qquad \text{(Eq. 2.1.5)}$$

Different class II LFERs correlating the electronic properties of substituents in aromatic molecules with physical-chemical constants have been developed. The most popular and most used was first described in the 20th century: the Hammett relationship (Hammett 1937); the reference reaction consists of the dissociation of *meta*- and *para*-substituted benzoic acids. The different equilibrium constants can be used to derive the Hammett parameters σ_X, where X is a specific *meta* or *para* substituent[4], as shown in Eq. 2.1.6:

$$\sigma_X = log(\frac{K_X}{K_H}) \qquad \text{(Eq. 2.1.6)}$$

K_X and K_H are the dissociation constants for substituted and unsubstituted benzoic acids, respectively. Hence, a smaller constant implies a higher electron donating power of X –therefore a lower acidity of the benzoic acid derivative– and *vice versa*. The Hammett constants can be used to rationalize the dependency of empirical data from a certain reaction involving aromatic substrates on electron donating/withdrawing power of substituents (Chapman & Shorter 1978; Kubinyi 1993). A common form to express the Hammett equation to describe a chemical reaction is represented in Eq. 2.1.7:

$$\frac{\log k_x}{\log k_H} = \sigma_x \rho \qquad \text{(Eq. 2.1.7)}$$

[3] Precisely: $\Delta G = -2.303\, RT \log K_{eq}$ and $\Delta G^{\ddagger} = 2.303\, RT \log k - 2.303\, RT log \kappa K_b\, T/h$; κ is the transmission coefficient, $K_b$the Boltzmann constant, R the gas constant, T the absolute temperature and h the Planck's constant.

[4] The use of *ortho* substituents is not considered because the additional steric factor would contribute to the property change.

Where the slope of the linear correlation ρ, which equals 1 for the dissociation of benzoic acids, measures the sensitivity of the reaction towards the changes of the substituents. Such correlations were shown to be quite broad and able to describe systems in different fields of chemistry (Kunal 2015; Putz 2013). The choice of different reference reactions allows the design of new constants which take into account different effects (Brown & Okamoto 1958; Hansch *et al.* 1991). The Taft constants σ_x^0 are defined using phenylacetic acid as substrate, which has no direct bonding of the carboxylic group to the aromatic ring and reflects the inductive effects of the substituents. Meanwhile, the electrophilic aromatic substitution constants σ_x^+ are defined using the solvolysis of *tert*-cumyl chlorides (Figure 2.1.12).

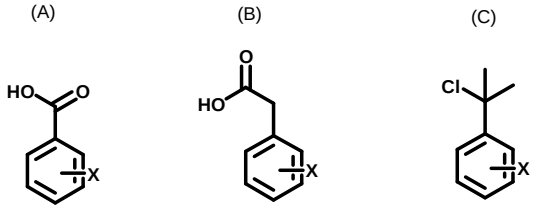

Figure 2.1.12: General substrate structures used to define Hammett (A), Taft (B) and electrophilic aromatic substitution (C) constants.

Benzoic acid (de)carboxylases coming from different microbial sources show different substrate scopes. For example, Rsp_DHBD shows a considerably narrow substrate scope when compared to the 2,3-dihydroxybenzoic acid (de)carboxylase from *Aspergillus oryzae* (Ao_DHBD) (Wuensch *et al.* 2014). In brief, Rsp_DHBD seems to strictly accept only dihydroxyphenols (catechol and resorcinol), *meta*-alkoxyphenols and *ortho*-alkylphenols, while Ao_DHBD accepts a remarkable variety of substrates. In order to have a greater amount of data to interpret, this study was conducted using Ao_DHBD (see Section 7.1 for details about cultivation and overexpression). Due to their similar biocatalysis and the same basic structural requirements – aromatic substrates with at least one phenolic group –, the same mechanism is assumed for both enzymes even though the structure and mechanism of Ao_DHBD are unknown. In this section, the equilibrium constants and the reaction rates for the carboxylation of different substituted phenolic compounds are quantitatively correlated using the electronic and steric parameters of the substituents. The effects are not considered with respect to the phenolic group but instead to the carboxylic group, which corresponds to the position of the reactive carbon –where the C–C bond formation occurs– (Figure 2.1.13).

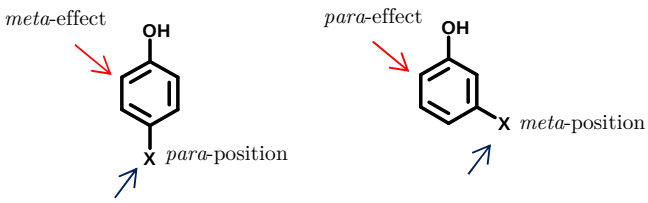

Figure 2.1.13: Effects of the substituents on the carboxylations reactive center in substituted phenolic compounds.

In order to evaluate the equilibrium conversions, steady-state concentrations of reactants and products obtained after a certain substrate dependent reaction time were measured. Enzyme inhibition phenomena may affect the steady-state concentrations and therefore the equilibrium constants are addressed as apparent ($K_{eq,app}$). Twelve different substrates with *meta* and *para* effects on the reactive carbon were studied. Using the Taft coefficients (σ^0), which mainly take inductive effects into account, a clear linear correlation could be found (Figure 2.1.14(A)):

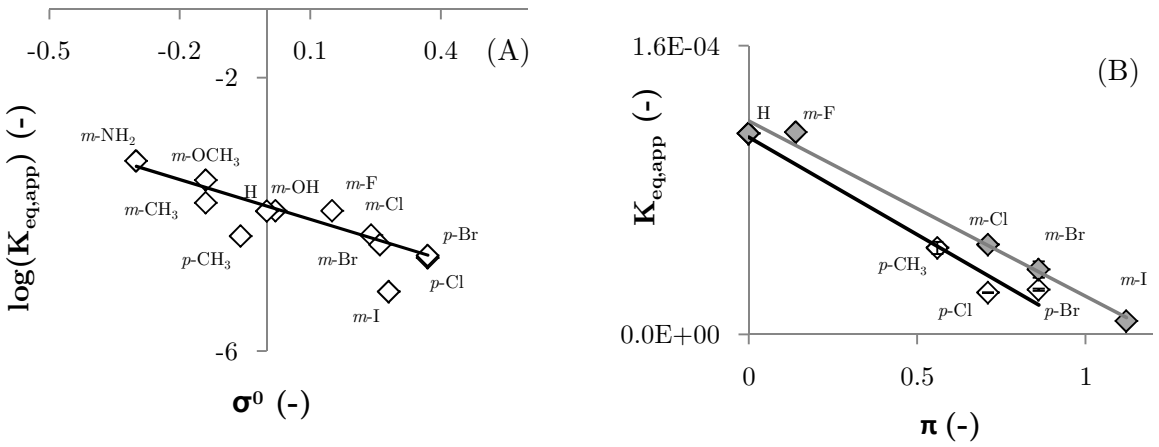

Figure 2.1.14: A: Correlation of the logarithm of the calculated $K_{eq,app}$ with respect to the Taft constants σ^0 ($R^2 = 0.93$); B: Correlation of the calculated $K_{eq,app}$ with respect to the hydrophobicity constants π ($R^2 = 0.98$ for *meta*-substituents; $R^2 = 0.97$ for *para*-substituents). Reaction conditions: 10 mM substrate, 30 mg mL^{-1} whole cells expressing Ao_DHBD (2.1 U mL^{-1}), in 3 M $KHCO_3$, at 30°C and 500 rpm.

Only two substrates, *meta*-methylphenol and *meta*-iodophenol, showed a significant deviation from linearity. From Figure 2.1.14(A) it can be concluded that: *i)* as the linear behavior is valid for both *para* and *meta* substituents, there is no differentiation of the regio-isomers, suggesting that the outcome is rather independent on the enzyme features, *ii)* the negative slope ($\rho = -1.9$) indicates that the reaction is favorable when the reactive center is electron rich, and *iii)* the deviation of *meta* methyl- and *meta* iodophenol are reasonably consequences of the

interactions with the enzyme. Conclusion *ii* is in accordance to what is known about the Kolbe-Schmitt reaction and in general about electrophilic aromatic substitutions, either chemical or enzymatic (Bathelt *et al.* 2004; Borkar *et al.* 2013; Lindsey A & Jeskey H 1957). Such a trend justifies why nitro-substituted phenols are not accepted by any (de)carboxylases described so far; nitrophenols require extremely harsh conditions to react under Kolbe-Schmitt protocols (Lindsey A & Jeskey H 1957). Figure A10 shows the correlation with the Hammett constants (R^2 = 0.87 with eleven phenols and ρ = –1.34) and the electrophilic substitution constants (R^2 = 0.91, with ten phenols and ρ = –0.87). From such results it is possible to speculate that inductive effects are more important for the observed variable. In order to evaluate the influence of enzyme-ligands interactions, a correlation with the hydrophobicity parameter π (Eq. 2.1.8) was attempted (Yang *et al.* 1986).

$$\pi = aV_w - bHB - c\mu + d \qquad \text{(Eq. 2.1.8)}$$

Where V_w is the Van der Waals volume, HB a hydrogen bonding factor, and μ the dipole moment of the substituents; a, b, c and d are corrective coefficients. It was found that *meta*- and *para*-halo-phenols are linearly correlated with the hydrophobicity of the substituents in two different series with R^2 = 0.98 and 0.97, respectively (Figure 2.1.14(B)). This differentiation may be due to different enzyme-regioisomer interactions. *para*-Methylphenol, deviating in the plot in Figure 2.1.14(A), behaves similarly to the other *para*-substituents. A similar correlation was found when considering only the Van der Waals volumes V_w, indicating the importance of the size factor (Figure A11). From this perspective, the steady-state conversion of *meta*-iodophenol is also a consequence of its size and interactions with the enzyme.

Similarly to what was observed for thermodynamics, an electron-donating group should also increase the rate of carboxylation. To rationalize this second variable, we determined the initial reaction rates in the carboxylation of different phenols. A good linear correlation could be identified between the logarithms of the reaction rates and the Taft coefficients (Figure 2.1.15):

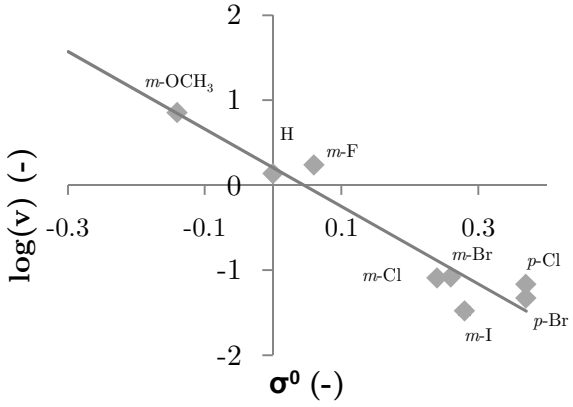

Figure 2.1.15: Correlation of the logarithm of the calculated $\log(v)$ with respect to the Taft constants σ^0 ($R^2 = 0.93$). Reaction conditions: substrate 10 mM, 30 mg mL^{-1} whole cells expressing Ao_DHBD (2.1 U mL^{-1}), in 3 M *KHCO₃*, at 30°C and 500 rpm.

The negative slope ($\rho = -4.5$) is expected for a mechanism involving a nucleophilic center. Significant deviations could be found for *meta*-methylphenol, *meta*-aminophenol and catechol. In particular, *meta*-aminophenol (*para* effect of the amino group on the reactive center) should have been the fastest in the chosen series because of its high electron donation. However, its conversion rate was ≈ 300 times lower than expected from the linear trend. Conversely, catechol (*meta*-effect of the OH group on the reactive center) was converted ≈ 200 times faster than expected, and was the fastest of the series. Even though the symmetry of catechol, which provides two different carboxylation positions available for catalysis, seems to be a reasonable explanation, its reactivity is about 8 times higher than that of phenol, as opposed to 2. For the amino-substituted phenol, a clue may come from docking simulations, where the top-ranking binding mode involves the coordination of the aspartate residue (Asp^{293}) to the amino group (Figure 2.1.16), rather than through the hydroxyl group, which is necessary for activation.

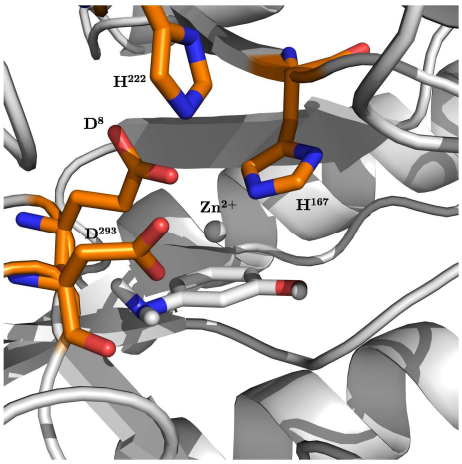

Figure 2.1.16: Docking of meta-aminophenol in the active site of the modelled Ao_DHBD. Visualization realized using Pymol.

The minor energy difference of 0.1 kcal mol^{-1} between the –NH_2 coordinating and the –OH coordinating conformations of may indicate non-selective binding.

As mentioned in the introduction, a so-called class I LFER shows the direct proportionality between equilibrium and rate constants of a certain reaction. Performing this analysis in our system, a different scenario was revealed (Figure 2.1.17).

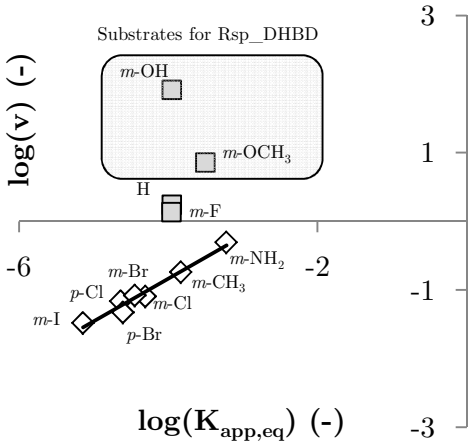

Figure 2.1.17: Class I LFER for the enzymatic *ortho*-carboxylation (R^2 = 0.97 for the linear regression).

It can be seen that seven phenols are directly correlated with each other (R^2 = 0.97), indicating that the substituents are influencing the two parameters in the same way. Interestingly, the four phenols H, –OH, –OCH_3, and –F do not fit on the linear regression and are also not correlated to each other. Such behaviors are known in literature when specific amino acids involved in stabilizing the transition states are

substituted (Fersht *et al.* 1986). Therefore, one of the explanations could be that, for these four phenols, diverse enzymes-substrate complexes are produced, resulting in significant rate increases. However, an explanation for catechol could derive from the establishment of an intramolecular hydrogen bond which would decrease the acidity of one phenolic group, consequently increasing its reactivity. Interestingly, catechol and *meta*-methoxyphenol are the only substrates included in this study that are also accepted by Rsp_DHBD[5]. Therefore, it could be speculated that the discrepancy in the substrate scope between the two enzymes is rather imputable to a lower efficiency of Rsp_DHDB, as only the substrates showing the highest reactivity are accepted (Figure 2.1.17). In fact, steric effects cannot explain the scope's differences (*e.g.*, the smaller phenol and *meta*-fluorophenol are not accepted by Rsp_DHBD). A comprehensive explanation for the observed differences and the outliers in the LFERs performed may come from the analysis of the interactions of the active sites with the phenolic substrates. Unfortunately, the structure of the Ao_DHBD is not yet solved and attempts to rationalize the empirical behaviors by molecular docking in a modeled active site – using Rsp_DHBD as the template – did not yield satisfactory explanations. Crystal data would provide a good basis for completing the evaluation.

Apart from the substrate promiscuity of the (de)carboxylases, a promiscuous hydrolytic activity was additionally discovered in this study. In fact, even though the realization of the homology model for the Ao_DHBD did not give any particularly useful insights in understanding the substrate scope, it revealed that this enzyme has a strong sequence homology with the *d*-metal-dependent amidohydrolase superfamily (EC 3.3.X.X), which catalyzes a diverse group of reactions, including C–C bond cleavages (Seibert & Raushel 2005). The creation of a phylogenetic tree depicts a strong evolutionary correlation of this enzyme group with Ao_DHBD and Rsp_DHBD (Figure A12). In particular, the active site of Rsp_DHBD shows strong resemblance with Zn^{2+}-dependent adenosine deaminases (Goto *et al.* 2006), which catalyze nucleophilic aromatic substitutions by activating the nucleophile via the metal center and a residue acting as general base (*e.g.*, glutamate). In order to find some catalytic basis for this similarity, we tested promiscuous hydrolytic activities using the purified Rsp_DHBD and we found out that the hydrolysis of *para*-nitrophenyl acetate could be hydrolyzed at significant rates (1 U mg^{-1}) (Figure

[5] *meta*-Methoxyphenol gives a steady-state conversion of only 15% with Rsp_DHBD, compared with a steady-state conversion of 50% using Ao_DHBD.

2.1.18(A)). Another lyase known to possess promiscuous hydrolytic activity towards activated esters is carbonic anhydrase (Lopez *et al.* 2011), which is also a Zn^{2+} metallo-protein. After comparing the mechanisms of cytosine deamination catalyzed by cytosine deaminase (Manta *et al.* 2014) and the hydrolytic activity of carbonic anhydrase, the mechanistic profile in Figure 2.1.18(B) is proposed.

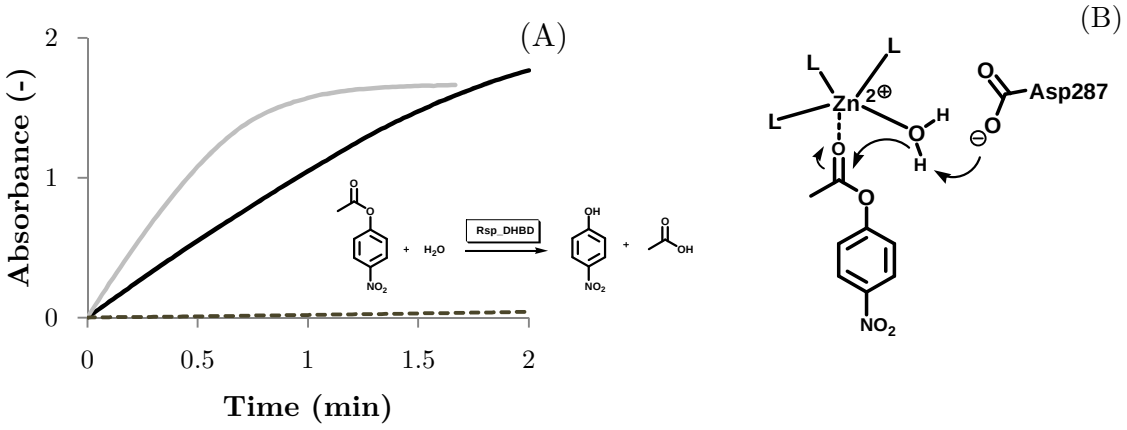

Figure 2.1.18: Promiscuous hydrolytic activity of Rsp_DHBD. A: hydrolysis of *para*-nitrophenyl acetate; dashed line: blank without enzyme, solid black line: assay with 0.75 mg mL^{-1} enzyme, solid grey line: assay with 1.5 mg mL^{-1} enzyme; reaction conditions: *para*-nitrophenyl acetate 1 mM, KP_i buffer 0.1 M, pH 7.0, room temperature; B: proposed substrates activation.

As for cytosine deaminase, water is coordinated with Zn^{2+} and additionally activated by a general base –in this case, Asp^{287-} [6]. As with carbonic anhydrase, the carbonyl coordination to the metal center activates the electrophile. The binding of uracile in cytosine deaminases also occurs by carbonyl coordination to the metal center (Manta *et al.* 2014).

In conclusion, this study points out that both chemical as well as biochemical factors are important determinants in describing the substrate spectra displayed by *ortho*-(de)carboxylases. The difference in reactivity seems to be a valid explanation for the remarkably distinct substrate promiscuity of Ao_DHBD and Rsp_DHBD. However, a comparison between the two crystal structures is mandatory to proceed with the study; this would likely allow us to answer other problems that remain unsolved, such as the non-reactivity of phenol derivatives containing *para*-electron donating substituents. The discovered reactions promiscuity points out a phenotypic as well as a functional similarity between these (de)carboxylases and the amidohydrolase superfamily. Further investigations in this direction may give insights into the biocatalytic determinants for nucleophilic/electrophilic aromatic

[6] A coordinated water molecule is also one metal ligand in Rsp_DHBD.

substitutions and hydrolytic reactions, potentially leading to the discovery of other promiscuous activities.

In conclusion:

- Initial reaction rates and steady-state conversions measured performing carboxylation reactions of different phenolic substrates catalyzed by Ao_DHBD were correlated with different chemical-physical parameters;
- Steady-state conversions showed negative correlations with Taft and Hammett electronic constants as well as with steric parameters (*e.g.*, Van der Waals volumes); the negative correlations with electronic parameters confirms that the reaction occurs by electrophilic aromatic substitution;
- The initial reaction rates showed a more complex behavior, suggesting that different activation modes are displayed by the enzyme depending on the phenolic substituent;
- The Rsp_DHBD displays a promiscuous hydrolytic activity towards an activated ester and a possible catalytic strategy was proposed.

2.1.4 CO_2 as (Indirect) Alternative Co-substrate via Amines Mediation

The ability to perform the biocatalytic carboxylation using (dissolved) CO_2 ($CO_{2(aq)}$) would be theoretically a great advantage for industrial applications, as conversions could be driven by pressure increase, such as in the Kolbe-Schmitt reaction. In literature, heterogeneous results for the behavior (de)carboxylases towards $CO_{2(aq)}$ are reported. We tested the possibility of using CO_2 for Rsp_DHBD under pressures of 50 and 80 bar. Using 80 bar would guarantee supercritical conditions ($scCO_2$) above 31°C, which showed to have significant impacts on the enzymatic carboxylation of pyrrole (Matsuda *et al.* 2001). The reactions were performed at 40°C because this would ensure the supercritical conditions in the technical apparatus used. As in the previous section was shown, the enzyme is indeed active at this temperature. Because CO_2 behaves as an acid in water, pH is a parameter that needs careful control. Although water pressurized with CO_2 at pressures greater than 30 bar has a pH of 3 at room temperature (Hofland *et al.* 2000), a decrease of only 0.5-1 pH units for both KP_i and bicarbonate buffers (0.2-1 M) pressurized with CO_2 was found. Hence, KP_i buffer (0.2 M, pH 8.0) was used to balance the pH decrease caused by

CO_2 dissolution in water. The results of catechol carboxylation are shown in Table 2.1.2:

Table 2.1.2: Carboxylation under carbon dioxide pressure. Reaction conditions: 10 mM catechol, 10 mM ascorbic acid, 0.5 mg mL^{-1} Rsp_DHBD in KP_i buffer 0.2 M pH 8.0, at 40°C and 500 rpm; CA = carbonic anhydrase (10 mg mL^{-1}). Reactions were run for 24 h.

CO_2 pressure (bar)	Max. conversion (%)
50	5
80	7
80, $KHCO_3$ (2M)	25
≈ 1*	2
50 + CA	5

* bubbling aeration

Close to the limits of accuracy, conversions of 5–7% were found at 50 and 80 bar, indicating no significant influence of the $CO_{2(aq)}$ concentration on the conversions. The supply of CO_2 by bubbling aeration afforded even lower conversions. According to data in the literature, the amount of dissolved CO_2 plateaus at a pressure of about 100 bar, which corresponds to a concentration of about 1.2 M; at 50 and 80 bar, the solubility of CO_2 is 0.87 and 1.1 M, respectively (Bamberger *et al.* 2000; Dodds *et al.* 1956). Taking the pH of the pressurized solution into account, the bicarbonate concentration can be estimated as 4 mM. This is considerably lower than the corresponding $KHCO_3$ concentration used at ambient conditions (0.1-3 M). Attempts to use carbonic anhydrase (CA) to achieve *ortho*-carboxylation with CO_2 were already reported and the inefficiency was interpreted as a consequence of enzyme inhibition by the phenolic substrate (Wuensch *et al.* 2012). However, by using CA just the time to reach the CO_2/HCO_3^- equilibrium would be shortened, resulting in a bicarbonate concentration too low to afford satisfactory conversions; Table 2.1.2 shows that even using 10 mg mL^{-1} of CA from bovine erythrocytes did not improve the conversions at 50 bar. Bicarbonate is the only effective species, as a conversion of 25% was achievable only in the presence of 2 M $KHCO_3$ under a gas pressure of 80 bar. These data underline that for Rsp_DHBD the co-substrate is bicarbonate rather than $CO_{2(aq)}$. From literature data, it seems that the ability to use CO_2 is strongly dependent on the enzyme type, even though enzymes involved in non-oxidative (de)carboxylations accept similar substrates and share a similar biological role. For instance, Mn^{2+}–dependent phenol carboxylase from *Thauera aromatica* catalyses the

para-carboxylation of phenylphosphate under a CO_2 atmosphere (1 bar) in the presence of 100 mM $NaHCO_3$ and 4 mM $MgCl_2$ with 90% yield (Aresta *et al.* 1998). The same enzyme also showed activity in $scCO_2$, albeit with a lower yield (5-10%) (Dibenedetto *et al.* 2006). Differently, metal-independent pyrrole-2-carboxylate decarboxylase from *B. megaterium* exhibited a higher reaction rate and conversion under CO_2 pressure (50 bar) in the presence of 3 M $KHCO_3$, with a bell-shaped curve for dependency on the pressure (Matsuda *et al.* 2001). However, it is very curious that the enzyme uses HCO_3^- as the reactive species[7] (Wieser *et al.* 1998). The behavior of Rsp_DHBD is similar to that of 2,6-DHBD from *Pandoraea* sp., where the conversion of resorcinol carboxylation decreased in the presence of $KHCO_3$ under supercritical CO_2 pressure[8] (Matsui *et al.* 2006). It follows, that the utilization of carbon dioxide in the *ortho*-carboxylation requires the establishment of a preliminary reaction which converts *in situ* carbon dioxide to bicarbonate. The conversions of acidic gases (*e.g.*, H_2S, COS and CO_2 itself) *via* reactions with alkanolamines (*e.g.*, ethanolamine, diethanolamine and N-methyldiethanolamine) are, since the 1950-1960s, established processes in the industry. In the case of CO_2, such processes are also known as "amine scrubbing", and are still of current research interest because of their environmental importance (Dutcher *et al.* 2015; Kaufhold *et al.* 2013). In aqueous media, the reactions of primary, secondary and tertiary amines lead to the formation of bicarbonates through different mechanisms. Therefore, these reactions seemed to be an ideal system to investigate in order to realize the *ortho*-carboxylation using gaseous CO_2 (Scheme 2.1.4).

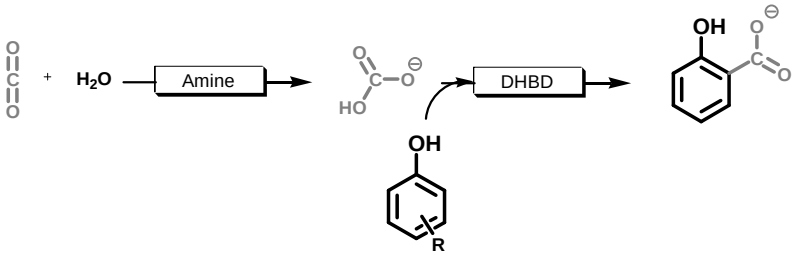

Scheme 2.1.4: Conversion of carbon dioxide to bicarbonate coupled with the biocatalytic carboxylation.

[7] The experiments under CO_2 pressure were realized using *Bacillus megaterium* whole cells, therefore the presence of other active enzymes cannot be ruled out.

[8] It is not clear whether or not and how the pH of the solution was controlled after pressurization with CO_2.

In general, the reactions of amines with carbon dioxide differ substantially in terms of mechanism, reaction rate and yield (usually discussed in terms of capacity in mol/mol). A brief overview on the different mechanisms is summarized in Scheme 2.1.5:

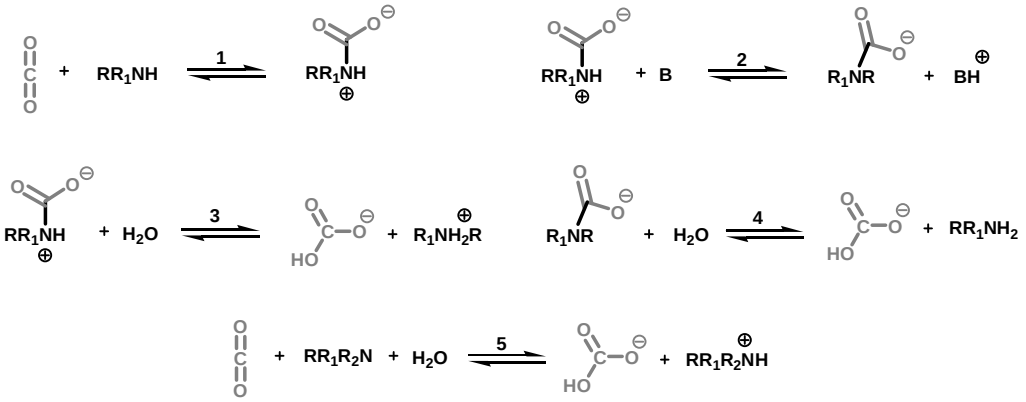

Scheme 2.1.5: *CO_2* conversion to bicarbonate for primary and secondary amines (reactions 1-4) and for tertiary amines (reaction 5).

In brief, primary and secondary amines react according to a zwitterion mechanism (Danckwerts 1979) where after the initial formation of a zwitterion, deprotonation by a base B (normally the amine itself) affords a carbamate (reactions **1** and **2**). Especially for sterically hindered amines, both zwitterion and carbamate can easily react with water, forming bicarbonate (reactions **3** and **4**) (Vaidya & Kenig 2007). Reaction **4** is particularly important because results in the regeneration of one amine molecule. An alternative termolecular mechanism has been also proposed (Crooks & Donnellan 1989; da Silva, Eirik F. & Svendsen 2004). Differently, tertiary amines are less likely to form carbamates (unless pH ≥ 12) and rather aid the hydration of carbon dioxide (Vaidya & Kenig 2007) (as carbonic anhydrase does) (reaction **5**). Brønsted relationships showed to be useful to rationalize the reactivities of different amine sub-groups (*e.g.*, primary and secondary amines, cyclic,…) (Khalili *et al.* 2012)(Singh *et al.* 2007, 2009). As a general reactivity trend, it is possible to state that: *i)* primary and secondary amines display higher reactivities than tertiary amines but lower than cyclic amines, *ii)* a higher hindrance of the substituents and the presence of α-carbons increase the yield, as well as the reactivity, *iii)* for hydroxyalkyl chains, the electron withdrawing effect of the –OH group is greater than the electron donation effect of the alkyl chain, *iv)* tertiary amines show normally higher capacity up to 1 mol/mol than primary and secondary ones (≈ 0.5 mol/mol) (Vaidya & Kenig 2007). Such trends are usually interpreted as

consequences of electronics, with respect to higher N-basicity, and sterics, with respect to higher carbamate instability.

Figure 2.1.19 shows the carboxylation of catechol conducted in the presence of CO_2 and 1 M triethylamine (TE) using Ao_DHBD as a biocatalyst. Surprisingly, the biocatalyst was able to catalyze the reaction more efficiently in the modified conditions, with a reaction rate almost five times higher and a steady-state conversion two times higher.

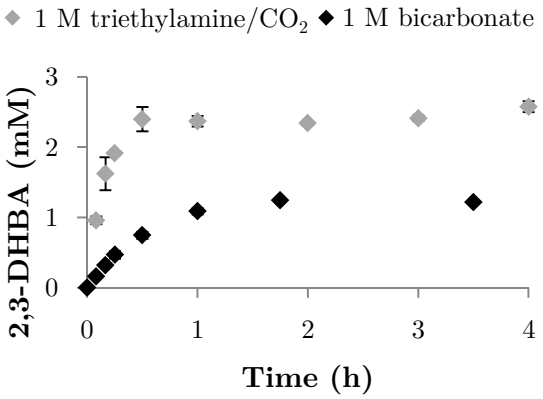

Figure 2.1.19: Biocatalytic carboxylation of catechol using bicarbonate (black diamonds) or CO_2/triethylamine (grey diamonds) as co-substrate; Reaction conditions: 10 mM catechol, 10 mM ascorbic acid, 3 mg mL^{-1} (2.3 U mL^{-1}) Ao_DHBD (whole cells) in KP_i buffer 0.1 M, pH 8.0, 1 M $KHCO_3$ or 1 M TE under CO_2 bubbling aeration 0.1 L min^{-1}, at 30°C and 500 rpm.

Carbon dioxide was supplied by bubbling aeration in the reaction solution through a needle. A 1 M aqueous TE solution (pK_a = 10.78 (Riddick *et al.* 1985)) in 0.1 M KP_i buffer pH 8.0 has a final pH of 11. In order to expose the catalyst exclusively to the pH value where the maximal activity is displayed, the aqueous solution containing the amine was pre-saturated with CO_2 for 1 hour prior to the reaction start. Such an experimental procedure allowed the establishment of a constant pH of ≈7.5, where bicarbonate is more than 90% of the whole carbon dioxide-derived species for the whole reaction time. Moreover, this method also allowed to exclude potential effects of the dissolution rate on the overall reaction kinetics. In Figure 2.1.11, it was demonstrated that, according to thermodynamics, the maximum conversion using 1 M potassium bicarbonate is approximately 14%. From the literature, it is known that the mol/mol capacity in amines scrubbing is less than 1 unless di- or tri-amines are involved (Singh *et al.* 2007, 2009). It follows that the bicarbonate concentration cannot exceed 1 M in the reaction. It can be concluded that, under the new experimental conditions, the amine or its counter cation exhibit a remarkably

positive effect on the reaction thermodynamics. Following these observations, a panel of different amines belonging to different "families" was screened under the same conditions (Table 2.1.3).

Table 2.1.3: Amines selected as mediators in the carboxylation reactions.

Name (abbreviation)	Structure	Family
Propylamine (PA)		Alkylamines (primary, secondary and tertiary)
Diethylamine (DE)	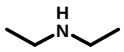	
Triethylamine (TE)	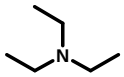	
Trimethylamine (TM)		
Ethanolamine (EA)		Alkanolamines (primary, secondary and tertiary)
Diethanolamine (DEA)	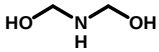	
Triethanolamine (TEA)	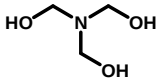	
Piperidine (PP)		Cyclic amines (secondary and tertiary)
N-methylpiperidine (MPP)	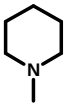	
1-(2-hydroxyethyl)- piperidine (HEP)	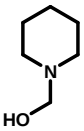	

Figure 2.1.20 shows the initial reaction rates and maximal conversions for catechol carboxylation for each amine mediator. In all cases, the pre-saturation step with CO_2 shifted the pH from 11-12 of the 1 M amine solution in buffer to approximately 7.5, which was maintained for the total duration of the reaction (Figure A13).

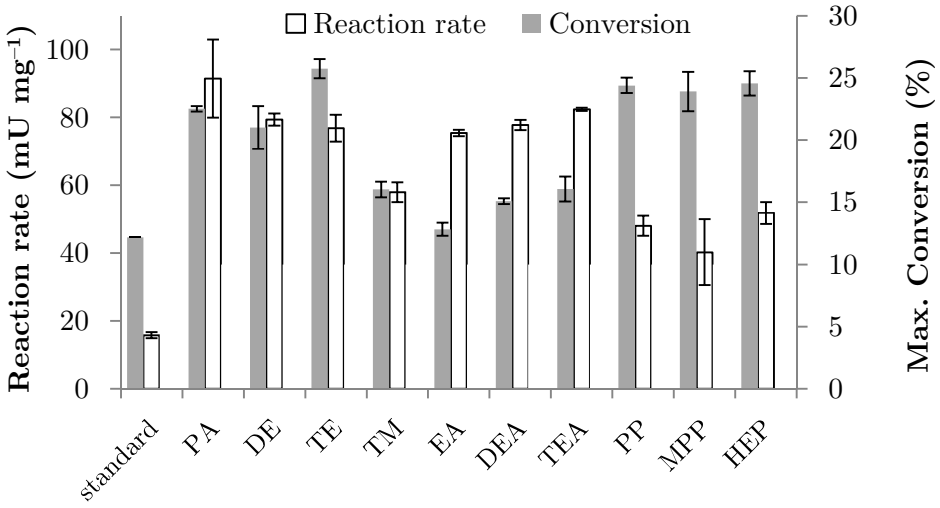

Figure 2.1.20: Biocatalytic carboxylation of catechol using CO_2/amines; Grey bars: max. conversion; white bars: initial reaction rate; Reaction conditions: 10 mM catechol, 10 mM ascorbic acid, 3 mg mL^{-1} (2.3 U mL^{-1}) Ao_DHBD (whole cells) in KP_i buffer 0.1 M, pH 8.0, 1 M amine, CO_2 bubbling aeration 0.1 L min^{-1}, at 30°C and 500 rpm.

The use of pyrrole, 1-methylpyrrole, tributylamine and aniline did not afford any conversion probably because of their low solubility in water. Interestingly, the catalytic enhancement as well as the conversion enhancement is quite general for all of the amines in Table 2.1.3, although in a quite heterogeneous way.

Regarding the maximum conversions, it can be observed that alkylamines generally perform superiorly, which could be attributable to the higher capacity of CO_2 "sequestration" due to the electron donation to the N atom effected by the alkyl chains. Moreover, a higher degree of substitution of primary and secondary amines seems to be beneficial to the conversion; this behavior can be explained when considering higher instability of the resulting carbamates (compare with Scheme 2.1.5, reactions **3** and **4**). The possibility that a different carbonate species behaves as co-substrate (*i.e.*, the zwitterion or the carbamate in Scheme 2.1.5) can be ruled out, as this would not explain the enhancement observed for tertiary amines. To evaluate the influence of carbon dioxide aeration during the whole reaction time, a series of experiments in which the co-substrate was supplied only during the pre-saturation step were conducted. The results are shown in Figure 2.1.21.

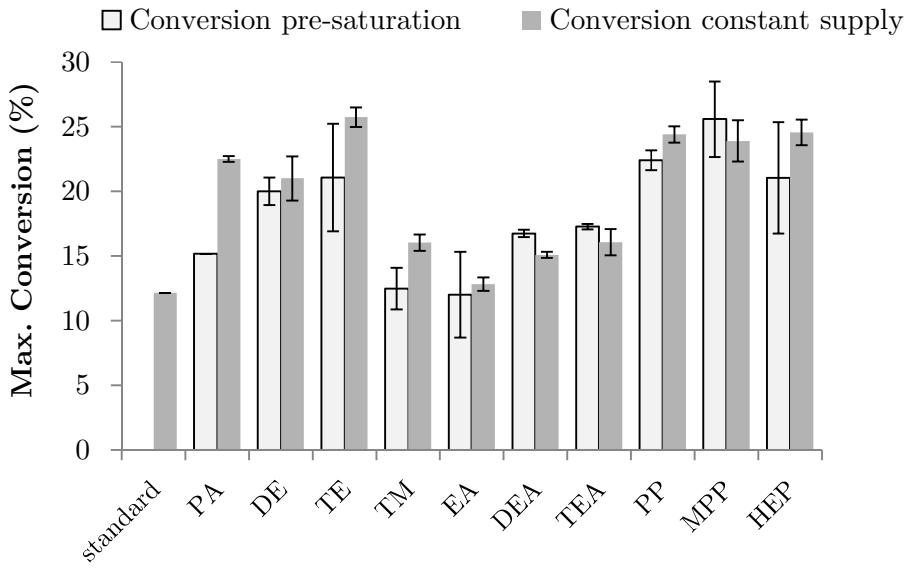

Figure 2.1.21: Biocatalytic carboxylation of catechol using CO_2/amines; dark grey bars: continuous CO_2 supply (from Figure 2.1.20); light grey bars: CO_2 supplied only in the 1 h pre-saturation phase; Reaction conditions: 10 mM catechol, 10 mM ascorbic acid, 3 mg mL^{-1} (2.3 U mL^{-1}) Ao_DHBD (whole cells) in KP_i buffer 0.1 M, pH 8.0, 1 M amine, CO_2 bubbling aeration 0.1 L min^{-1}, at 30°C and 500 rpm.

It can be observed that the conversions do not significantly differ in most cases, suggesting that the pre-formation of the ammonium salts is most responsible for the enhancements with respect to potassium bicarbonate and highlighting a direction for possible process optimization.

The reaction of amines with carbon dioxide is a reversible stoichiometric reaction. Therefore, we would expect that higher bicarbonate concentrations could be ensured simply by changing the amine concentrations. Figure 2.1.22 shows that the enhancement in conversion does occur for TE concentrations between 0.5 and 2 M, while no conversion could be observed at 3 M, even after 24 h of incubation, indicating that such a high concentration of TE causes enzyme deactivation. It is important to note that the conversion enhancement with respect to $KHCO_3$ holds true at every amine concentration tolerated by the enzyme.

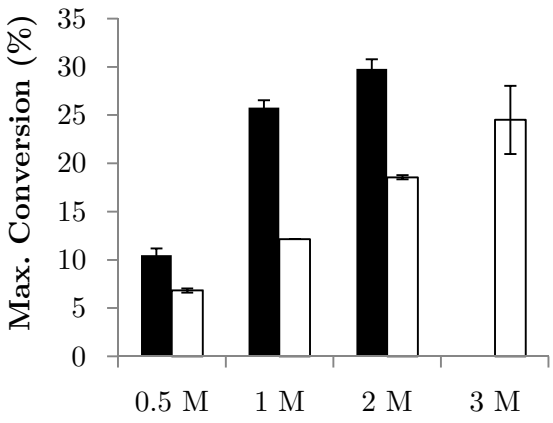

Figure 2.1.22: Biocatalytic carboxylation of catechol using different $KHCO_3$ (white bars) or TE (black bars) concentrations; Reaction conditions: 10 mM catechol, 10 mM ascorbic acid, 3 mg mL^{-1} (2.3 U mL^{-1}) Ao_DHBD (whole cells) in KP_i buffer 0.1 M, pH 8.0, $KHCO_3$ or TE/CO_2 bubbling aeration 0.1 L min^{-1}, at 30°C and 500 rpm.

In order to study the effect of pressure and possibly higher bicarbonate concentrations, the reaction was also performed with CO_2 at 50 bar using selected amines. A very low reproducibility of the results, up to 100% standard deviation, was observed. This can be explained by the reversibility of both chemical (*i.e.*, bicarbonate formation) and biochemical (*i.e.*, carboxylation) reactions. In fact, the pressure release after the incubation time would cause a decrease in CO_2 concentration and therefore shift the reaction equilibrium towards the side of the starting materials. The irreproducible release, cooling and sampling times would justify the discrepancy in the carboxylation's results. In order to prevent the reversibility of the biocatalytic reaction, the vessel was heated to 90°C for 5 minutes before releasing pressure. The modified overheating protocol allowed highly reproducible results (Figure 2.1.23).

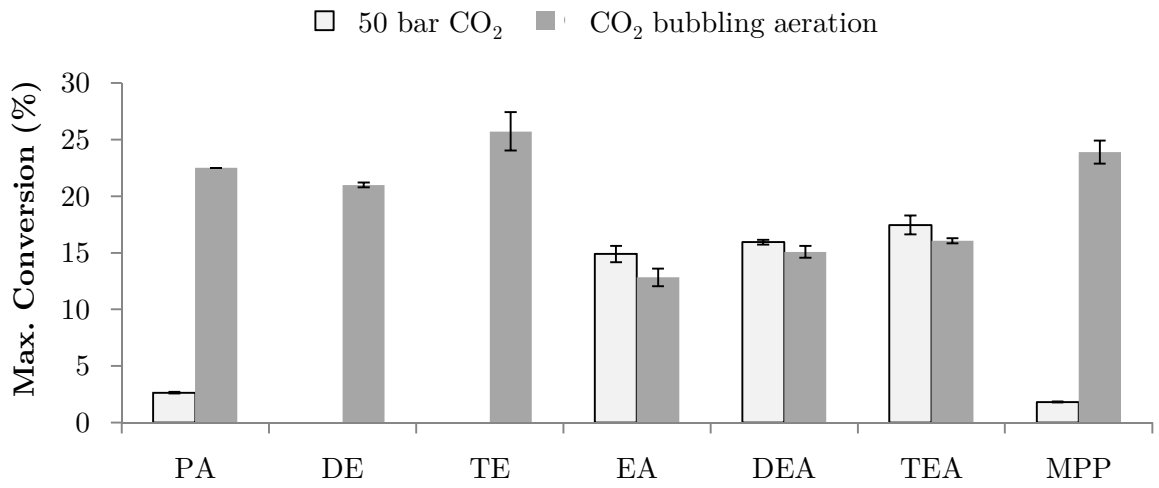

Figure 2.1.23: Biocatalytic carboxylation of catechol using CO_2/amines under a carbon dioxide pressure of 50 bar; Reaction conditions: 10 mM catechol, 10 mM ascorbic acid, 3 mg mL^{-1} (2.3 U mL^{-1}) Ao_DHBD (whole cells) in KP_i buffer 0.1 M, pH 8.0, 1 M amine and 50 bar CO_2, at 30°C and 500 rpm. Reactions were run for 24h.

A different interfacial areas in the experimental set-up under pressure and under bubbling aeration would affect the overall reaction rate due to a different time to reach the equilibration of carbon dioxide. Literature data regarding the study of carbon dioxide equilibration in aqueous solutions under pressure, in set-ups that are similar to the one reported in this thesis, show that 12 hours is the largest time needed (10 mL autoclave) (Wen & Olesik 2000), while in other cases 60 minutes (magnetically stirred 100 mL autoclave) (Ferrentino *et al.* 2016) and 5 minutes (mechanically stirred 100 mL autoclave) (Garcia-Gonzalez *et al.* 2010) are needed. Hence, it is reasonable to assume that 24 hours as the overall reaction time is sufficient to ensure carbon dioxide and reaction equilibration. Figure 2.1.23 shows that alkanolamines afforded slightly higher conversions under pressure. The differences can be rationalized with the establishment of higher concentrations of bicarbonate due to higher solubility of CO_2 at high pressures. However, the differences are very subtle. Alkylamines were not efficient under pressure. Such a discrepancy with the bubbling aeration protocol is imputable to the modified operational procedure that was used. In fact, while the biocatalyst in the experiments at ambient conditions was added at slightly basic pH (after the pre-saturation with CO_2), in the pressure experiments the vessel had to be pressurized on the biocatalyst/amine aqueous mixture (pH 10-12). Therefore, the difference is ascribable to enzyme deactivation occurring in the 10-20 minutes necessary for the preparation

of the set-up. In order clarify this behavior, we performed a biotransformation using bubbling aeration and 1 M trimethylamine without the pre-saturation step; a conversion of only 10% was obtained after 24 h, pointing towards enzyme deactivation.

The increases in conversion observed in the CO_2/amine systems both at ambient and high pressure are not easy to rationalize, especially because of a lack of fundamental information about such reaction system. The use of different bicarbonate salts for the *ortho*-carboxylation of resorcinol using Rsp_DHBD has been already described in the literature (Wuensch *et al.* 2013b). A subtle conversion increase for resorcinol carboxylation was reported for trimethylammonium bicarbonate, which resembles our results in Figure 2.1.20. The authors correlated the results obtained with different counter cations to the Hofmeister series, for which chaotropic cations (*e.g.*, lithium and guanidinium) afforded significantly lower conversions than cosmotropic ones (*e.g.*, potassium or tetramethylammonium). In our results, the conversion difference with respect to the standard protocol using potassium bicarbonate is significantly higher. Therefore, the reason must be related to a different energy balance between the product and starting materials in the reaction media.

Three other phenolic compounds were investigated under similar conditions using the amines producing the best results in order to verify the generality of the approach and to be able to gain more knowledge about the influence of the substrate on rate and conversion increases. *meta*-Aminophenol and *meta*-methoxyphenol were subjected to the carboxylation reaction using 1 M propylamine (PA) and continuous carbon dioxide supply by bubbling aeration, and the results were compared with reactions using 1 M $KHCO_3$. Interestingly, both transformations showed approximately the same conversions, 24% for *meta*-aminophenol and 27% for *meta*-methoxyphenol, either using potassium bicarbonate or PA/CO_2 (≈ 3% higher in the amine system). The case of *meta*-methoxyphenol was investigated in more detail; the conversion using diethylamine (DE) and trimethylamine (TM) were as high as in the other conditions. The carboxylation of phenol was also performed using 1 M $KHCO_3$ and 1 M TM/CO_2. Both conditions showed comparable conversions of 11-14 %, about 3% higher in the amine system. These results strongly suggest that the thermodynamic boost observed in the amine/CO_2 system is substrate-specific and reasonably related to specific interactions between the di-phenol moiety and the ammonium cations. Literature shows that ammonium and alkylammonium ions can

interact with aromatic molecules in a variety of ways, which are both qualitatively and quantitatively diverse (Rodríguez-Sanz *et al.* 2013; Zhu *et al.* 2000). Phenol can undergo cation-π interactions as well as cation-OH hydrogen bonding, with an enthalpy difference of –6 kcal mol^{-1} in favor to the hydrogen bonding interaction (Rodríguez-Sanz *et al.* 2013). The decrease in relative free energy of the carboxylated product with respect to catechol due to the formation of a hydrogen bond network would be able to explain our results. However, obtaining crystal structures together with computing the complex formation in solution are necessary to validate these hypotheses. With respect to the kinetic behavior represented in Figure 2.1.20, it is fundamental to separate the influence of the amines and their protonated forms on the enzyme catalysis from the kinetics of carbon dioxide conversion to bicarbonate. Through the use of inline Fourier Transform-Infrared (FT-IR) spectroscopy it could be observed qualitatively that the conversion of CO_2 was complete during the 1 hour pre-saturation step (Figure A15). Bicarbonate can, in fact, be detected following the signal increase at around 1350 cm^{-1}, corresponding to its C–O–H in-plane bending; for all of the amines tested, no appreciable changes of the signal could be observed after 40 min–1 h aeration (Figure A15). Reaction times of the same order of magnitude in similar reaction conditions were already reported in the literature (Singh *et al.* 2007, 2009). This suggests that the kinetics of the carboxylations is mostly determined by the interactions of the amines or of the resulting ammonium ions with the biocatalyst. Support for this finding also comes from the comparison of the total reaction progress using the two supply methods described when discussing Figure 2.1.21. As the example in Figure A14 shows, no significant differences can be observed in terms of reaction rates. Attempts to correlate the initial rates with the pK_a of the amines failed. On the other hand, looking at the different polarity of the amines, quantified by their *logP* (taken from Sangster 1989), many cases show that a higher hydrophobicity results in lower reaction rates (Figure 2.1.24).

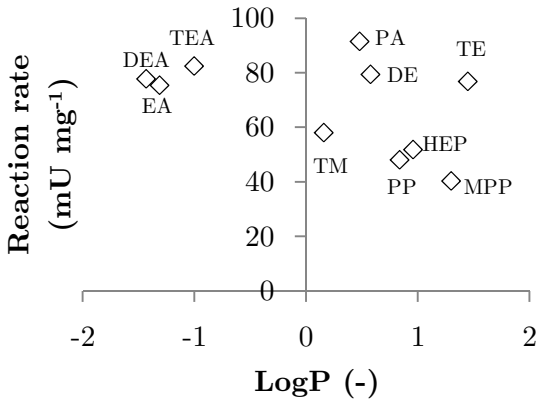

Figure 2.1.24: Correlation of the initial reaction rate for catechol carboxylation with the *logP* of the amine mediators.

Notable exceptions are the alkylamines PA, DE and TM; with the exception of these 3 amines, the other 7 show a linear correlation with $R^2 = 0.93$. As it has been already discussed, it can be assumed that the conversion of carbon dioxide reached the equilibrium at the start of each reaction; therefore, the reason behind the rate differences have to be searched in the molecular interactions between the enzyme and the amines. Figure 2.1.24 may suggest that for a group of amines a higher polarity corresponds to a higher rate. However, more data about the specific enzyme-amine interactions have to be acquired to draw any general conclusions.

To verify the generality of the behavior and to understand if the faster rates are due to specific interactions of the substrate with the ammonium ions at the active site, reaction progresses were also performed for the carboxylation of *meta*-methoxyphenol using PA, DE and TM. Figure 2.1.25 shows that the initial reaction rates in the newly established reaction media are comparable to each other and only slightly lower when compared with the standard potassium bicarbonate medium.

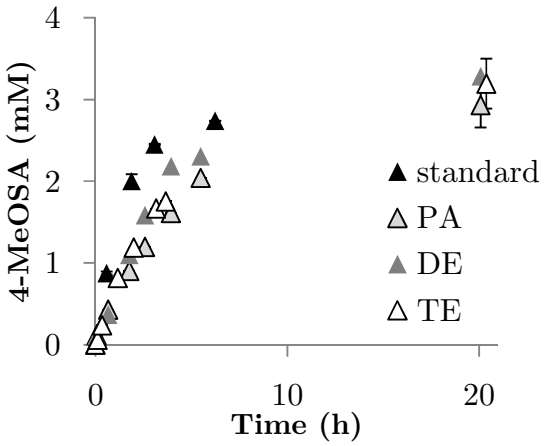

Figure 2.1.25: Biocatalytic carboxylation of *meta*-methoxyphenol using CO_2/amines; Reaction conditions: 10 mM catechol, 10 mM ascorbic acid, 3 mg mL^{-1} (2.3 U mL^{-1}) Ao_DHBD (whole cells) in KP_i buffer 0.1 M, pH 8.0, 1 M amine and CO_2 bubbling aeration 0.1 L min^{-1}, at 30°C and 500 rpm.

The simplest phenol, which was also subjected to carboxylation in potassium bicarbonate and in TM/CO_2, also showed no significant differences in initial rates.

A more challenging reverse decarboxylation reaction due to the formation of a complex between 2,3-DHBA (product of catechol carboxylation) and the alkylammonium ions would justify the increase in reaction rates observed with catechol. Therefore, it was expected that, by performing decarboxylation kinetics on 2,3-DHBA, different catalytic efficiencies could be measured when running the assays in potassium phosphate buffer or in alkylammonium phosphate buffer. On the other hand, since almost no kinetic differences were observed in the carboxylation of *meta*-methoxyphenol, it was speculated that the same kinetic efficiencies in the decarboxylation of *para*-methoxysalicylic (4MeOSA) acid would be observed with the two phosphate buffers. Tables 2.1.4 and 2.1.5 show the kinetic parameters for the decarboxylation of 2,3-DHBA and 4-MeOSA in different reaction media.

Table 2.1.4: Catalytic constants for 2,3-DHBA decarboxylation in different reaction media. Reaction conditions: 0-2 mM 2,3-DHBA, 0.015 U mL^{-1} (8.8 mg mL^{-1}) CFE containing 2,3-DHBD from *A. oryzae* in 0.1 M P_i buffers, pH 8.0. Non-linear fit (black line) were performed with Microsoft Excel.

Buffer	K_M **(mM)**	V_{max} **(µmol min^{-1} mg^{-1})**	$V_{max}\,K_M^{-1}$ **(mL min^{-1} mg^{-1})**
KP_i 0.1 M	0.36 ± 0.17	3.5 ± 0.4	11 ± 4
KP_i 1 M	0.26 ± 0.08	2.5 ± 0.2	10 ± 2
TEP_i 0.1 M	0.3 ± 0.01	3.5 ± 0.01	11 ± 0.5
TEP_i 1 M	0.57 ± 0.03	2.7 ± 0.1	5 ± 0.1

Table 2.1.5: Catalytic constants for 4-MeOSA decarboxylation in different reaction media. Reaction conditions: 0-3 mM 4-MeOSA, 0.15 U mL^{-1} (59 mg mL^{-1}) CFE containing 2,3-DHBD from *A. oryzae* in 0.1 M P_i buffers, pH 8.0. Non-linear fit (black line) were performed with Microsoft Excel.

Buffer	K_M **(mM)**	V_{max} **(nmol min^{-1} mg^{-1})**	$V_{max}\,K_M^{-1}$ **(nL min^{-1} μg^{-1})**
KP_i 1 M	1.8 ± 0.5	1.2 ± 0.2	0.7 ± 0.1
TEP_i 1 M	6.4 ± 1.5	1 ± 0.2	0.15 ± 0.005

Even though the activity towards 4MeOSA is significantly lower, looking at the V_{max}/K_M ratios, it is possible to see that, for both compounds, the decarboxylation is least efficient in triethylammonium phosphate buffer. This fact indicates that the reason for catalytic enhancement in the case of catechol lies in the specific interactions between the phenolic substrate and the alkylammonium ions at the active site of the (de)carboxylase. The effects of monovalent cations (M^+) on enzyme activity have been extensively studied in the literature. Unlike divalent M^{2+}, which are directly involved in catalysis, M^+ are usually involved in stabilizing enzyme structure and the catalytic intermediates, and in aiding correct substrate positioning (Page & Di Cera 2006). The difference between the two metal types is also a clear consequence of the different charge densities. In many cases, the selectivity for a certain M^+ is not high and the activity increases in the presence of the larger K^+, NH_4^+, Cs^+ ions. The M^+ preferences are normally described by invoking the salting in/out properties of the Hofmeister series. However, it is important to remember that every protein has its own features and that it is very difficult to draw general conclusions. For example, kinases normally require K^+ as an activator, and the similar NH_4^+ and Rb^+ display activation as well, in contrast to smaller (*e.g.*, Li^+) and bigger (*e.g.*, Cs^+) cations (Page & Di Cera 2006). Another very detailed experimental/computational study on the M^+ specificity of a haloalkane dehalogenase shows a very weak preference towards Cs^+. The poor differentiation between the cations was explained as a consequence of limited access to the active site (Štěpánková *et al.* 2013). In this study, a general enzyme activation due to enzyme-alkylammonium ion interactions can be ruled out because the effect is revealed only using catechol as substrate. It follows that a specific interaction must occur between catechol and the ammonium ions at the active site; Figure 2.1.26 depicts a possibility by which such activation could occur.

Figure 2.1.26: Proposed interactions of catechol (left) and phenol (right) in the presence of alkylammonium ions (primary, secondary or tertiary); the grey frame represents the binding site for the alkylammonium ions.

As already discussed in the previous section about LFERs, the highest reactivity of catechol can be justified through the increased acidity of the phenolic group due to an intramolecular hydrogen bond. The interaction of the ammonium ion with the second hydroxyl group would establish a hydrogen bond network that facilitates the most effective orientation of the two hydroxyl groups while stabilizing the negative charge that develops. In order to validate this model, the resolution of the enzyme's crystal structures containing the two ligands is necessary.

In conclusion:

- Carboxylation experiments conducting using carbon dioxide in various reaction conditions point out that bicarbonate is the effective co-substrate;
- The formation of bicarbonate *in situ* by the combination of dissolved carbon dioxide and primary, secondary or tertiary amines can be used as an alternative co-substrate;
- When catechol is used as the substrate, a higher reaction rate and equilibrium conversion were measured in the newly developed reaction conditions, while when other phenolics are used, no appreciable differences can be observed with respect to the standard conditions using the sole potassium bicarbonate;
- The analyses of the decarboxylation kinetics of 2,3-dihydroxybenzoic acid and 4-methoxybenzoic acid in potassium and trialkylammonium phosphate buffers suggest that the reason for the enhanced catalytic activity in the case of catechol carboxylation lies on the specific interactions between the phenolic substrate and the alkylammonium ions in the active site.

2.2 Applications: Overcoming the Thermodynamic Barrier

The previous sections of this study showed that the enzymatic *ortho*-carboxylation suffers from both thermodynamic and kinetic limitations ($K_{eq} \approx 10^{-4}$ and $k_{cat} \approx 0.1$ s^{-1} for catechol with Rsp_DHBD). These intrinsic characteristics of the system appear to be, to some extents, less severe for electron-rich aromatics (*e.g.*, *meta*-methoxyphenol). Due to the unfavorable equilibria and substrate deactivation, an approximately 300 molar excess of the co-substrate (bicarbonate salts) needs to be used to achieve conversions which, in most of the cases, are less than or equal to 30%. When assessing the environmental balance of the reaction (*e.g.*, such as determining the E-factor (Sheldon 2007)), a copious amount of unreacted salt will have to be included in the calculation and regarded as waste. The only solution for aiming at a more efficient biochemical Kolbe-Schmitt reaction is to investigate reaction engineering strategies which would afford higher conversions with lower co-substrate loadings. Considering the functional groups of product and starting material, a collection of strategies to push/pull the equilibrium of the enzymatic carboxylation are summarized in Table 2.2.1. The feasibility of each strategy will be discussed in this chapter.

Table 2.2.1: Reaction engineering methods investigated for enzymatic *ortho*-carboxylation.

Strategy	Approach	Principle	Possible limitation
In situ product removal	Adsorption on ion exchangers	Selective adsorption of the product	Low selectivity
	Extraction of the alkylammonium carboxylate	Selective extraction in a second organic phase	Low selectivity/activity of the biocatalyst
Medium engineering	Use of co-solvents	Change of the thermodynamic balance	Unfavorable thermodynamics/activity of the catalyst
Follow up reaction	Reduction of the carboxylic acid	Pull of the reaction equilibrium	Low activity of the catalyst and compatibility

In general, it is worth mentioning that a realistic process based on this biotransformation should be easy and cheap; this is a consequence of the fact that the chemical counterpart is a simple and established method requiring the heating of

the starting material using pressurized carbon dioxide. Moreover, as a consequence of the aforementioned points, salicylic acids are relatively cheap bulk products.[9]

2.2.1 Adsorption on Ion-Exchangers

In situ product removal represents a tool of enormous value for biotechnological processes, either based on enzymes, resting cells, or fermentation (Lye & Woodley 1999). It is possible to state that, in most cases, this is due to the typical occurrence in such processes of product inhibition/toxicity and often of an unfavorable thermodynamic equilibrium. The design of an *in situ* product removal strategy requires the analysis of the target molecules' properties in the given reaction medium and, more importantly, by which characteristics it differs from starting materials and reactions additives (Freeman *et al.* 1993). The sole chemical feature that can be exploited to selectively remove the product in our reaction system is obviously the carboxylic functionality. Salicylic acids generally show pK_a around 3, resulting in an almost complete deprotonation at the reaction pH of about 8.0. The reaction medium where the carboxylation takes place must also be regarded. In fact, the need of –excess– bicarbonate as co-substrate has as consequences: *i)* the necessity of an aqueous medium, *ii)* the setting of the pH value at around 8.0, and *iii)* the presence of an excess of negatively charged ions chemically resembling the newly introduced functionality of the product. Attempts to achieve selective product removal were performed using adsorption on ion exchangers and extraction of product/tetraalkylammonium ion pairs in a second organic phase. However, as it will be shown, the intrinsic properties of the medium, in addition to the similarities between the phenolic substrate and its product (aromatic ring and phenolic group) make both strategies infeasible for applications because of lack of selectivity.

The adsorption of carboxylic acids on ion scavengers is based on the establishment of ionic interactions between the carboxylate functional group and an ammonium group present on a polymeric matrix, typically based on polyacrylate, polystyrene or silica. Two major types of anion exchangers can be distinguished: weak and strong. Scheme 2.2.1 shows the working principle of both resins towards carboxylic acids.

[9] The price strongly varies depending on the specific salicylic acid derivative. For example, simple salicylic acid has a cost of ≈ 0.05 € g^{-1}, while 4-fluorosalicylic acid has a cost of ≈ 20 € g^{-1} (gram-scale, Alfa Aesar, June 2016).

Scheme 2.2.1: Working principles of weak (left) and strong (right) anion exchangers.

Weak anion exchangers are based on a tertiary amino group which, upon protonation by a carboxylic acid, is able to establish electrostatic interactions with the formed carboxylate. Consequently, these adsorbers work at acidic pH, where the acid is partially protonated (Zhou *et al.* 2011). Moreover, anions such as bicarbonate will not be adsorbed. Both acrylate- and styrene-based weak anion exchangers (the commercially available Amberlite IRA67® and Dianion WA30®, respectively) were tested for the adsorption of catechol and 2,3-DHBA. As expected, the adsorption of 5 mM product on 100 mg of adsorber in 1 mL volume was complete after approximately 30 minutes of incubation at pH 5.5, while at pH 8.0, the condition of carboxylation, the adsorption only reached 60%. At both pH values, catechol was completely adsorbed and even faster than 2,3-DHBA at pH 8.0 (see Figure A16 for both reaction time plots). This is clearly a consequence of the adsorption of the hydrophobic compound on the polymeric matrixes, which were studied in detail in the literature, as they are effective for the removal of phenolic compounds from wastewaters (Hararah *et al.* 2010). Competition can also occur by hydrogen bonding of the phenolic groups to the amino group acceptor (Zhen-mao *et al.* 2007). Strong anion exchangers, on the other hand, are based on quaternary ammonium functionalities. Consequently, they are effective at all pH values. For the same reason, they adsorb bicarbonate as well. Also in this case, the competitive adsorption of catechol on the polyacrylate or polystyrenic matrix (Amberlyst A26® and Amberlite IRA958®, respectively) constitutes a major problem; the selectivity, as well as the capacity, are also influenced by the concentration of bicarbonate, which competes for the electrostatic interactions. The adsorption of 2,3-DHBA is almost five times lower at 2 M bicarbonate than at 0.2 M, while the adsorption of catechol is approximately 50% for all bicarbonate concentrations (Figure A17). In conclusion, the hydrophobicity of the aromatic ring represents the biggest challenge for selective product removal. The use of a hydrophilic matrix as an alternative to a hydrophobic one could be a valid solution to achieve higher selectivity towards products adsorption. Silica-based strong anion exchangers are also commercially available and

were tested for selective adsorption in bicarbonate as well as in organic solvent, where they are supposed to show the best selectivity (SiliabondTMA®, Figure 2.2.1).

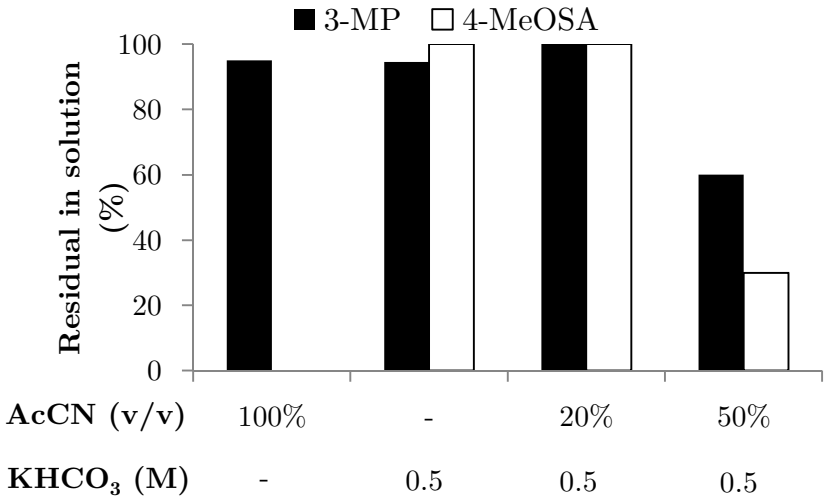

Figure 2.2.1: Adsorption of *meta*-methoxyphenol and 4-methoxybenzoic acid on strong anion exchanger (SiliabondTMA®, silica based); Reaction conditions: 10 mM *meta*-methoxyphenol/4-methoxybenzoic acid, 50 mg adsorber in 1 mL acetonitrile (AcCN) or 0.5 M $KHCO_3$, at 30°C and 500 rpm. Percents reported refers to the v/v % of acetonitrile used as co-solvent.

No adsorption was observed for either the substrate or product in the aqueous bicarbonate, which is reasonable because of the competition of the inorganic ions even at 0.5 M. As shown in Figure 2.2.1, a good selectivity was achieved in acetonitrile. The addition of 20-50% acetonitrile in aqueous bicarbonate did not improve the selectivity. Despite these results, such a technique would be useful for downstream processing because the co-substrate bicarbonate is not soluble in organic solvents. In conclusion, the property of the reaction medium and the hydrophobic features of the phenolic substrate make an *in situ* product removal strategy by adsorption impractical for applications. Table 2.2.2 summarizes the strategies attempted and the outcomes.

Table 2.2.2: Summary of adsorption´s selectivity studies for the biocatalytic carboxylation.

Anion exchanger	Matrix type	Notes
Weak base	Polyacrylate Polystyrene	Reaction pH limits product adsorption Competition of the substrate
Strong base	Polyacrylate Polystyrene	Competition of substrate and co-substrate
	Silica	Competition of the co-substrate Good selectivity in organic solvent

2.2.2 Extraction in Organic Solvent

Reactive extraction is a known method applied in fermentation technology when producing carboxylic acids (Hong *et al.* 2001; Wasewar 2012). The working principle is similar to what was discussed regarding the adsorption of carboxylic acids using a weak base anion exchanger. In brief, a long chain alkylamine solution in a so-called "diluent" is used to extract the acid, which is present in an aqueous solution at acidic pH, by formation of an ammonium-carboxylate *via* acid-base reaction. This is extracted from the aqueous in the organic phase. Processes based on this principle are implemented commercially, such as for the recovery of citric acid from fermentation broth using trioctylamine in a mixture of 1-octanol and hydrocarbons (Hong *et al.* 2001). "Diluents" used for reactive extraction are classified as active or inactive. Active diluents, such as halogenated solvents, show high solvation capacities towards the carboxylate-ion pairs, while inactive diluents, such as linear hydrocarbons, are used for the regeneration, where the chemical extractor is recycled for a new extraction step. As already mentioned while discussing the weak-base adsorption, an acidic pH cannot be used in the carboxylation conditions. Therefore, the possible extraction of the salicylic acid derivatives has to occur using tetraalkylammonium ions. For this purpose, the possibility to perform the reaction in 2 liquid-phase systems (2LPS) in the presence of tetrabutylammonium chloride in the aqueous phase was studied, which was meant to aid the selective extraction of the product in the organic phase. Preliminary experiments conducted on *meta*-methoxyphenol and its carboxylation product showed that 96-99% of 4-methoxysalicylic acid could be extracted from the aqueous phase in dichloromethane (DCM) when mixed with tetrabutylammonium chloride (TBACl, molar ratio acid/amine 1:1-18:1). However, the substrate *meta*-methoxyphenol was also almost completely extracted in the same conditions, indicating the establishment of interactions with the phenolic group as well (Figure A18). Similar trends were observed using catechol and 2,3-DHBA. In order to evaluate different solvents for extraction, catechol/2,3-DHBA were subjected to the 2LPS conditions using a 1:1 ammonium/phenolic molar ratio. At the same time, the possibility for the (de)carboxylase to work in the presence of a water immiscible organic phase (20-60 v/v %) was also verified using whole cells and crude extracts. In terms of the carboxylation reaction, conversions as high as those in the simpler aqueous system were obtained using n-heptane, while solvents with higher polarity showed inferior performances (Figure 2.2.2).

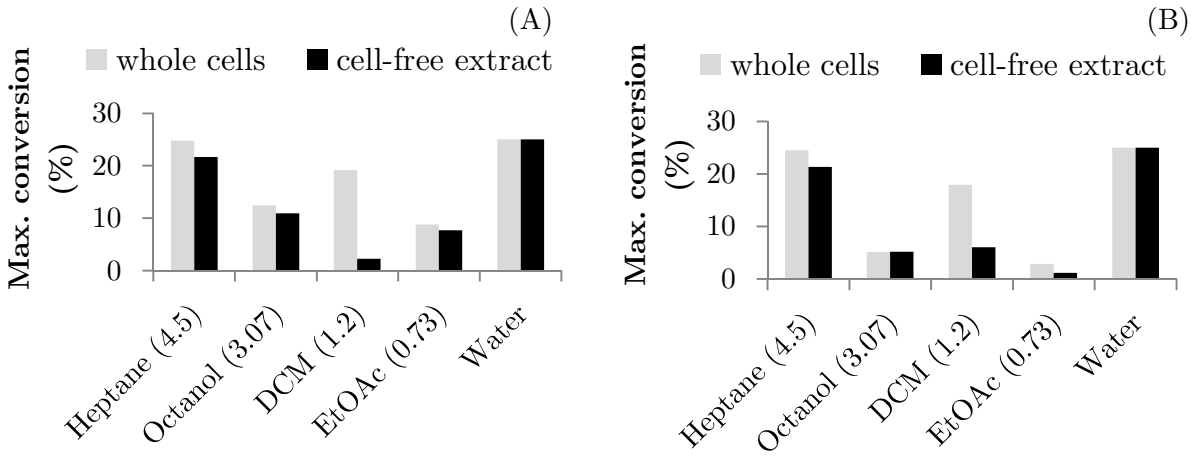

Figure 2.2.2: Carboxylation of catechol in 2LPS using 20% (A) or 60% (B) of organic phase (*logP* are indicated in parentheses); Reaction conditions: 10 mM catechol, 10 mM ascorbic acid, 2 M $KHCO_3$, Rsp_DHDB as biocatalyst either as whole cells (30 mg mL^{-1}) or CFE (80 µL), at 30°C and 500 rpm.

An interesting exception is the case of DCM using whole cells as biocatalyst, where the cell "wrapping" may behave as protective layer. The low conversions with the other solvent types are likely consequent of enzyme stability in combination with substrate unavailability due to extraction, even though details about this differentiation were not investigated. The influence of TBACl on the extraction of both components is shown in terms of partition coefficients in Figure 2.2.3.

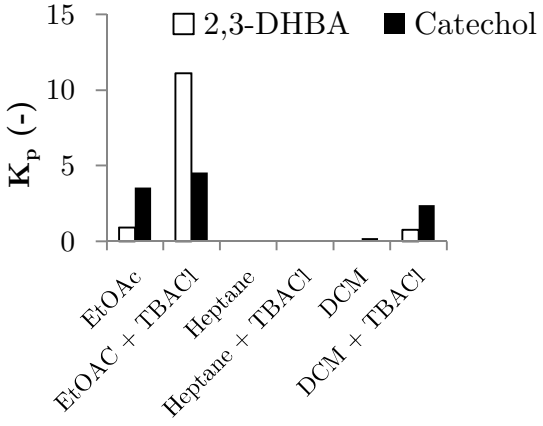

Figure 2.2.3: Extraction of catechol and 2,3-DHBA in 2LPS in the presence and absence of tetrabutylammonium chloride; Reaction conditions: 10 mM catechol/2,3-DHBA, TBACl/phenolic 1:1 mol:mol, 2 M $KHCO_3$, aqueous:organic 1:1 v/v, shaking for 10 minutes at 30°C and 500 rpm.

As it can be seen, and as it was also expected from the behaviors of the different diluent types in reactive extractions of carboxylic acids, the poorest performances were achieved using hydrocarbons such as n-heptane, where the biocatalysis

otherwise performs at its best. The fact that catechol shows a high partition in organic solvents such as DCM –even higher than the product– demonstrates that this approach is also not feasible for applications.

2.2.3 Use of Water-Miscible Co-solvents

Another strategy that was investigated to overcome the unfavorable thermodynamic equilibrium is to make use of alternative reaction media by means of organic miscible co-solvents. Such media engineering approaches have been widely used in the biocatalysis field to influence thermodynamics (Voutsas *et al.* 2009), kinetics and selectivity (Stepankova *et al.* 2014), especially in the hydrolases enzyme class, where a deep understanding has been achieved also at the molecular level (Castillo *et al.* 2016). Looking at the mechanistic explanations about (de)carboxylation reactions in Chapter 1, it appears clear that polar solvents would favor carboxylation reactions, as when pH > pK_a, the polar carboxylate would be stabilized, while non-polar solvents would facilitate decarboxylations and provide a "comfortable" environment for the – neutral and hydrophobic – CO_2 molecule which is cleaved. Evidence that the latter strategy is effective to aid decarboxylation can be found in the high hydrophobicity of the active sites of many decarboxylases (Frank *et al.* 2012; Sigman 1992). The use of organic co-solvents in the *ortho*-carboxylation catalyzed by Rsp_DHBD has recently been reported in the literature (Wuensch *et al.* 2013b). In summary, resorcinol conversions after 24 h of reaction were shown to increase from 32% to 45% in a 3 M $KHCO_3$ aqueous solution with water miscible co-solvents such as acetone or N,N-dimethylformammide. Stimulated by the recent interest in glycerol carbonate (GlC, 4-hydroxymethyl-2-oxo-1,3-dioxolane) as a water-like solvent in biocatalysis (Ou *et al.* 2011), the influence of water-GlC mixtures on the enzymatic carboxylation of catechol was studied. Figure 2.2.4 shows how the presence of GlC as co-solvent improves the maximum conversion as $KHCO_3$ concentrations approach the solubility limit and at different GlC v/v %.

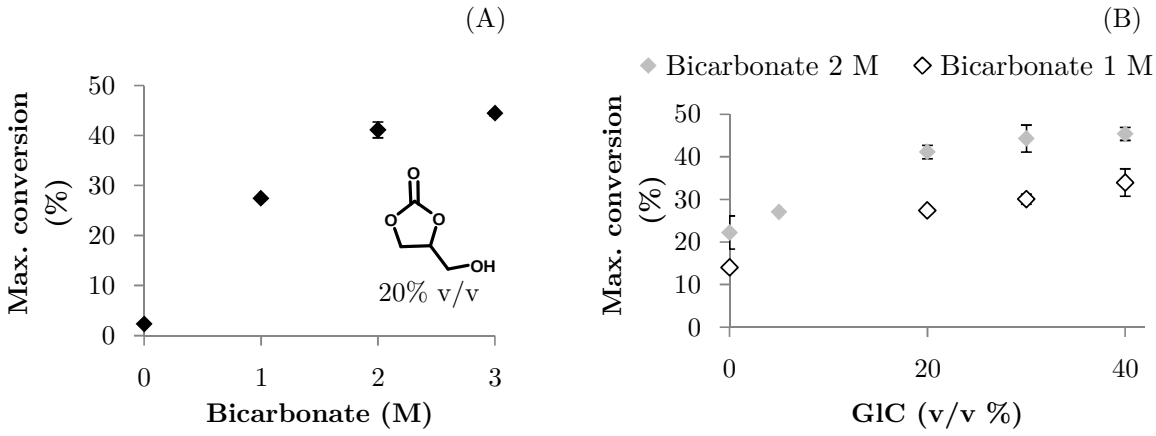

Figure 2.2.4: Maximum conversion of catechol carboxylation in aqueous-GlC mixtures varying bicarbonate (A) and GlC (B) concentrations; Reaction conditions: 20 mM catechol, 20 mM ascorbic acid, 30 mg mL^{-1} Rsp_DHBD (whole lyophilized cells) in 0-3 M *KHCO₃* and 0-40% v/v GlC, at 30°C and 500 rpm.

GlC is hydrolyzed to glycerol (Gl) and bicarbonate at basic pH (Sonnati *et al.* 2013)(Scheme 2.2.2):

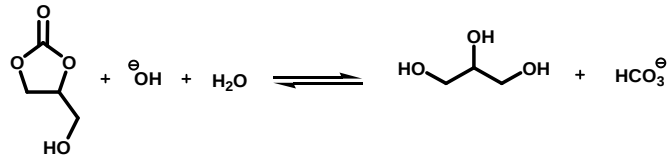

Scheme 2.2.2: Hydrolysis of GlC in alkaline solutions.

In order to verify whether the increase in conversion is due to Gl and not to GlC, we performed reactions using Gl as co-solvent; as it will be later discussed, this co-solvent also affords an increase in conversion, albeit lower when compared with GlC. The fact that the hydrolysis reaction is not significant is also proved in Figure 2.2.4(A), where it is shown that in the absence of bicarbonate the reaction does not proceed efficiently. The equilibrium conversion increases can be rationalized with the solvent properties of GlC, particularly its dielectric constant (ε). In fact, unlike other water miscible organic solvents, GlC and water are characterized by a similar ε (82 and 78, respectively). Acetonitrile, for example, has ε = 36. On the one hand, this explains why enzymes are active in GlC, as it guarantees ionization states of the amino acids residues similar to those in water (Ou *et al.* 2012). The occurrence of enzyme activity in this solvent cannot in fact be justified when considering the *logP* criteria, stating that solvents with *logP* < 2 are not suitable for biocatalysis (Laane *et al.* 1987). The *logP* for GlC is –0.25 (Ou *et al.* 2011), considerably lower than, for

example, the one of tetrahydrofuran (0.46 (Sangster 1989)), which is generally considered a strong enzyme denaturing agent and has been shown also to have a negative impact on Rsp_DHBD (Wuensch *et al.* 2013b). On the other hand, such dielectric properties justify a higher solvation of the carboxylate ion, increasing its stability. Interestingly, the conversion levels at ≈ 30 v/v % GlC and at 2 M $KHCO_3$, with a maximum of 45%, double of that without the co-solvent. The same maximum conversions were obtained changing the catalyst to the Ao_DHBD, strongly suggesting that the observed maximum conversions are a consequence of thermodynamics. A temperature change to 20°C allowed a further thermodynamic boost, as the carboxylation is an exothermic reaction, reaching a maximum conversion of 50% using 30% v/v GlC and 2 M $KHCO_3$ (Figure A19). In order to quantitatively express the increase in solvation of the carboxylate, we quantified and compared the solubility properties of the used reaction media using the Hansen Solubility Parameters (HSPs) (Hansen 2007). In brief, these parameters quantify the cohesive energy of a given compound by three different quantities: atomic dispersion forces (δ_D), molecular permanent dipole-permanent dipole forces (δ_P) and hydrogen bonding forces (δ_H). These cohesive energies depend on the interactions of two molecules of the same kind. Consequently, two species with similar HPSs have higher affinities to one other. Every molecule can be described in a tridimensional space where the x, y, and z axes represent the HSPs. Therefore, the relative affinity/solubility of two components 1 and 2 ($R_{a(1-2)}$) can be geometrically represented as the distance between the two points in the HSPs space (Williams & Kuklenz 2009) (Eq. 2.2.1):

$$R_{a(1-2)} = \sqrt{(2\delta_{d,1} - 2\delta_{d,2})^2 + (\delta_{h,1} - \delta_{h,2})^2 + (\delta_{p,1} - \delta_{p,2})^2} \qquad \text{(Eq. 2.2.1)}$$

In case of a mixture of n solvents, the mixture´s HSPs can be calculated using the following additive equation (Hansen 2007):

$$\delta_{mix(1-2)} = (X_1\ \delta_1) + (X_2\ \delta_2) + \cdots + (X_n\ \delta_n) \qquad \text{(Eq. 2.2.2)}$$

Where X_n is the volume fraction of the n^{th} component. The HSPs values can be determined experimentally or mathematically. A high amount of data can be found in existing handbooks (Hansen 2007). The HSPs of the media used in the enzymatic carboxylation were compared with the ones of sodium benzoate (Bustamante *et al.* 2000), which is the compound most similar to the biotransformation products for which the three parameters are known. Figure 2.2.5(A) shows that the R_a distances

between the solvent and sodium benzoate progressively decrease going from water to glycerol carbonate, indicating a higher affinity in the last one. The R_a were also calculated for the water-solvent mixtures where the reactions were performed, including 20 and 40% v/v glycerol (Gl) (Figure 2.2.5(B)) and a qualitative trend correlating higher affinity to higher equilibrium conversion can be observed.

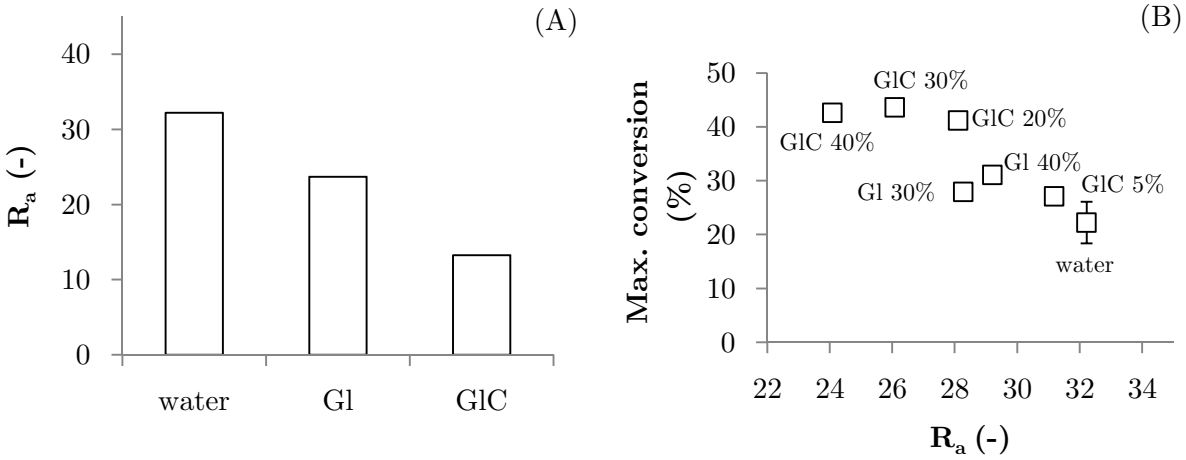

Figure 2.2.5: Correlation of the conversion with the solubility of sodium benzoate in different solvents; A: sodium benzoate/solvent R_a according to the HSPs; B: Correlation of the maximum conversion in solvent mixtures with the sodium benzoate/solvent R_a ; Reaction conditions: 20 mM catechol, 20 mM ascorbic acid, 30 mg mL^{-1} Rsp_DHBD (whole lyophilized cells) in 2 M *KHCO₃* and 0-40% v/v GlC or 30-40% Gl, at 30°C and 500 rpm.

The reaction mechanism requires the elimination of a water molecule. Therefore a change in the water activity could be used as an explanation for the increased conversion. However, it is known that a polyol such as glycerol decreases the activity of water, therefore not justifying the increased concentration of product at equilibrium. The generality of the increase in conversion was assayed with other phenolic compounds using 30% v/v GlC and 2 M *KHCO₃*. The results are summarized in Table 2.2.3.

Table 2.2.3: Carboxylation of phenolic compounds in aqueous bicarbonate and 30% v/v GlC; Reaction conditions: 10 mM phenolic compound, 40 mg mL^{-1} Rsp_DHBD (whole lyophilized cells) in 2 M *KHCO₃* and 30% v/v GlC or 30-40% Gl, at 30°C and 500 rpm.

Substrate	Max. conversion in water (%)	Max. conversion in 30% v/v GlC (%)
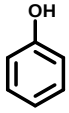	22	28
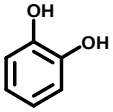	22	44
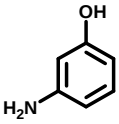	56	68
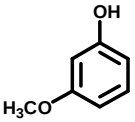	38	47

The results show that the conversion increase is substrate independent, even though it is higher for catechol. Reaction time courses where analyzed to compare the reaction velocities in the different media. Figure 2.2.6(A) shows the progress of the biotransformation in water (black diamonds), 30% v/v Gl (white diamonds) and 30% v/v GlC (grey diamonds), and Figure 2.2.6(B) shows the respective initial reaction rates.

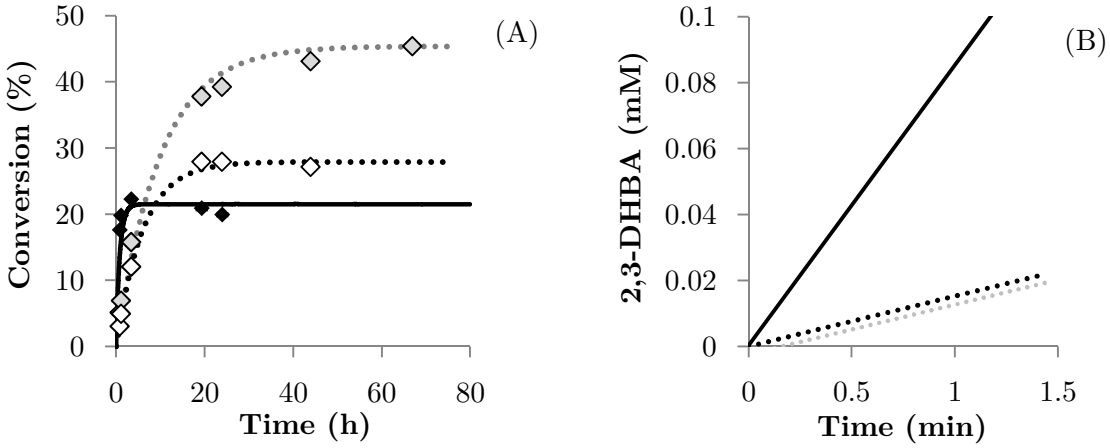

Figure 2.2.6: Reaction progresses for catechol carboxylation in different reaction media (A) and the respective initial reaction rates (B); solid black line corresponds to the simulation performed with equation 2.1.2, dotted black and grey lines correspond to a fit to the experimental points; Reaction conditions: 20 mM catechol, 20 mM ascorbic acid, 30 mg mL^{-1} Rsp_DHBD (whole lyophilized cells) in 0-3 M *KHCO₃* and 0-40% v/v GlC, at 30°C and 500 rpm.

In the presence of either Gl or GlC, the biotransformation is slowed down more than 5 times compared to the reaction in water. This could be a consequence of their higher viscosities.

In general, the properties of the reaction medium, characterized by molar concentrations of a negatively charged ion as co-substrate, the presence of a millimolar concentration of the main substrate, and the structural similarities between the starting material and the product, make reaction engineering strategies based on adsorption and extraction not applicable as tools for *in situ* product removal due to lack of selectivity. The use of a bio-compatible co-solvent such as glycerol carbonate was demonstrated to afford higher conversions with respect to solely aqueous medium, but, being lower or equal to 50%, it is still far from applicability standards,. Therefore, the application of this reaction shows to have major constraints. However, the biocatalytic *ortho*-carboxylation constitutes a very interesting reaction from a fundamental point of view as it sheds light on the different strategies that nature uses to perform a transformation that has been only in relatively recent times performed by man. Moreover, its study also revealed interesting – and unexpected – effects that alkylammonium ions have on the reactivity displayed by catechol.

In conclusion:

- *In situ* product removal by adsorption on ion exchangers or by extraction in organic solvent show considerable issues due to the poor selectivity towards the product and the properties of the reaction medium;
- The use of glycerol or glycerol carbonate as co-solvents at up to 30% v/v can push the equilibrium conversions towards more product (up to 2 times in the case of glycerol carbonate);
- The reaction rates decrease considerably in the presence of the co-solvents;
- A higher affinity of the carboxylation product towards the water/co-solvent mixtures, evaluated considering the solubility parameters of the individual components, can justify the increased equilibrium conversions.

3 *para*-Decarboxylation of Hydroxycinnamic Acids

3.1 Fundamental Studies on a Phenolic Acid Decarboxylase

Trans-hydroxycinnamic acids are important phytochemicals that are either attached to the cell walls as esters, amides and glycol-conjugates or present in free form in the cytoplasm (Figure 3.1.1) (Faulds & Williamson 1999).

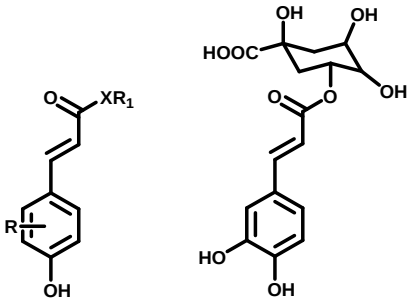

Figure 3.1.1: General structure of hydroxycynnamic acid derivatives (left) and chlorogenic acid (right). X = N, O

Chlorogenic acid (Figure 3.1.1 right) is, for example, an abundant soluble form of caffeic acid. The most common hydroxycynnamic acids are *para*-coumaric, ferulic and sinapic acids, which derive from the three basic monolignols constituting lignin (*para*-coumaryl alcohol, coniferyl alcohol and sinapyl alcohol) (Davin & Lewis 2005). These three acids and their derivatives constitute the primary source of aromatic compounds in plant cells and they are also involved in maintaining cells integrity and in defending against pathogens (Faulds & Williamson 1999). Without too much surprise, microorganisms have learned how to make use of these derivatives for their "diet" by cleaving the ester/amide bonds *via* cinnamoyl ester hydrolases (Landete *et al.* 2010), releasing the acids, which become substrates for different metabolic reactions (*e.g.*, decarboxylation, reduction and demethylation) (Rosazza *et al.* 1995). Because of their high abundance, and considering the concepts of green and sustainable chemistry, hydroxycynnamic acids can be addressed as modern building blocks for aromatic compounds. The decarboxylation reaction is catalyzed by phenolic acid decarboxylases (PADs, EC 4.1.1.-, including ferulic acid and *para*-coumaric acid decarboxylases), which constitute a family of lyases with similar structural as well as functional features, and yields 4-hydroxystyrenes. Hydroxystyrenes – together with various other alkyl/vinyl phenols – are aroma compounds present in different types of food and beverages and often provide a

significant contribution to the overall flavor. For example, 4-vinylguaiacol (4VG, decarboxylation product of ferulic acid (FA), Scheme 3.1.1) contributes to the aroma of beer, tortilla chips, rice bran and also raw arabica coffee beans (Shahidi & Naczk 2003).

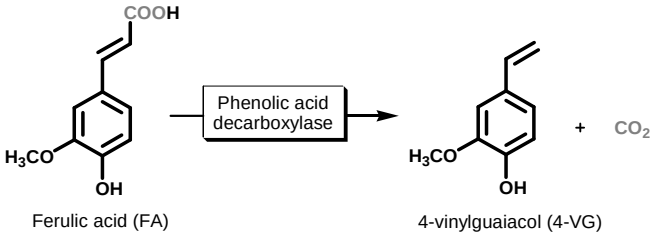

Scheme 3.1.1: Decarboxylation of FA yielding 4VG catalyzed by PAD.

As 4VG is a Food and Drug Administration (FDA) approved flavouring agent used as food additive, there is an industrial interest for its synthesis (Burdock 2010). In order to study this biotransformation for its technical application, a phenolic acid decarboxylase from *Mycobacterium colombiense* (McPAD) was studied in detail to elucidate challenges and limitations of the system. In particular, this chapter will discuss:

i) the general features of the biocatalyst in terms of activity and stability,
ii) the enzyme kinetics, with a particular focus on product inhibition,
iii) the evaluation of two liquid-phase systems (2LPS) to realize the *in situ* product removal. The reaction system in Scheme 3.1.1 was used throughout this work.

3.1.1 Enzyme Characterization

After the first discovery of this enzymatic decarboxylation reaction by Herzog and Ripke in 1906 (Rosazza *et al.* 1995) and the first cloning and overexpression of the PAD from *Bacillus pumilus* in *E. coli* in 1995 (Zago *et al.* 1995), this biotransformation has been of relatively intensive interest only in the last five-six years. During this time, efforts have been concentrating in the elucidation of structures (Bhuiya *et al.* 2015; Rodríguez *et al.* 2010), mechanisms (Sheng *et al.* 2015) and in the development of applications as well (Jung *et al.* 2013; Leisch *et al.* 2013). The most characterized enzymes come from bacterial sources, while detailed studies on PAD from yeast have only appeared recently (Bhuiya *et al.* 2015). A sequence comparison between McPAD and the 6 most characterized bacterial PADs

shows the presence of a similar number of amino acids (between 161 and 178) and a pairwise sequence identity around 53% (Figure A20). The conservation of the amino acids residues can be appreciated especially between the β strands motif, which composes the hydrophobic internal cavity and the active site (Rodríguez *et al.* 2010). In order to evaluate the correlation of McPAD with structurally characterized PADs, we constructed a homology model based on the PAD from *Bacillus subtilis* (PDB code: 2P8G, sequence identity 54%, GMQE 0.77,). The active site shows a high number of aromatic as well as aliphatic hydrophobic residues described to be involved in substrate recognition and in supporting CO_2 release (Frank *et al.* 2012; Rodríguez *et al.* 2010). Docking of FA in the active site is in agreement with previously reported binding modes, in which the 4-hydroxyl group and the carboxylic group bind to amino acid residues *via* hydrogen bonds (Tyr^{23}, Tyr^{31} and Glu^{76}, see Figure 3.1.2(A)) (Frank *et al.* 2012; Rodríguez *et al.* 2010). The mechanism is accepted to proceed in two-steps via a *para*-quinone methide intermediate, formed after deprotonation of the phenolic group, and which generates an electron flow leading to CO_2 release and vinyl double bond formation (Figure 3.1.2(B)). However, recent theoretical studies show that for the PAD from *B. subtilis* the tyrosine residues interact with the phenolate rather than with the carboxylate (Sheng *et al.* 2015). Moreover, the nature of the proton donor to the C–C double bond is still not clear. Interestingly, the same methide intermediate was proposed for an organocatalyzed decarboxylation which follows the treatment of vanillinin under Knovenagel condensation conditions; the methide intermediate is formed after the elimination of piperidine –acting as an organocatalyst–, covalently bound to the propanoic side chain (Aldabalde 2011) (Figure 3.1.2(C)).

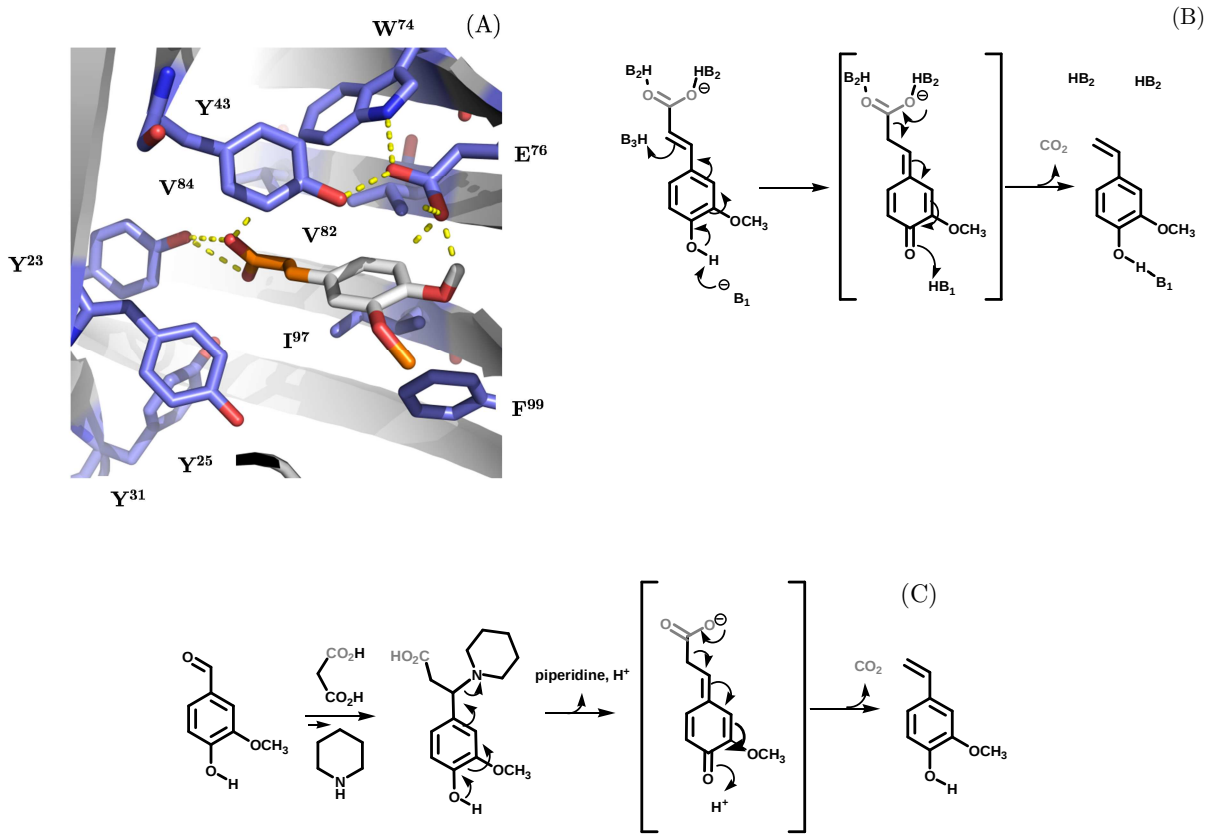

Figure 3.1.2: (A): docking of FA in the active site of McPAD (details in the experimental section), visualization created using Pymol; (B): mechanism of the enzymatic decarboxylation of FA; (C): mechanism of the Knovenagel condensation using vanillin as substrate. The common intermediate is shown in brackets.

The presence of the *para*-hydroxyl group is necessary for both chemical and biochemical variants, indicating the necessity of an "electron sink" for both reactions. It has been demonstrated that PADs are also able to act in the reverse carboxylation direction forming hydroxycynnamic acids from styrenes (Wuensch *et al.* 2015). As with the *ortho*-carboxylation, this reaction is thermodynamically limited. Therefore, molar concentrations of bicarbonates are necessary to achieve less than 50% conversion. Even though this reaction does not seem to be interesting for applications (at least for the abundant natural hydrocynammic acids), it is worth to mention that no chemical counterpart is known (Wuensch *et al.* 2012). Considering the pH range (< 8) that was used in this study and the mM concentrations of substrate, the decarboxylation reaction is assumed to be irreversible. The plasmid containing the McPAD gene was transformed in *E. coli* BL21(DE3) and fermentation was performed using standard shaken flasks protocols (see details in the

experimental section). Being a previously uncharacterized enzyme, its behavior with pH and temperature was investigated (Figure 3.1.3).

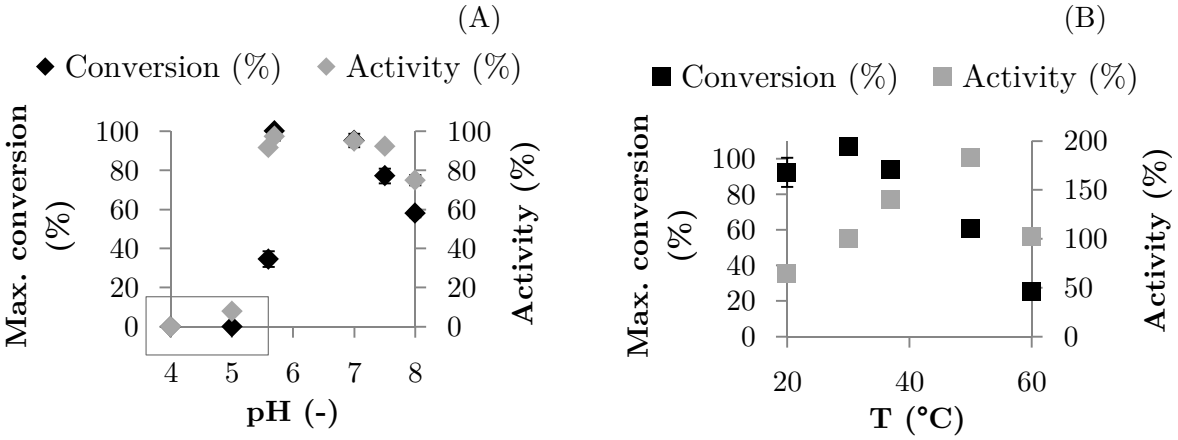

Figure 3.1.3: (A): Dependency of enzyme activity (grey diamonds) and maximum conversion (black diamonds) on pH. The grey frame indicates the assays performed with acetate buffers; (B): dependency of the enzyme activity (grey squares) and conversion (black squares) on temperature. Reaction conditions: 5 mM FA, 0.1 M KP_i or acetate buffers, 0.39 U mL^{-1} (6 mg mL^{-1}) McPAD at 700 rpm.

The highest values of activity and max. conversion were in the pH range 6-7 using KP_i buffers. Outside this interval, the activity decreased and quantitative conversions could not be reached. The pK_a of ferulic acid is 4.5 and the maximum activity is displayed when the acid is mostly in deprotonated form. Being pH <5.7 beyond the capacity of phosphate buffers, to investigate the performances at pH 4-5 a potassium acetate buffer was used. This buffer type displays additional negative effects on the enzyme, as at pH 5.6 the activity was 70% less than with KP_i at pH 5.7. The lower max. conversion at pH >7 can be attributed to a higher product inhibition rather than to a change in thermodynamics; even though steady-state concentrations of reactants/product were observed after 60 minutes of reaction and preserved during overnight incubation, it is assumed that waiting long enough ,considering enzyme stability, quantitative conversions could have been achieved. Such an optimal pH range has been already described for other PADs –bacterial and from yeast– in terms of activity, indicating a strong mechanistic similarity (Bhuiya *et al.* 2015; Hu *et al.* 2015; Landete *et al.* 2010; Rodríguez *et al.* 2010). Regarding the temperature, the activity increased progressively between 20 and 50°C (Figure 3.1.3(B)). However, quantitative conversions could be observed only between 20 and 37°C, due to deactivation beyond this value. In fact, a half-life of the enzyme of

approximately 1 h at 50°C was determined. For further studies, a 0.1 M KP_i buffer at pH 7.0 and 37°C were chosen, once the stability of the enzyme under these conditions was proven (40% residual activity after 24 h). The enzyme kinetics was studied using the purified McPAD, in order to calculate the enzymes mass-specific activities. McPAD, containing a histidine tag, was purified by routine Ni-NTA affinity chromatography. From the SDS-PAGE analysis and from the low protein yield (0.3%[10]) it appears clear that the fermentation procedure needs optimization for future applications (Figure A21). We ran kinetic experiments at increasing substrate concentrations up to 10 mM FA by measuring initial rates using a HPLC-based discontinuous assay. Figure A22 shows some examples for initial rates measurements while Figure 3.1.4 shows the concentration dependency of the initial rate.

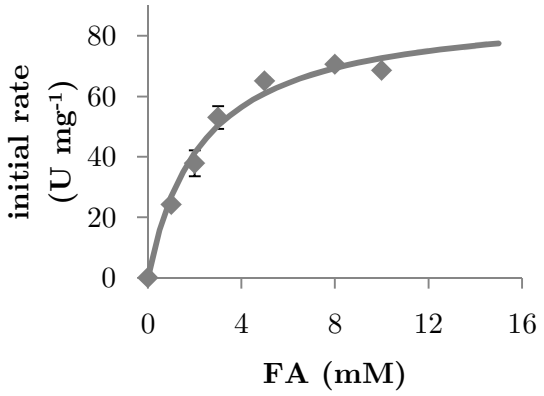

Figure 3.1.4: Saturation kinetics for McPAD-catalyzed decarboxylation of FA. Fit to the Michaelis–Menten equation realized using Microsoft Excel by the least squares method. Reaction conditions: 1–10 mM FA, 0.1 U mL^{-1} (1.7 µg mL^{-1}) McPAD, in 0.1 M KP_i buffer pH 7.0, at 37°C and 700 rpm

The typical saturation curve was fitted using the single substrate Michaelis-Menten equation and the catalytic parameters are summarized in Table 3.1.1.

Table 3.1.1: Kinetic parameters for McPAD-catalyzed decarboxylation of ferulic acid (FA).

K_M (mM)	V_{max} (U mg^{-1})	k_{cat} (s^{-1})	K_i (mM)	K_i/K_M (-)
2.4 ± 0.1	90 ± 1	22.0 ±0.1	0.14 ± 0.04	0.06 ± 0.01

[10] The yield refers to the mass of the (de)carboxylase with respect to the mass of the total proteins in the crude extract.

By comparing the literature values of the previously investigated PADs, the K_M values are all in the same range, with most of them between 0.8 and 2 mM and in general below 10 mM. For example, K_M values for PADs from *Candida guillermondi*, *Bacillus subtilis*, *Enterobacter* sp., *Lactobacillus brevis* and *Saccharomyces cerevisiae* are 5.3 mM (Huang *et al.* 2012), 1.1 mM (Cavin *et al.* 1998), 2.4 mM (Gu *et al.* 2011), 0.96 mM (Landete *et al.* 2010) and 0.79 mM (Bhuiya *et al.* 2015) for their phenolic substrates, respectively. On the other hand, V_{max} values are more diverse: the PAD from yeast has a value of 6.8 $\times 10^{-3}$ µmol min^{-1} mg^{-1}, the one from *C. guillermondi* 378 µmol min^{-1} mg^{-1} and the enzyme from *L. brevis* 10 µmol min^{-1} mg^{-1}. The considerably lower efficiency for the PAD from *S. cerevisiase* compared with the other known PADs could be explained by the absence of hydrogen bond acceptors stabilizing the carboxylate (Bhuiya *et al.* 2015), which are present in the other cases (Figure 3.1.2(A)). The 4-hydroxyl group is necessary for substrate recognition in the active site, therefore it is not surprising that PADs are inhibited by the product. So far, the inhibition has been seldom quantitatively characterized and the only reported K_i is 0.46 mM for 4-hydroxystyrene for the enzyme from *B. amiloliquefaciens* (Jung *et al.* 2013). Assuming a mechanism involving competitive product inhibition (*i.e.*, the product binds reversibly to the enzyme forming an enzyme-product complex which impedes substrate binding, see Scheme 3.1.2), the progress of batch reactions were fitted to Eq. 3.1.1 by regression of the inhibition constant K_i.

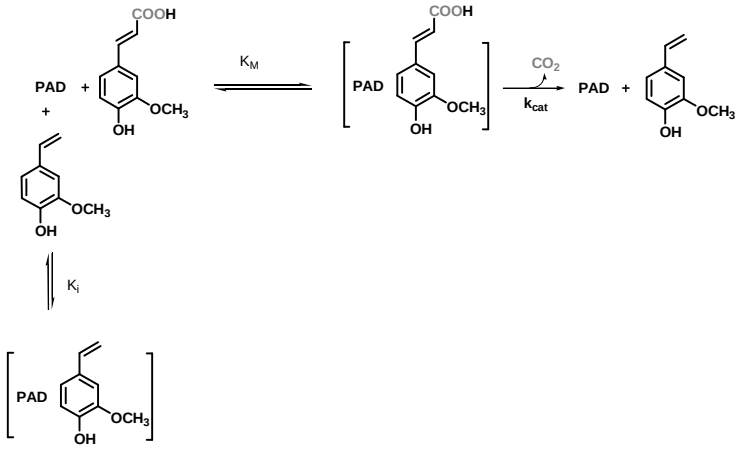

Scheme 3.1.2: Proposed catalytic pathway for the decarboxylation of FA catalyzed by McPAD.

$$\boldsymbol{v} = \frac{\boldsymbol{V_{max}}\,[\boldsymbol{FA}]}{\boldsymbol{K_M}\,(\mathbf{1}+\frac{[\boldsymbol{4VG}]}{\boldsymbol{K_i}})+[\boldsymbol{FA}]} \qquad \text{(Eq. 3.1.1)}$$

The equation represents the proposed catalytic mechanism, where $[FA]$ and $[4VG]$ are the concentrations of substrate and product. The inhibition constant is determined to

be 0.14 mM, which is in the same order of magnitude of the one reported by Jung *et al.* (Jung *et al.* 2013). As pointed out in literature ,originally by Lee and Whitesides (Lee & Whitesides 1986; Liese *et al.* 1996), a biotransformation characterized by a K_i/K_M ratio < 1 would not proceed efficiently to complete conversion and therefore product inhibition by 4VG represents a major problem for this biotransformation. To validate the kinetic model, the experimental data were compared with the numerical solutions of the mass balance equations Eq. 3.1.2 and 3.1.3 (Figure 3.1.5 and A23). $[PAD]$ is the enzyme concentration whike k_d is the deactivation constant for the enzyme ($k_d = 6.3 \times 10^{-4} \pm 1 \times 10^{-4}$ min^{-1}, see details below and in Figure 3.2.1).

$$-\frac{d[FA]}{dt} = [PAD]e^{-k_d t}\, v \qquad \text{(Eq. 3.1.2)}$$

$$\frac{d[VG]}{dt} = [PAD]e^{-k_d t}\, v \qquad \text{(Eq. 3.1.3)}$$

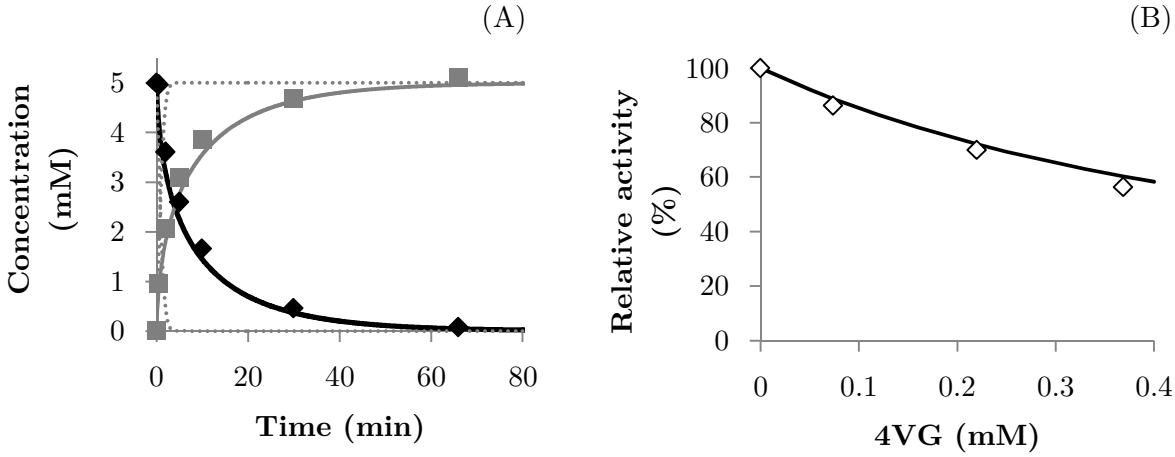

Figure 3.1.5: (A): Comparison of the experimental data (black diamonds: FA; grey squares: 4VG) with the simulation of the kinetic model (solid lines). Dashed lines represent the kinetic model without competitive product inhibition. Reaction conditions: 5 mM FA, 3.8 U mL^{-1} PAD (59 µg mL^{-1}) McPAD in 0.1 M KP$_i$ buffer pH 7.0, at 37°C at 700 rpm; (B): Enzyme inhibition tests. Reaction conditions: 5 mM FA, 0–0.38 mM 4VG, 0.2 U mL^{-1} (3 µg mL^{-1}) McPAD in 0.1 M KP$_i$ buffer pH 7.0 at 37°C at 700 rpm. Solid black line corresponds to the simulation performed using the kinetic model.

Figure 3.1.5 shows the good agreement of the experimental with simulated data (black and grey solid lines) and the significant effect of the product inhibition (grey dashed lines, simulated without inhibition) on the overall reaction progress. As already mentioned, the reaction is reasonably irreversible, therefore, in the absence of

enzyme deactivation, the reaction should proceed to complete conversion also at relatively high substrate concentrations (molar range). In this respect, Figure 3.1.6 shows the effect of the substrate amount on the maximum conversion and the deviation from the theoretical data derived from the kinetic model.

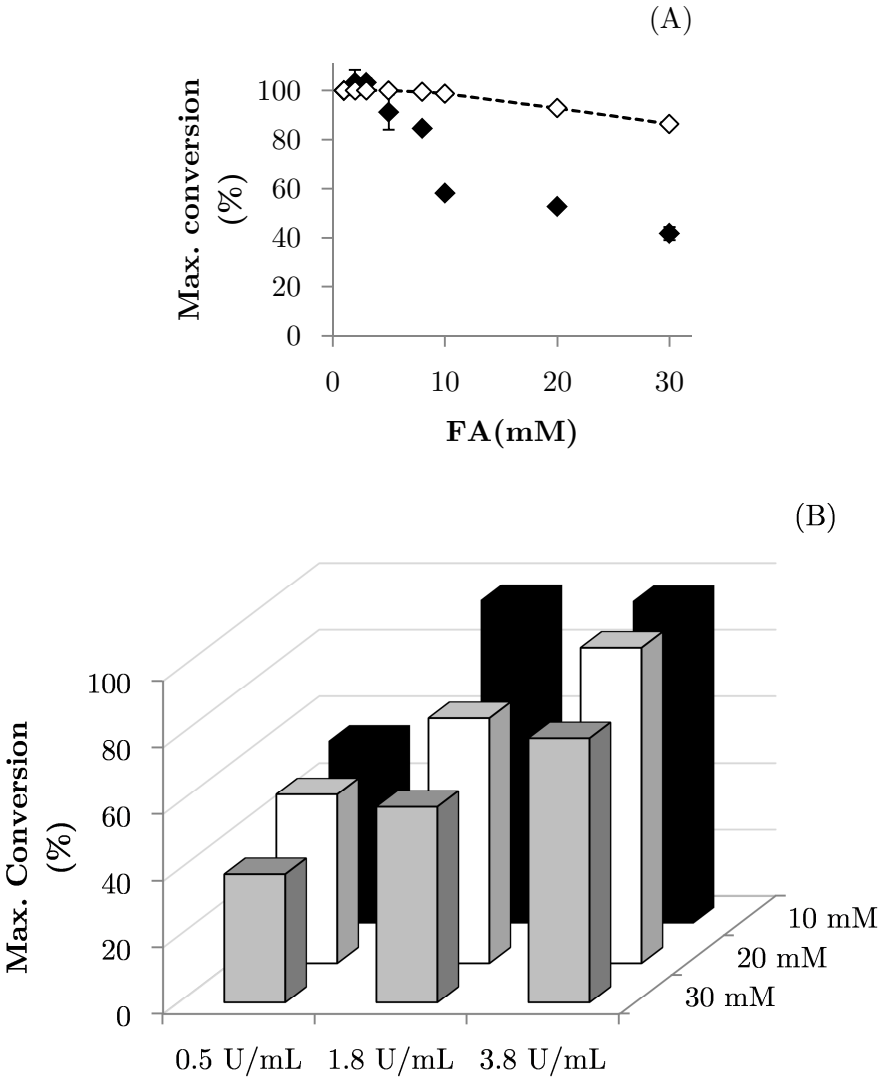

Figure 3.1.6: (A): Influence of the substrate concentration on the maximum conversion. Black diamonds: max. conversion; white diamonds: theoretical max. conversion according to Eq. 3.1.1 at 24 h. Reaction conditions: 1–30 mM FA, 0.5 U mL^{-1} (8 µg mL^{-1}) McPAD, in 0.1 M KP_i buffer pH 7.0, at 37°C at 700 rpm; (B): The influence of the substrate concentration on the maximum conversion. The PAD concentrations correspond to 8, 29 and 59 µg mL^{-1}, respectively; standard deviations in duplicates <7%.

Such a trend does not derive from the excess substrate inhibition (*i.e.*, the substrate binds to the enzyme-substrate complex), as the kinetic data do not support this hypothesis. Possible explanations could be found in enzyme deactivation due to the high product concentrations or in the establishment of a different inhibition mechanism when the product overcomes a certain threshold value. In that respect, the maximum conversion should be dependent on the catalyst amount. Figure 3.1.6(B) shows the increase in the maximum conversion due to increased amount of biocatalyst at different FA concentrations (10-30 mM). Data supporting this observation were also reported by Leisch and co-workers (Leisch *et al.* 2013). Almost complete conversion could be achieved at 20 mM using 59 µg mL^{-1} McPAD, but not at 30 mM. At 20 and 30 mM FA and 59 µg mL^{-1} McPAD, the analytical yields were slightly lower (6-7%) than the conversions, owing to the product solubility limit. To further study the influence of the enzyme/substrate ratio in determining the maximal conversion, reaction progress curves at different biocatalyst concentrations were compared (Figure 3.1.7). In the absence of the deactivation or of any changes in the catalytic mechanism, conversion *versus* time × PAD concentration data points should fall on the same line (Selwyn 1965). The results show that this holds true at 5 mM FA but not at 10 mM, where different enzyme concentrations generate different progress curves at the last stage of the reaction (Figure 3.1.7).

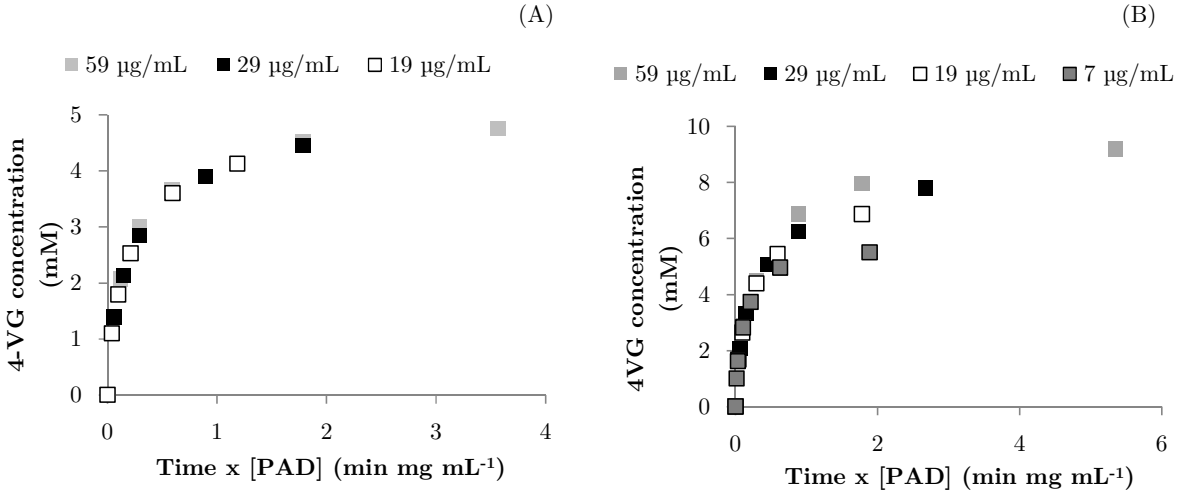

Figure 3.1.7: Deactivation anlysis at 5 mM FA (A) and 10 mM FA (B). The time difference between the last two data points in each curve is of approximately 20 h. Reaction conditions: 5 or 10 mM FA, McPAD, in 0.1 M KP_i buffer pH 7.0, at 37°C at 700 rpm.

Hence, the Eq. 3.1.1 for this reaction system seems to be valid at high FA concentrations only when the enzyme concentrations are high enough (PAD(µg mL^{-1})/FA (mM) ratio ≈ 6). This becomes evident by comparing the experimental and simulated data at 10 mM FA using two different enzyme amounts (Figure A23(B),(C)). Inhibition or deactivation of PADs by the reaction products have not been described in detail in the literature so far. Our data show an influence of 4VG concentration on the enzyme, which could be exerted either by (irreversible) deactivation or by the establishment of a different inhibition mechanism. In this regard, a more detailed comprehension of the conformational changes of the enzyme upon product binding may be useful. PADs are reported to be dimers or tetramers in solution and to have mobile loops that regulate substrate access to the active site, at the same time shielding the entrance of water, suggesting the occurrence of significant modifications upon ligand binding (Frank *et al.* 2012; Gu *et al.* 2011; Rodríguez *et al.* 2010).

In conclusion:

- Phenolic acid (de)carboxylase from *Mycobacterium colombiense* (McPAD) was expressed in *E. coli* and characterized regarding its behavior towards pH and temperature for the decarboxylation of ferulic acid;
- A detailed kinetic study allowed to evaluate the catalytic constants and to propose and validate a rather simple catalytic pathway including reversible product inhibition;
- Combined experimental and simulated data point out that a different catalytic pathway is established when the ratio of enzyme to ferulic acid is approximately < 6, due to substrate deactivation or to the establishment of a different inhibition mechanism.

3.1.2 Biotransformation in Two Liquid Phase System

From a practical point of view, to achieve high conversions in this system, as a rule of thumb the concentration of the product should be maintained below 10 mM when PAD concentration is less than 20 µg mL^{-1}. In order to employ higher FA concentrations maintaining 4VG under the 10 mM threshold, the possibility for the McPAD to work in two liquid phase systems (2LPSs) was investigated, where an organic phase would continuously remove the formed product. The establishment of

an efficient biotransformation in a 2LPS requires a trade-off between partition coefficients of the product and enzyme/activity stability in the chosen system. Figure 3.1.8 shows the logarithms of the partition coefficients K_p and the reaction rates for extraction of 5 mM 4VG for solvents in the *logP* (octanol/water partition coefficients) range 0.7-4.

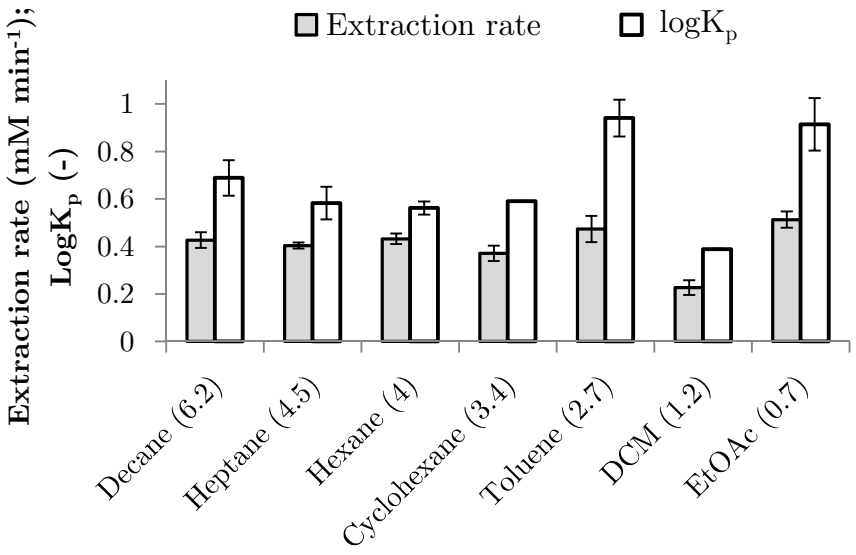

Figure 3.1.8: Extraction rates and partition coefficients of 4VG in buffer/organic solvent systems. The *logP* of each solvent is indicated in brackets. 5 mM 4VG, 1:1 solvent ratio, in 0.1 M KP$_i$ buffer pH 7.0, at 37°C at 700 rpm. Equilibrium was reached in all cases after approximately 1 h. DCM: dichloromethane, EtOAc: ethyl acetate.

The highest partition in the organic phase was observed for toluene and ethyl acetate, while the differences in reaction rates are not as significant. Biotransformations were performed in 1.8 mL scale using 5 mM FA to verify whether the McPAD was compatible (Table 3.1.2).

Table 3.1.2: Conversion in 2LPS. Reaction conditions: 5 mM FA, 0.78 U mL^{-1} (12 µg mL^{-1}) McPAD, in a 2LPS (organic: aqueous, 1:1 (v/v)), aqueous medium 0.1 M KP$_i$ buffer at pH 7 and 37°C, 700 rpm.

Solvent	Solubility in water*	*LogP*	Conversion (%)
Hexane	<0.1	4	99
Toluene	<0.1	2.7	99
DCM	1.3	1.2	99
EtOAc	8.7	0.7	5

* g in 100 mL

The reaction runs to completion in hexane, toluene and DCM but not in EtOAc, possibly because of its higher polarity and water solubility, leading to enzyme deactivation. These results show that the biocatalyst is able to work in the presence of relatively hydrophobic organic solvents. The second part of this chapter is focused on the optimization of the reaction conditions to synthesize 4VG and in the establishment of a reaction sequence leading to 4-ethylguaiacol (4EG), another industrially relevant fragrance compound.

In conclusion:

- The use of a second organic phase which could behave as a product sink is proposed as a strategy to overcome product inhibition;
- A solvent survey combining data about the extraction of the decarboxylation product 4-vinylphenol and the activity of the enzyme in two liquid-phase systems show that hexane, toluene and dichloromethane are the most promising solvents.

3.2 Applications: Synthesis of Fragrance Compounds

The fact that McPAD is able to work in 2LPSs can be exploited on the one hand to counteract product inhibition/deactivation and on the other hand to ensure a straightforward downstream processing through phase separation and organic solvent evaporation. Moreover, the vinyl functionality can be used to design further (chemocatalytic or biocatalytic) reaction steps leading to other industrially relevant compounds. For example, the hydrogenation of 4VG yields 4-ethylguaiacol (4EG), which is another FDA-approved flavouring agent (Burdock 2010). 4EG is a natural substance present in cooked asparagus, raw Arabica coffee beans, scotch whiskey and tequila as well as in soy souce and cloves (Shahidi & Naczk 2003). In this part of the work, the synthesis of 4VG in 2LPS and of 4EG by a chemoenzymatic reaction sequence is studied and demonstrated up to the gram scale. After the decarboxylation reaction, 4EG was obtained by performing a Pd on charcoal (Pd/C)-catalyzed hydrogenation of 4VG without intermediate isolation, as the chemical reaction was performed directly on the organic phase (Scheme 3.2.1).

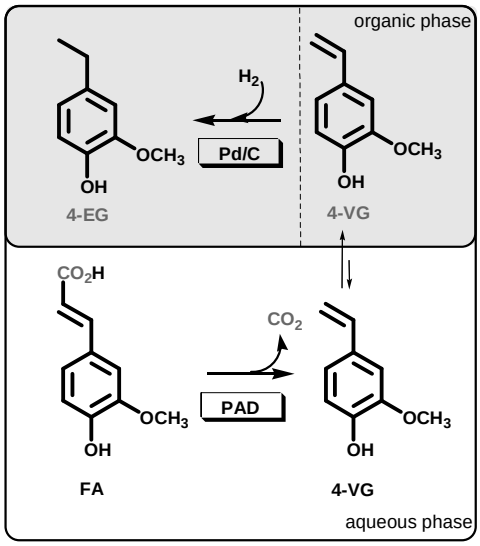

Scheme 3.2.1: Reaction sequence of PAD-catalyzed decarboxylation of FA and subsequent Pd-catalyzed hydrogenation in the organic phase. The dashed line indicates that the hydrogenation takes place subsequently in a second reactor.

3.2.1 Kinetics in Two Liquid Phase System and Synthesis of 4-Vinylguaiacol

Hexane, toluene and DCM were selected for our further studies. Experiments performed with 20 mM FA and 8 µg mL^{-1} enzyme concentration in 10 mL volume using either hexane or toluene as the second phase showed already a consistent improvement with respect to the reaction performed in buffer, as quantitative conversion was obtained after less than 10 h of reaction. The 4VG concentration in buffer remained below 4 mM (Figure A24). The rate of ferulic acid conversion in the 2LPS was 69% of the rate observed in the one-phase system. The organic phases contained only the target product, therefore a straightforward work-up afforded the isolation of 4VG. However, in the case of toluene, the product was isolated as a yellow oil (Figure A25), indicating a low purity (probably due to the higher solubility of the crude extract components in toluene). This has also been observed by Leisch *et al.* (Leisch *et al.* 2013). Using hexane, 4VG could be isolated with more than 70% yield as transparent oil. The maximum conversion in the presence of DCM was around 75%. This is probably due to the longer exposure of the enzyme to the organic phase, leading to its deactivation. Due to the aforementioned observations, hexane was chosen for further optimization studies. As mentioned in Chapter 3.1, enzyme stability in the presence of organic solvents is a critical factor for the selection of a solvent. In the case of PADs, their stability was reported to be an issue

in 2LPSs (Hu *et al.* 2015; Jung *et al.* 2013; Wuensch *et al.* 2013b). Therefore, the stability of McPAD in a reaction medium composed of buffer/hexane was studied. Surprisingly, a more than three-fold increased stability of the enzyme was detected in the presence of hexane. Figure 3.2.1 shows that less than 20% of activity is lost when the enzyme is exposed to hexane for ≈ 27 h while in the sole buffer the activity loss is of 60%. In terms of half-life time, $\tau_{1/2}$ of McPAD in buffer is 15 h, while in buffer:hexane is 53 h.

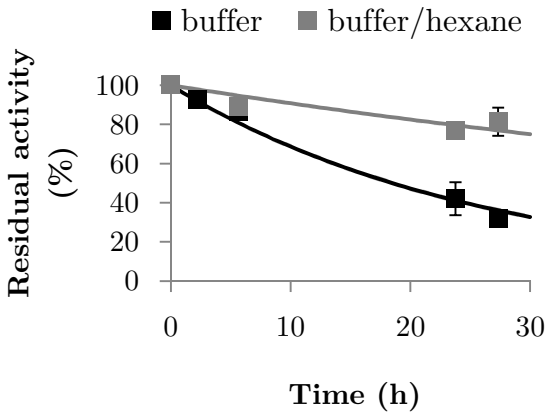

Figure 3.2.1: Stability of the McPAD in buffer and buffer/hexane. Solid black and grey lines represent an exponential fit to the experimental data. Reaction conditions: 5 mM FA, 0.39 U mL^{-1} (6 µg mL^{-1}) McPAD; in a 2LPS (organic: aqueous, 1:2 (v/v)), aqueous medium 0.1 M KP_i buffer pH 7.0, at 37°C, 700 rpm.

The decreased activity and the increased stability in a 2LPS suggest the establishment of a rigid McPAD conformation. In fact, more flexible conformations facilitate substrate-enzyme interactions (PADs have also been characterized with regard to their mobile loop) and at the same time decrease the thermostability (Carrea & Riva 2000; Klibanov 2001). Such flexibilitys' properties changes may occur either at the interphase or by the direct action of solubilized solvent molecules. In fact, even though the solubility of hexane in water is very low, assuming a concentration of 1 g L^{-1}, this would result in a hexane/PAD molar concentration ratio of approx. 20–30 (with specific values depending on the enzyme loading). It is worth mentioning here that the PAD from *B. licheniformis* CGMCC 7172 (solvent tolerant microorganism) showed a remarkable stability towards high ***logP*** organic solvents (Hu *et al.* 2015). The construction of a kinetic model would allow a better understanding of the reaction and the *in silico* planning of further improvements of the reaction for technical-scale applications. Assuming no changes in the enzymatic

mechanism, the kinetic equations for product formation in the aqueous phase v_1 and in the organic phase v_{-1} can be written as in Eq. 3.2.1 and 3.2.2.

$$v_1 = v - k_1[4VG]_{aq} + k_{-1}[4VG]_o \quad \text{(Eq. 3.2.1)}$$

$$v_{-1} = k_1[4VG]_{aq} - k_{-1}[4VG]_o \quad \text{(Eq. 3.2.2)}$$

Where $[4VG]_{aq}$ and $[4VG]_o$ are the product concentrations in aqueous and organic phase, v is Eq. 3.1.1, k_1 is the rate constant for the extraction into the organic phase and k_{-1} is the rate constant for the reverse direction. The two constants k_1 and k_{-1} were estimated measuring extraction velocities in 5 mL thermostated vessels using 1 mL buffer and 2 mL hexane at two different 4VG concentrations, obtaining k_1 = 0.097 min^{-1} and k_{-1}= 0.0078 min^{-1} –calculated dividing k_1 by the partition coefficient measured using an organic:aqueous ratio of 2 (v/v) ($logKp$ = 1.08). Since the catalytic constants of the enzyme would probably change in the presence of the second phase, a fit of the proposed mass balance (using the deactivation constant for the enzyme k_d =1.6 $\times 10^{-4}$ ± 7.9 $\times 10^{-5}$ min^{-1}) to the reaction progress was realized and the results show that this is a realistic model for the reaction (Figure 3.2.2 and A26). The determined parameters are showed in Table 3.2.1.

Table 3.2.1: Kinetic parameters for the two-phase system calculated via non-linear fitting of the kinetic model to progress curves. Details in the experimental section.

K_M (mM)	V_{max} (U mg^{-1})	K_i (mM)	k_1 (min^{-1})	k_{-1} (min^{-1})
2.6±0.1	80±13	0.22±0.01	0.09±0.02	0.009±0.02

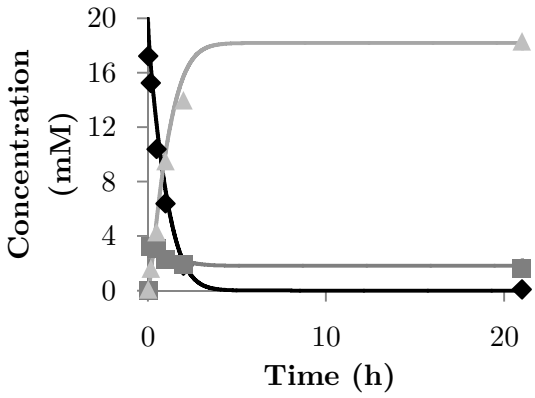

Figure 3.2.2: Comparison of the experimental data with the kinetic model (solid lines). Black diamonds: FA; grey squares: 4VG in buffer, grey triangles: 4VG in hexane. Reaction conditions: 20 mM FA, 0.58 U mL^{-1} (9 µg mL^{-1}) McPAD, in a 2LPS (organic:aqueous, 1:2 (v/v)), aqueous medium 0.1 M KP_i buffer pH 7.0, at 37°C, 700 rpm.

Figure 3.2.2 shows a typical reaction progress in the 2LPS, where the product accumulates in the aqueous medium reaching a maximum and the extraction into the organic phase continues up to an equilibrium point. Initial attempts to run the reaction at 50–100 mM failed because of the pH increase to 8.0 during the course of the reaction. In fact, in order to solubilize FA in KP_i buffer (0.1 M, pH 7.0) KOH was added (final concentration 70 mM), and, as the acid is converted, the pH of the reaction mixture would become increasingly alkaline. As mentioned above, incomplete conversions were found at basic pH values. Table 3.2.2 shows that the increase in the buffer concentration from 0.1 to 0.5 M allowed the establishment of a constant pH value (≈ 7) and consequently improved, for example, the conversions at 100 mM FA from 41% to 95%.

Table 3.2.2: Influence of pH control on the conversion; reaction conditions: 50–200 mM FA, 0.84 U mL^{-1} (13 µg mL^{-1}) McPAD, in a 2LPS (organic: aqueous, 1:2 (v/v)), aqueous medium 0.1 M KP_i buffer at pH 7 and 37°C, 700 rpm.

Concentration (mM)	KP_i buffer Concentration (M)	Max. Conversion (%)
100	0.1	41
50	0.1	66
50	0.5	99
100	0.5	95
200	0.5	30
200	0.1[a]	60
120	0.5	87

[a] Reaction operated with pH control and autotitrator.

The results show that in the presence of an appropriate buffer concentration, the reaction can proceed to high conversions (87%) up to 120 mM. The reaction cannot proceed efficiently at 200 mM, even with continuous pH titration, due to the establishment of inhibitory product concentrations in the aqueous phase (consequence of the partition coefficient). The employment of higher FA concentrations would require a higher hexane/buffer ratio. Table 3.2.3 shows the process parameters for the reaction at 100 mM FA and 0.5 M KP_i buffer at pH 7.

Table 3.2.3: Process parameters for the following reaction conditions: 100 mM ferulic acid, 0.5 M KP_i buffer at pH 7, 37°C, 700 rpm. X = conversion; Y = isolated yield; TON = turnover number (moles of product/moles of enzyme); EC = enzyme consumption (kg product/g of enzyme).

FA ($g\ L^{-1}$)	PAD ($mg\ L^{-1}/(U\ L^{-1})$	X (%)	Y (%)	TON ($mol\ mol^{-1}$)	TON ($Kg\ g^{-1}$)
19	0.09/5.8	95	79	11734	89

At this concentration, the reaction progress can be simulated with a good agreement only in the first 2 h of the reaction (A26(C)); afterwards it proceeded slower than expected. A possible reason can be the presence of product concentrations higher than 10 mM in the aqueous phase, causing enzyme deactivation or a different product inhibition, as mentioned above. The reaction was demonstrated also at gram scale (1.9 grams FA) in 100 mL reaction volume, affording the production of 1 gram of 4VG with 89% conversion and 75% isolated yield. A limitation of this system is caused by the partition coefficient of 4VG, which generates a steady-state product

concentration in the aqueous phase of about 2 mM. This also limits the use of higher FA concentrations. As already mentioned, these problems could be circumvented by using higher organic solvent volumes. Instead, this issue was addressed by designing a recycling system that allows the reduction of the amount of hexane used, while at the same time facilitating product purification. The system is presented in Figure 3.2.3 as picture and flow sheet.

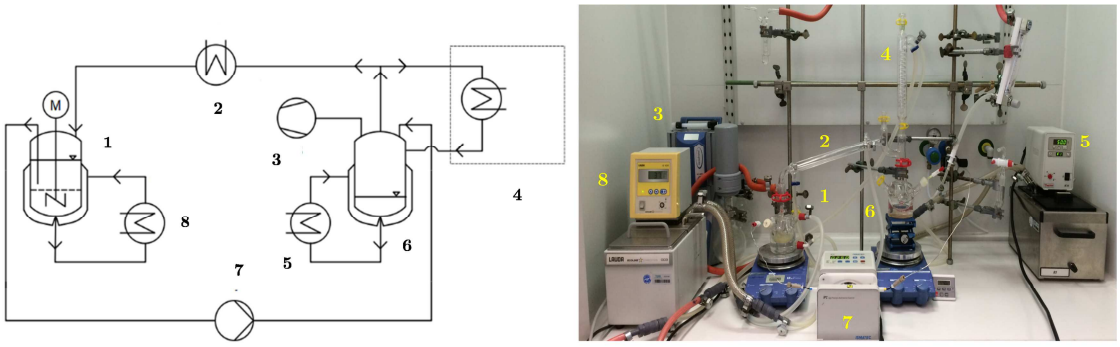

Figure 3.2.3: Flow sheet (left) and picture (right) of the extraction/distillation reactor set-up. 1: two-phase reactor; 2: distillation condenser (4°C); 3: vacuum pump connected with the distillation system (400–450 mbar); 4: bubble condenser (4°C); 5: thermostat (50–55°C); 6: vessel collecting product solution; 7: tube pump (0.25 mL min^{-1}); 8: thermostat (37°C).

In this reactor set-up, the organic phase containing the product is continuously pumped (7) into a second reactor (6) where hexane is distilled under vacuum to enter again the two-phase reactor. Having a boiling point of 220°C, 4VG accumulates in the distillation vessel (6) at a pressure of 400-450 mbar. Figure 3.2.4 shows the comparison between the reaction run in the simple 2LPS set-up that has been described so far and in the set-up depicted in Figure 3.2.3.

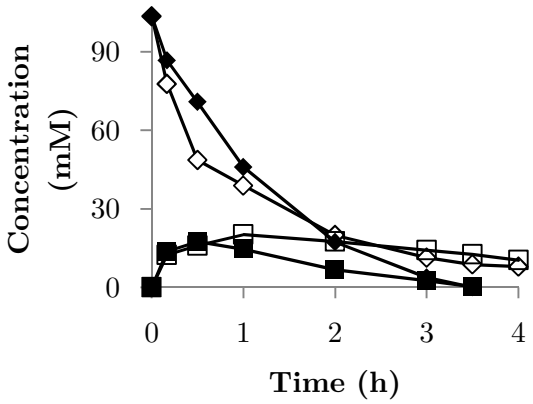

Figure 3.2.4: Decarboxylation of FA in 2LPS (FA: white diamonds; 4-VG: white squares) and in the extraction-distillation apparatus (FA: black diamonds; 4-VG: black squares). Reaction conditions: 100 mM FA, 3.9 U mL^{-1} (60 µg mL^{-1}) McPAD, in a 2LPS (organic:aqueous, 1:2 (v/v)), aqueous medium 0.1 M KP_i buffer pH 7, at 37°C, 700 rpm.

Using the integrated recycling system, quantitative conversions were achieved in a shorter time and with complete extraction of the product from the aqueous phase. This set-up was also successfully used at 170 mM substrate concentration (with 92% conversion). Moreover, since at such high FA concentrations a continuous autotitration system is necessary the reaction was performed in distilled water (without using buffer), therefore reducing the input material (Table 3.2.4).

Table 3.2.4: Comparison of reactor set-ups involving distillation.

FA (mM)	FA (g L^{-1})	Conditions	X (%)
100	19.4	Extract./distill.	>99
200[a]	38.8	0.1 M KP_i buffer pH 7.0	60
170	33	Extract./distill.[b]	92

a Data from Table 3.1.4 inserted as comparison.

b Reactions operated in distilled water with pH control and autotitrator (3M HCl).

Hexane was chosen as a solvent because of the satisfactory performance in view of conversion, enzyme stability, product purity and boiling point (allowing faster product isolation). However, hexane is considered in modern solvent selection guides to be a non-desirable solvent, and for this reason alternative solvents were investigated (Table 3.2.5).

Table 3.2.5: Conversion in 2LPS. Reactions performed using 29 μg mL^{-1} (1.8 U mL^{-1}) McPAD, in 0.1 M KP_i buffer (0.5 M in case of 100 mM FA) pH 7.0 and a buffer:solvent ratio 1:2 (v/v).

Solvent (mM)	Solubility in water*	LogP	Concentration (mM)	X (%)
Heptane	0.01	4.5	5	>99
Heptane	0.01	4.5	100	90
MTBE	1.4	1	5	96
MTBE	1.4	1	100	45
2-MeTHF	4.4	0.7	5	9**

* g 100 mL^{-1}, 20°C; ** High standard deviation

Alternatives such as methyl *tert*-butyl ether (MTBE), 2-methyl-THF (2-MeTHF) and heptane were tested. The reaction could proceed smoothly to 96% conversion at 5 mM FA using MTBE as the second phase but only to 45% at 100 mM. 2-MeTHF probably causes an instantaneous enzyme deactivation, since it provided similar results as those obtained with EtOAc, given in Table 3.1.2. Heptane seems to be the best alternative, as the reaction could perform as well as in hexane. In general, solvents with $logP$ lower than ≈ 1 and water solubility higher than ≈ 2 g in 100 mL are found to be detrimental to the enzyme. This behavior can be related to the stripping of water molecules by hydrophilic solvents that are tightly bound to the enzyme, therefore distorting the active conformation (Laane 1987).

In conclusion:

- McPAD showed to have a 3.5 times higher stability in buffer:hexane with respect to the sole buffer;
- The kinetics of the enzyme in the two liquid-phase system (2LPS) was used to propose and validate a kinetic model including product extraction in the organic phase;
- The use of a 0.5 M potassium phosphate buffer allowed the employment of 100 mM substrate concentration affording 95% conversion and 79% isolated yield in mg scale; the reaction, performed in gram scale, afforded the isolation of the target product in 75% yield;
- A reactor set-up including solvent distillation and product isolation improved the reaction at 100 mM ferulic acid (>99 % conversion) and allowed the use of 170 mM ferulic acid (92% conversion);

- Solvent screening showed that heptane is a valid alternative to be used for this reaction in an industrial context.

3.2.2 Synthesis of 4-Ethylguaiacol via Chemoenzymatic Sequence

The hydrogenation of 4VG was attempted in a 2 mL scale using the homogeneous Wilkinson catalyst (*$RhCl(PPh_3)_3$*) and the heterogeneous Pd/C. The use of the Wilkinson catalyst (1-10 mol%) afforded low starting material conversion (less than 10%) after 1 h of reaction at room temperature under a hydrogen atmosphere. The reaction did not proceed further. Temperature increase up to 40°C and change of the solvent (toluene, methanol, DCM) did not improve the reaction performance. These results point out that the catalyst is inhibited/deactivated by the substrate, possibly *via* coordination of the phenolic group. Pd/C, on the other hand, was able to catalyze the transformation very efficiently (Scheme 3.2.2).

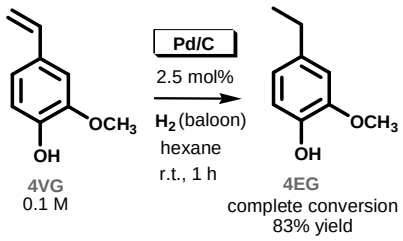

Scheme 3.2.2: Hydrogenation of 4VG to 4EG using Pd/C as catalyst.

The reaction afforded the expected product 4EG with complete selectivity in 83% isolated yield after a simple filtration of the catalyst and solvent evaporation. The complete two-step PAD-Pd/C sequence was performed on a gram scale (1.9 grams FA) in 100 mL volume, where after the biocatalytic reaction the organic layer was withdrawn with a syringe and transferred into the reactor containing the metal catalyst. An isolated yield of 70% for the final product was achieved. In Figure A27 two vials containing 1 g 4VG and 1.1 g 4EG synthesized in the preparative scale experiments are shown. The identity of both products was verified by TLC and HPLC by comparison with commercial reference materials, and by GC-MS (Figure A27). The different performances in terms of reaction rates and conversion displayed by the two steps show that the bottleneck of the whole system is the enzymatic step, which needed more research efforts to be optimized in view of substrate

concentration, biocatalyst loading and reaction conditions. The whole sequence can be performed using heptane as a more industrially preferred solvent, as also the hydrogenation step can be performed in heptane maintaining the performances unchanged.

In conclusion:

- Palladium on charcoal allows a rapid and convenient hydrogenation of 4-vinylguaiacol to 4-ethylguaiacol, in contrast to the use of the (Rh-based) Wilkinson catalyst, probably due to the catalyst deactivation;
- A decarboxylation-hydrogenation reaction sequence was demonstrated up to the gram scale yielding the final target product with 70% isolated yield.

4 Discussion and Outlook

Despite the enormous amount of information about biocatalysis, research efforts are continuously applied in different aspects of this highly interdisciplinary field. This is evident through the publication of related research reports in a variety of different scientific journals, which traditionally deal with either pure biology, chemistry or engineering. However, the knowledge and understanding of biocatalysis at the molecular level has been only achieved in the last 50 years, a relatively recent time if compared with its closest relatives biology and chemistry. This indicates that there is still a strong need to understand how enzymes manage to catalyze their reactions; such knowledge, aside from contributing to (chemical) biology, is also necessary for designing applications. The most straightforward application of enzymes is in chemical production, for which the knowledge of the catalytic system is needed for designing reaction engineering as well as enzyme engineering strategies in order to find the best desired performances. In this work, phenolic (de)carboxylases (EC 4) were analyzed from a fundamental point of view and for application purposes. Despite their biological role, they are capable of catalyzing both carboxylation and decarboxylation directions. Therefore, the "(de)" is applied in parentheses. The enzymes studied were two *ortho*-(de)carboxylases (Rsp_DHBD and Ao_DHBD) and one *para*-(de)carboxylase (McPAD). Having different selectivities and being studied focusing in different reaction directions, the two types of (de)carboxylases will be discussed separately.

The two *ortho*-(de)carboxylases were studied with respect to the carboxylation direction due to greater relevance for applications. In fact, such an enzymatic route has the potential to substitute the large scale synthesis of salicylic acids, realized since the 1860s *via* the Kolbe-Schmitt (KS) method (Schmitt 1885). The KS reaction utilizes high energy inputs for pressure and temperature and is not completely regio-selective, therefore presents environmental and safety issues (Lindsey A & Jeskey H 1957). From a plan view, *ortho*-decarboxylases can be included in the group of metalloenzymes where Zn^{2+} behaves as Lewis acid, or, in other terms, as a superacid, with the purpose of polarizing substrate molecules. Members of this group with their respective functions are shown in Table 4.1.

Table 4.1: Summary of the reactions catalyzed by Zn(II)-dependent enzymes.

Enzyme class	Catalytic function	Example
Hydrolases	Hydrolysis reactions (C–N, C–O, C–Cl, C–S and O–P)	Thermolysin (hydrolysis of peptides)
Lyases	Nucleophilic addition of OH^-	Carbonic anhydrase (hydration of CO_2); phloretin hydrolase (cleavage of aromatic hydroxy-ketones)
	C–C bond formation/cleavage	
Oxidoreductases	Nucleophilic addition of H^-	Alcohol dehydrogenase (reduction of ketones)

What makes Zn^{2+} so useful for enzyme catalysis is its potential to establish labile four-, five- and six-coordinated complexes, ensuring versatile binding and unbinding events with amino acids, water and substrate molecules (Andreini *et al.* 2008). Dihydroxybenzoic acid (de)carboxylases (DHBDs), although structurally not comprehensively studied, are Zn^{2+}-dependent lyases where the metal ion activates bicarbonate in the carboxylation direction (increasing its electrophilicity) and behaves as an "electron sink" in the decarboxylation direction. Similar to the chemical KS reaction, the carboxylation of phenolic compounds catalyzed by DHBDs occurs *via* electrophilic aromatic substitution. Interestingly, there is a striking similarity between the protein sequences of DHBDs and the amidohydrolases (AHs) superfamily; these enzymes constitute a well characterized superfamily of mononuclear or binuclear *d*-block metallo-proteins. They are comprised of a typical $(\beta/\alpha)_8$-barrel structural fold and catalyze a plethora of hydrolytic reactions[11], including nucleophilic aromatic substitution by water (adenosine deaminases) (Seibert & Raushel 2005). In fact, the DHBD from *Rhizobium* sp. (Rsp_DHBD, also known as γ-resorcylate decarboxylase) is considered a member of this superfamily because it shows sequence identities of 99 to 72% (query coverage of 100 to 98%) with respect to different AHs from related organisms. It is important to stress that the two enzyme types belong to different EC classes. As a matter of fact, the similarity is also mechanistic because the DHBDs are non-oxidative (de)carboxylases which, considering the carboxylation direction, form the C–C bond with the consequent elimination of one water molecule. We demonstrated that there is even a functional similarity by showing that Rsp_DHBD is able to catalyze the hydrolysis

[11] 18 different structurally and functionally characterized AHs have been reported.

of an activated ester bond with significant activity (1 U mg^{-1} for *p*-nitrophenylacetate as substrate). AHs such as carboxylate esterases and Zn-dependent lyases (*i.e.*, carbonic anhydrases) are able to act on similar phenyl esters (Xiang *et al.* 2014). This fact additionally highlights the common role of the Zn^{2+} catalysis in the metallo-proteins summarized in Table 4.1. Looking at the vast collection of reactions contained in such metal-containing active sites, it appears clear that the elucidation of the catalytic determinants for hydrolytic activities and for aromatic substitution reactions is highly desired to define substrate specificity and the synthetic creation of novel activities by protein engineering. As already mentioned, the DHBD-catalyzed *ortho*-carboxylation occurs via electrophilic aromatic substitution. In brief, the C–2 aromatic carbon is activated for nucleophilic attack by an aspartate residue which is hydrogen-bonded to the phenolic group, while the electrophile (*i.e.*, bicarbonate) is polarized by the metal-center. This mechanism is confirmed by our linear free energy relationship studies realized with the DHBD from *Aspergillus oryzae* (Ao_DHBD), for which the logarithms of both –apparent– equilibrium constants and enzyme activities increase with increasing electron donation of the substituents to the nucleophilic center. Such a behavior is typical for this reaction type and also known for the classical chemical KS reaction. (Bio)chemical factors are probably behind the unexpected non-reactivity of phenolics with electron donors in *para* positions as well as for the unexpected high reactivity of 1,2-dihydroxybenzene (catechol) and *meta*-methoxyphenol. At the same time, further biochemical studies would be necessary to determine the reasons for the highly restricted substrate scope of Rs_DHDB compared to Ao_DHBD. The fact that only catechol and *meta*-methoxyphenol are accepted by the *Rhizobium* sp. variant suggests that a detailed look into the catalytic pathway at the transition-states level may provide satisfactory answers.

The (de)carboxylation of aromatic compounds *in vivo* is part of different catabolic pathways which deal with the transformations of phenolics and hetero-aromatics. Even though these biocatalysts are able to catalyze the transformation in both reaction directions, each enzyme appears to have only one physiologically important function. In particular, the carboxylation of the phenolic moiety in the *para* position is required in the anaerobic metabolism of phenol (*e.g.*, in *Thauera aromatica*, a denitrifying and facultative aerobe bacterium) (Schühle & Fuchs 2004) while the *ortho*-decarboxylation (*e.g.*, in *Rhizobium* sp. an aerobe bacterium) is required for the degradation of salicylic acids and hetero-aromatics such as indole

(Santha *et al.* 1995; Yoshida & Nagasawa 2000). Scheme 4.1 compares the metabolic pathways for the catabolism of phenol and 2,6-dihydroxybenzoic acid in the two bacterial strains mentioned as examples.

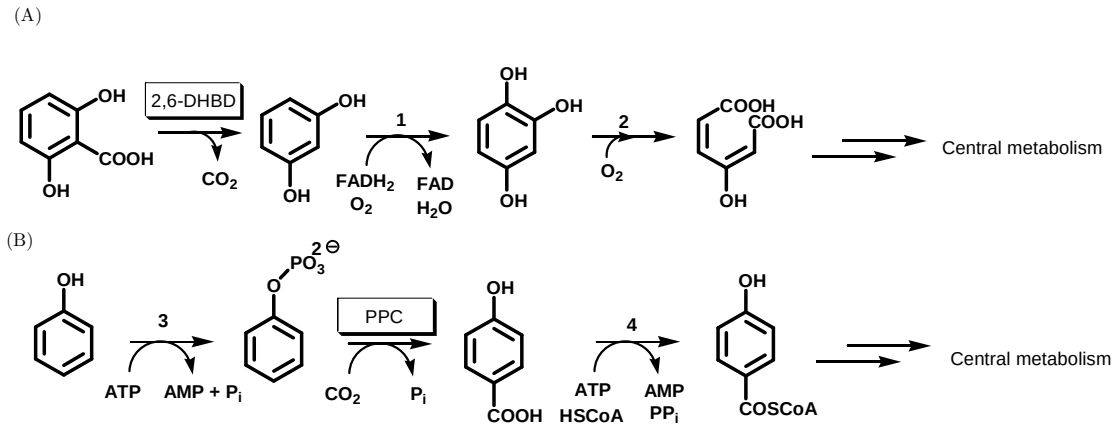

Scheme 4.1: (A) aerobic biodegradation of γ-resorcilic acid in *Rhizobium* sp.; **1**: resorcinol hydroxylase, **2**: hydroxyquinol 1,2-dioxygenase; (B) anaerobic biodegradation of phenol in *Thauera aromatica*, **3**: phenylphosphate synthase, **4**: 4-hydroxybenzoate CoA ligase.

In fact, there are no known metabolic pathways where the *ortho*-carboxylation is the physiologically relevant direction. These differences in biological functions can also be discussed by looking at the kinetics and mechanistic differences. It was shown that the K_M values for the Rsp_DHBD-catalyzed *ortho*-carboxylation are 35 mM for catechol as substrate and more than 800 mM for bicarbonate, which are far beyond the concentrations that occur *in vivo*[12]. This, in addition to a specificity constant (V_{max}/K_M) for the decarboxylation direction which is two and three orders of magnitude bigger than for the carboxylation (for catechol and bicarbonate, respectively), would make the carboxylation a very inefficient metabolic reaction to be pursued by living cells. As mathematically clarified by the Haldane equation, such differences in the kinetic constants are typical for thermodynamically constrained reactions. In this view, the *ortho*-carboxylation appears more as an "unnecessary" and "useless" reverse activity of the enzyme. Contrarily, the *para*-carboxylation of phenol catalyzed by phenylphosphate carboxylase (PPC) is the direction which effectively occurs *in vivo*. The thermodynamic constraint is overcome, in this case, by using phenylphosphate as substrate, which, by hydrolysis at the active site, provides a significant negative free energy contribution (Schühle & Fuchs 2004). Moreover, the upstream ATP hydrolysis to realize phenol phosphorylation provides a further

[12] The concentration of phenolic metabolites *in vivo* is in the µM-mM range, while the concentration of CO_2 is in the tenths of mM range.

favorable thermodynamic contribution to the metabolic network involved with *para*-carboxylation. Dissolved carbon dioxide is the effective substrate for the *para*-carboxylation and its K_M of 1.5 mM additionally supports this statement because of the order of magnitude of the *in vivo* concentrations (Schühle & Fuchs 2004). The strict preference for bicarbonate or dissolved CO_2 is an interesting feature of the two enzyme types which, since the structure of the PPC has so far not been elucidated, cannot yet be comprehensively explained. That carbon dioxide is the substrate for PPC can be justified by its higher electrophilicity, which would ensure higher reactivity. The necessity of Mg^{2+} as a cofactor may be necessary to bind CO_2 and increase its electrophilicity, but how this is realized and why specifically Mg^{2+} is used still remain unsolved questions. In general, this would be a necessary step to understand the different activation strategies. For the DHBDs studied in this work, the only possibility to run the biotransformation using CO_2 was to establish an *in situ* pre-conversion to bicarbonate using primary, secondary or tertiary amines in concentrations up to 2 M. The biocatalysts showed comparable performances in the novel reaction medium compared with the standard procedure in potassium bicarbonate and even improved performances in terms of both initial reaction rate and equilibrium conversion when catechol was used as the substrate. For example, a five-fold reaction rate and a two-fold increase in equilibrium product concentration were achieved using 1 M diethylamine/CO_2 instead of $KHCO_3$. The reason for such improved features are not clear at this stage and further fundamental chemical and biochemical studies, such as enzyme crystallization in the presence of catechol and alkylammonium bicarbonates are required.

Even though the enzymatic *ortho*-carboxylation appears to be non-relevant in metabolic pathways, its implementation in the industry would provide a milder and more selective route to salicylic acids, which are important industrial intermediates (Boullard *et al.* 2000; Ritzer & Sundermann 2000). A collection of stoichiometric as well as catalytic routes to these compounds is presented in Scheme 4.2.

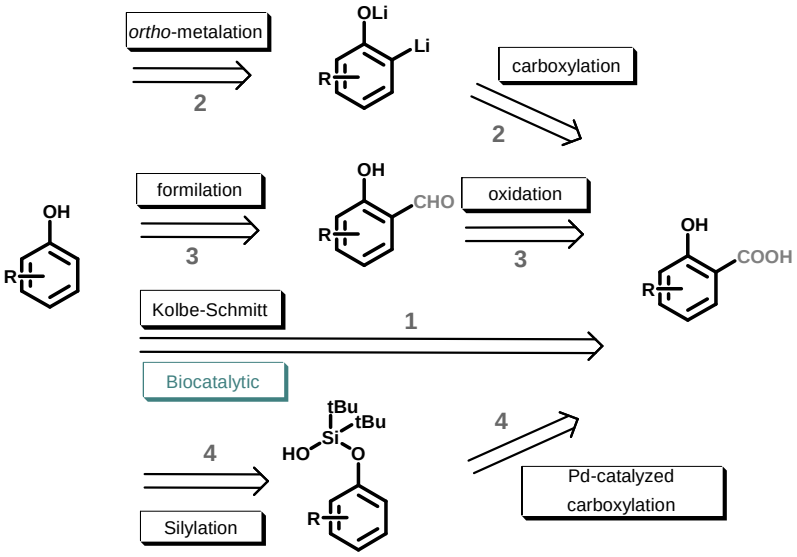

Scheme 4.2: Retrosynthetic analysis for the synthesis of salicylic acids.

As it can be easily seen, only the KS reaction –the only one implemented at large scale– and the enzymatic variant described in this work allow the direct carboxylation of phenols (Route 1). Route 2 and 4, for example, require the preliminary formation of a C–Li bond or of phenolic group silylation (Posner & Canella 1985; Wang & Gevorgyan 2015), respectively. However, the reaction thermodynamics in the conditions of the enzymatic carboxylation is extremely unfavorable, so that a 30-fold molar excess of co-substrate is needed to reach equilibrium conversions which are average 25%; in exceptional cases, when an electron donating group is in *meta* to the phenolic group, equilibrium conversions are as high as 70%. Converting in mass ratio of co-substrate to substrate, it is possible to say that ≈ 300 g of potassium bicarbonate are needed to produce ≈ 0.5 g of salicylic acid. Moreover, downstream processing is also problematic because the substrate and the product have to be separated from a concentrated salt solution. The easiest strategy would probably be medium acidification to protonate the salicylic acid and extraction in organic solvent. However, the acidification of a 1-3 M bicarbonate solution generates salt waste and carbon dioxide. Therefore, reaction engineering needs to play a key role in view of the implementation of this reaction. After conducting studies on *in situ* product removal (ISPR) approaches to selectively adsorb or extract the product, it is possible to conclude that due to the specific reaction conditions (concentrated aqueous bicarbonate solution at pH 8.0) and the similarity the products with their substrates (phenolic aromatic ring and carboxylate

functional group of the co-substrate), such strategies are not feasible for application due to the lack of selectivity. Interestingly, organic co-solvents are able to increase the equilibrium conversion up to two-fold, likely due to the decrease of salicylic acid free energy. However, the increased conversions are still below 50% and do not solve issues such as the use of molar bicarbonate concentrations and the subsequent problematic downstream processing. Recently, it has been shown that the carboxylation of catechol and resorcinol can be pulled to complete conversion by precipitating the reaction products with long-chain tetra-alkylammonium salts (Ren *et al.* 2016). This represents the first example of an enzymatic *ortho*-carboxylation protocol which runs until complete substrate consumption. It is reasonable to state that such a procedure probably has a promising future only on the lab bench because of comparable prices of the salicylic acids and the ammonium-based additive –which has to be added in two-molar fold–, the unsolved issue of the downstream processing and the limited substrate scope, which was verified in our laboratories by performing the reaction in the same reported conditions with two mono-hydroxy phenols. In general, the *ortho*-carboxylation of phenolics represents an interesting system to study from a fundamental point of view; as this work shows, this biotransformation generates "surprises" which contribute to the understanding of how enzyme catalysis works and how it differs from the known chemical methods. The applicability on large scale is, at this stage, limited by the intrinsic thermodynamics of the system. In future works, attention could be given on the establishment of reaction cascades to pull the equilibrium, forming additional products from salicylic acids (Scheme 4.3).

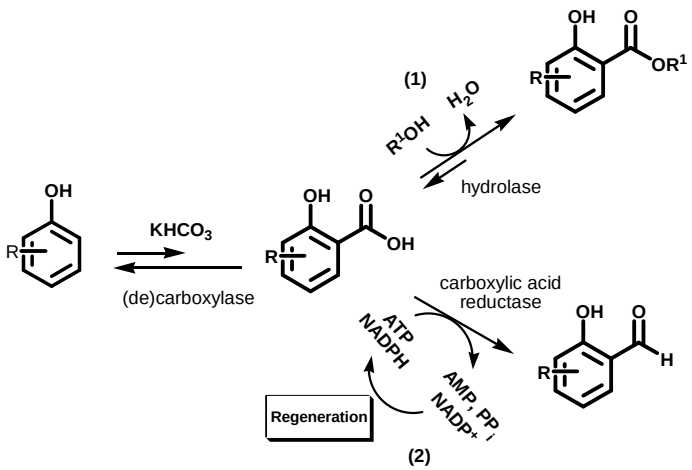

Scheme 4.3: Enzymatic cascades which would drive the enzymatic carboxylation of phenolics;.

Examples in this regard could be esterification with hydrolases (Scheme 4.3, route 1) –such as *Candida antarctica* lipase A, capable of performing esterification in aqueous media– or reduction by ATP-NADPH dependent carboxylic acid reductases (Scheme 4.3, route 2) (Brenneis & Baeck 2012; Gross & Zenk 1969; Li & Rosazza 1997). Important issues for both coupling reactions regard the low activity of the most current reported biocatalysts towards salicylic acid scaffolds. Carboxylic acid reductases show the additional drawback of requiring expensive cofactors, which follows the need to establish cofactors regeneration methods The low reactivity of carboxylic acids make the developments of chemoenzymatic strategies to pull the equilibrium also infeasible at this stage of knowledge. The development of chemocatalytic systems able to reduce the carboxylic functionality in water and ambient conditions would be highly desirable, though none have been discovered so far (Falorni *et al.* 1999; Kanth & Periasamy 1991).

The phenolic acid (de)carboxylase from *M. colombiense* (McPAD) studied in this work belongs to a well characterized family of proteins (Pfam entry: PF05870) which catalyze the decarboxylation of hydroxycynnamic acid, which are associated with the metabolism of lignin compounds and common to both bacteria and fungi. Contrary to the DHBDs, these enzymes show a complete *beta*-selectivity (on the C–C double bond). In the last 3-4 years, it has been demonstrated that PADs are also able to work in the carboxylation direction –with a thermodynamic profile very similar to that described for the *ortho*-carboxylation– (Wuensch *et al.* 2015) and that they are able to catalyze a promiscuous asymmetric hydration of hydroxystyrenes on the C–C double bond, although with enatioselectivities ≤ 70%, (Wuensch *et al.* 2013a). As with DHBDs, the natural function of PADs is in the "downhill" decarboxylation direction. The decarboxylation mechanism seems to be common to all PADs characterized so far and follows acid-base catalysis principles, where the required *para*-phenolic group serves as an electron sink to drive CO_2 release. As structural data show, the phenylacrylic acid decarboxylases acting on cinnamic acids, lacking the phenolic group, use a different catalytic strategy (Kopec *et al.* 2011; Rangarajan *et al.* 2004; Richard *et al.* 2015). Hydroxycinnamic acids, and in particular the three lignin-derived building blocks ferulic acid, sinapic acid and *para*-coumaric acid, are abundant and cheap biomass-derived starting materials. Once subjected to suitable "deoxygenation" protocols (*i.e.*, removal of the high oxygen content of biomass-derived substances), these three molecules could be utilized as

"modern" building blocks for aromatics. The use of PADs to remove the carboxylic group generating the versatile vinyl moiety has generated increased interest in the last years. The C–C double bond could be exploited to realize follow-up reactions; in fact, a strategy to subsequently polymerize 4-vinylguaiacol (4VG, product of ferulic acid decarboxylation) has been recently reported (Leisch *et al.* 2013). The combination of PAD-catalyzed decarboxylation and Pd-catalyzed hydrogenation to produce 4-ethylguaiacol (4EG) from ferulic acid (FA) was investigated. 4EG is an FDA-approved flavoring agent characterized by a smoked aroma which appears in nature in a variety of vegetables and beverages such as wine and beer. The intermediate of the reaction sequence, 4-vinylguaiacol (4VG), is also an industrially produced flavoring agent, the use of which is approved by the FDA, and it is characterized by a pleasant, sweet-smoked aroma. The price ratio (€ kg^{-1}) between 4VG, 4EG and FA (3.3 and 5, respectively[13]) indicates that the development of new and cleaner routes (*e.g.*, according to the principle of green and sustainable chemistry) are of current interest. A detailed investigation on research papers and patents show that the main routes to access 4VG and 4EG are the ones showed in Scheme 4.4:

[13] Prices for substances purity of 98-99% from Sigma Aldrich and Alfa Aesar catalogues (June 2016) considering the largest stocks available.

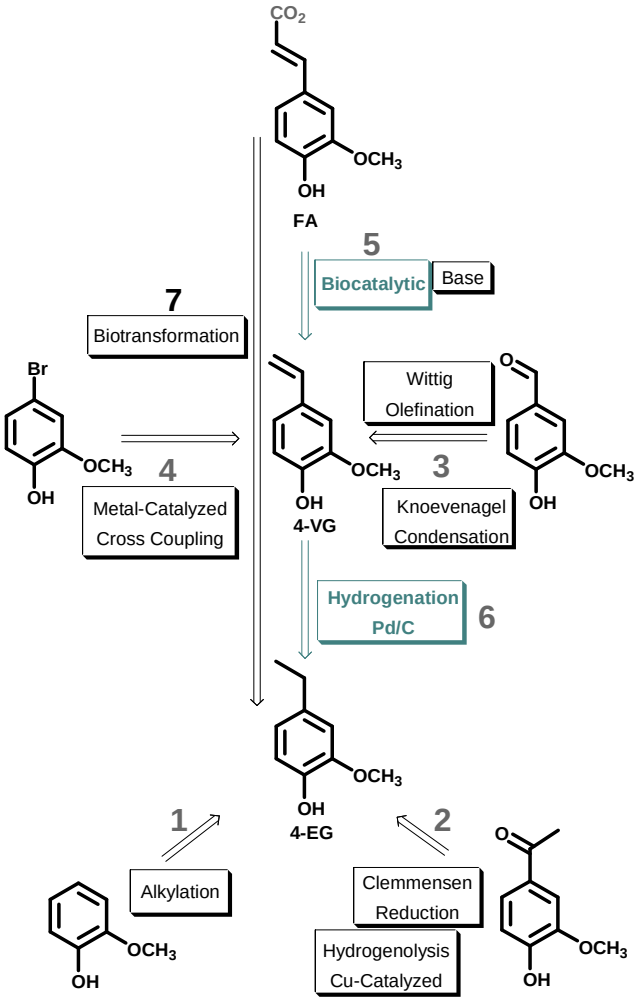

Scheme 4.4: Retrosynthetic analysis for the syntheses of 4VG and 4EG.

Route 1 to 4-EG *via* Friedel–Crafts alkylation was inserted as a reference from traditional organic chemistry, as on paper it is probably the least desirable. In fact, recent selectivity studies using acid catalysts show a high competition between C- and O-alkylation and incomplete regioselectivity in the C-alkylation due to the activation of multiple carbon atoms exerted by the phenol and methoxy groups (Yadav & Pathre 2007). Route 2 is selective and involves complete C=O-reduction of acetovanillone, a classic example of the Clemmensen reduction, a stoichiometric synthesis approach with the use of amalgamated Zn in acid under reflux conditions (Chittimalla *et al.* 2014). A recently developed alternative is the Cu-doped porous metal oxide-catalyzed hydrogenolysis, with low catalysts loading (0.3 mol%) and methanol as solvent (Petitjean *et al.* 2016). In addition to its full chemo-selectivity, this method uses an abundant metal in catalytic amounts. However, drawbacks include the need for a H_2 pressure of 40 bar and a temperature of 180°C. Milder hydrogenation conditions can be applied using palladium on charcoal (Pd/C)

catalysis (route 6). 4VG can be synthesized starting from the corresponding aldehyde (route 3) in a Knoevenagel–Doebner condensation using malonic acid and piperidine as an organocatalyst (Simpson *et al.*) in pyridine (Aldabalde 2011) or by Wittig olefination (Rein *et al.* 2005). Regarding cross-couplings using aryl bromides (route 4), the efficient Heck cross-coupling catalyzed by palladacycles at low ethylene pressure can only be used if the phenolic hydroxyl group is protected (Smith & Rajanbabu 2010). Alternatives are the Pd-catalyzed cross-coupling using vinyl Grignard reagents (Bumagin & Luzikova 1997) or the Stille coupling (Littke *et al.* 2002). Route 5 indicates the decarboxylation of FA. In addition to the PAD-catalysis, this reaction can also be performed chemically by treating FA with a base and with high energy inputs (inorganic base in refluxing dimethylformammide (Kunitsky *et al.*) or under microwave irradiation using either DBU (1,8-diazabicycloundec-7-ene) or $NaHCO_3$/*[Hmim]Br* (ionic liquid) (Bernini *et al.* 2007; Sharma *et al.* 2008)). It is worth mentioning that fermentation protocols using either wild-type fungal strains (*Candida* and *Aspergillus* (Baqueiro-Peña *et al.* 2010; Suezawa & Suzuki 2007) or engineered *E. coli* strains (Kang *et al.* 2015)) yielding 4VG and 4EG from FA were established (route 7); 4-VG can also be reduced enzymatically by NADH-dependent vinyl phenol reductases (Tchobanov *et al.* 2008). However, this *in vivo* strategy yields, in general, low productivities due to the use of low initial FA concentrations. As already discussed, routes 5 and 6 constitute the focus of this work. Previously uncharacterized, the McPAD studied shows similar features to other reported PADs, hence: *i)* its ability to catalyse the decarboxylation reaction to complete conversion –as already discussed, the decarboxylation is virtually irreversible–, *ii)* a K_M for FA in the mM range, *iii)* a relatively high V_{max} (90 U mg^{-1}, although lower than for other reported PADs), *iv)* a slightly acidic-neutral pH optimum and *v)* strong inhibition by the product (K_i = 0.14 mM; K_M/K_i = 17). Product inhibition strongly limits the reaction at high substrate and low enzyme concentrations (McPAD/FA ratio ≈ 6 when enzyme is in µg mL^{-1} and FA is in mM). Moreover, our kinetic data and their validation through computer simulations suggest that reversible competitive product inhibition is not the only mechanism playing a role when the concentration of the product is high with respect to the McPAD concentration. Further elucidation of this unexpected behaviour would need further molecular as well as structural data to be clarified. From a practical point of view, a two liquid-phase system (2LPS) is able to continuously extract the product in the organic phase, limited by its partition coefficient in the specific reaction

conditions, restricting its interactions with the enzyme. After solvent screening, we found hexane to be a good choice because of the partition coefficient ($logK_P = 0.5$), extraction rate (0.4 mmol L^{-1} min^{-1}), enzyme stability (> 3 times higher with respect to the sole buffer) and product purity (transparent oil giving a single peak in HPLC, GC-MS analyses and a single spot in TLC). After the optimization by choosing the temperature, pH, buffer capacity, FA concentration and organic:aqueous solvent ratio, the biotransformation was carried out at 0.1 M FA obtaining 79% isolated yield of 4VG. Conversions higher than 90% were demonstrated also at 0.17 M FA using a modified reactor set-up which tackles the partition coefficient at high 4VG concentrations. A straightforward hydrogenation conducted in the organic phase using Pd on charcoal (Pd/C) under a hydrogen atmosphere afforded 4EG with an isolated yield of 70%.

Even at early stage of developments, the evaluation of a chemical process in terms of its environmental impact is a good practice in modern organic chemistry. In this context, the E-factor ($kg_{waste}/kg_{product}$) is a simple but indicative estimation of the environmental impact of a synthetic procedure (Sheldon 2007). The whole environmental impact (*e.g.*, quantified by "life-cycle assessment") requires the integration of many factors, dealing with economics (*e.g.*, price/synthesis of starting materials, products, catalysts, waste disposal, etc.) and human and environmental safety. However, calculations of E-factors allow quantitative comparison of methodologies even at the first stages of development and the understanding of where improvements are necessary. Therefore, E-factors for the first PAD-catalyzed step, leading to 4VG, and for the whole PAD-Pd/C reaction sequence, leading to 4EG, were calculated and compared. According to Scheme 4.4, the comparison for the 4VG synthesis was realized with the routes 3, 4 and 5 (base-catalyzed decarboxylation). E-Factors were calculated separately for the reaction (Figure 4.1(A)) and for the product isolation (Figure A28(A)); solvents were addressed separately and expressed as solvent demand (mL solvent per gram of product, Figure A28(B)).

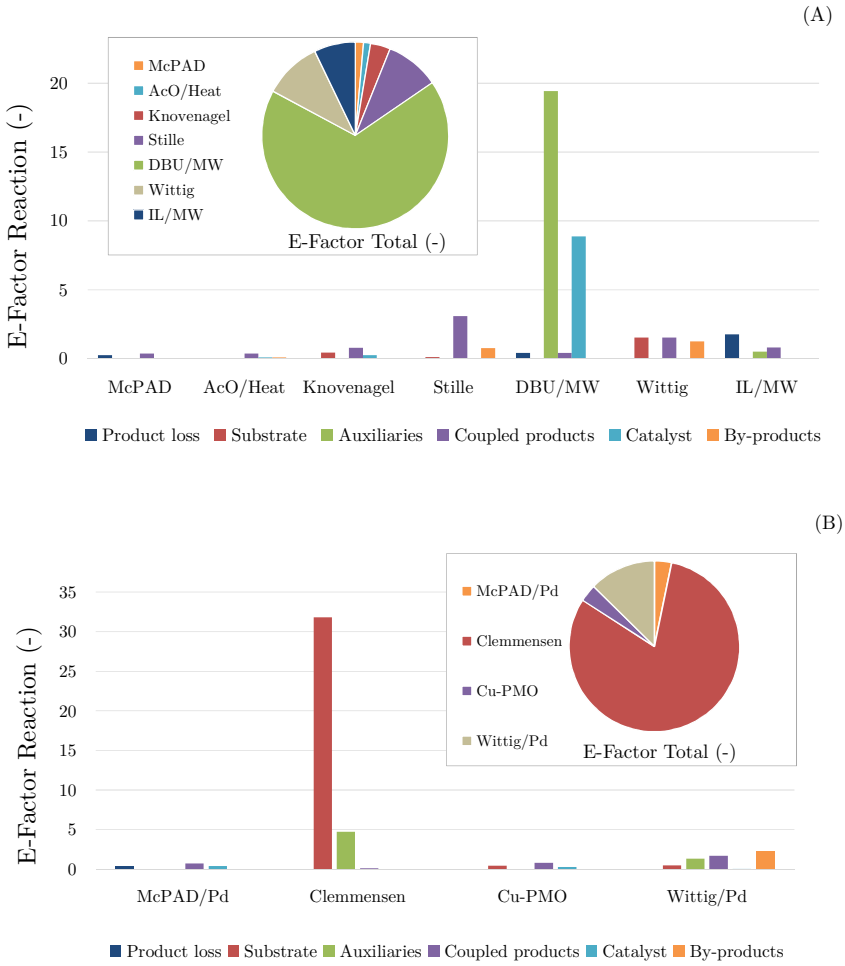

Figure 4.1: (A): Comparison of E-factors for the synthesis of 4VG, AcO/heat decarboxylation from reference (Kunitsky *et al.*), Knovenagel condensation from reference (Aldabalde 2011), Stille coupling from reference (Littke *et al.* 2002), DBU/MW decarboxylation from reference (Bernini *et al.* 2007), Wittig reaction from reference (Rein *et al.* 2005), IL/MW decarboxylation from reference (Sharma *et al.* 2008); (B): Comparison of the E-factors for the synthesis of 4EG, Clemmensen reduction from reference (Chittimalla *et al.* 2014), Cu/PMO hydrogenolysis from reference (Petitjean *et al.* 2016), Wittig-Pd sequence from reference (Broekhof 1986).

The chemical route (acetate-catalyzed under heating) and the biocatalytic route from FA appear to be comparable, most likely due to the fact that these routes avoid the more complex construction of C–C bonds. The advantage of the enzymatic route becomes clear when considering the E-factor for the work-up and isolation (Figure A28(A)), which brings, for example, an increase of approximately 150-fold for the heat/base decarboxylation, without considering chromatography. However, due to the enzyme features and the partition coefficient of the product, the reaction's solvent demand for the enzymatic route is the highest (Figure A28(B)). The sub-molar reactant concentrations in enzymatic reactions are in fact a preponderant

cause of high E-factors (Ni *et al.* 2014). However, considering both reaction and isolation together, the biocatalytic route has the second lowest value among the seven routes (Figure A28(B)). The synthesis of 4EG in the two-step sequence was compared with route 2 and 3 –*via* the stoichiometric Clemmensen reduction, the recent catalytic reduction, and the Wittig/hydrogenation sequence–. The alkylation route is difficult to compare because of the unavailability of data, especially for selectivity, and because these reactions are normally conducted in the gas phase in continuous flow. Figure 4.1(B) shows the results in terms of the E-factor for the reaction. The superiority of the catalytic routes is evident. Due to the relatively low concentration of the starting material in the enzymatic reaction, the E-factor for work-up/isolation and the solvent demand are quite high. Such values are direct consequences of the large volumes used (Figure A29). Solvent recycling, as shown in Figure 3.2.3-3.2.4 is clearly an appealing solution to substantially decrease the overall solvent load. In addition to that, high substrate concentrations would also lower the E-factor. Therefore, in order to be truly appealing, research efforts need to be concentrated to achieve ideal molar starting FA concentrations, either by means of reaction or protein engineering. The design of additional chemo-enzymatic follow-up reaction to the PAD-catalyzed decarboxylation would make hydroxycinnamic acids very useful aromatic building blocks. Examples in this context could be the synthesis of chiral epoxides or of more complex (aromatic) alkenes (*e.g.*, resveratrol) by methatesis reactions.

5 Conclusions

- A detailed study of the biocatalytic *ortho*-carboxylation of phenolics afforded the determination of kinetic and thermodynamic parameters and the proposal and validation *via* simulation of a rapid-equilibrium reversible random bi-uni mechanism. The parameters, all determined by experimental measurements, are in accordance with the intrinsic thermodynamic constraint.
- Linear Free Energy Relationships correlating kinetic and thermodynamic parameters of the reaction with steric and electronic constants of the substrates' substituents confirmed the nature of the mechanism used by the enzyme (*i.e.*, electrophilic aromatic substitution) and disclosed additional features of the *ortho*-decarboxylases, hence: the ability to exert different activation modes and the promiscuous hydrolytic activity towards activated phenyl esters.
- Studies on the nature of the co-substrate (CO_2 or HCO_3^-) show that the *ortho*-(de)carboxylases catalyze the carboxylation exclusively in the presence of bicarbonates. A new carboxylation reaction protocol using dissolved carbon dioxide in the presence of amines was developed and characterized. Higher reaction rates and equilibrium conversions with respect to the standard protocol were obtained when catechol is used as substrate.
- Attempts to "pull" the thermodynamic equilibrium by *in situ* product removal strategies showed that, due to substrates and reaction medium´s features, the biotransformation is not feasible for applications, especially because of high chemical similarity between product and starting materials (causing low selectivity for adsorption and extraction) and problematic downstream processing. The use of glycerol carbonate as additive was demonstrated to be a practical tool to increase equilibrium conversions up to two-fold.
- The kinetics of a phenolic acid (de)carboxylase for ferulic acid decarboxylation was studied *via* initial rate measurements as well as non-linear fitting. A catalytic mechanism was proposed and validated through simulations. Product inhibition was shown to be the most limiting factor for an efficient biotransformation.
- The decarboxylase-catalyzed ferulic acid conversion was investigated in two liquid phase systems (2LPS). Hexane-buffer was studied in more detail, also with the formulation and verification of a kinetic model. The

biotransformation was demonstrated on analytical as well as on preparative (gram) scale at 0.1 M substrate concentration and afforded the isolation of 4-vinylguaiacol (4VG) in 79% yield.

- A reaction sequence yielding 4-ethylguaiacol (4EG) after 4VG catalytic hydrogenation using Pd/C was demonstrated on analytical as well as on preparative scale starting from FA. The final product was obtained with an isolated yield of 70%.
- The synthesis procedures of 4VG and 4EG were compared to other protocols known in the literature in terms of E-factors. The methods developed in this work show a low E-factor in comparison with other chemical (stoichiometric as well as catalytic) methods. Increase of the starting FA concentration is critical for lowering the E-factor for product isolation and the solvents demand.

6 Experimental details

6.1 Materials

Chemicals. Starting materials and solvents were purchased from Sigma Aldrich, Roth and Alfa Aesar and used without further purification. Ready-to-use gels for SDS electrophoresis, sample and running buffers and coloring agent were purchased from Expedeon. *E. coli* BL21(DE3) for transformation were purchased from BioLabs. Ni-NTA agarose for protein purification was purchased from Quiagen.

Enzymes. The plasmid vectors pET21a+ containing the genes of the (de)carboxylases were kindly provided by Prof. Kurt Faber and Dr. Silvia Glueck (Graz University, Graz, Austria).

6.2 Methods

Competent cells transformation. This transformation procedure was followed for all of the three (de)carboxylases used in this work. In the pET21a+, Rsp_DHBD and McPAD genes are between HindIII and XhoI, while Ao_DHBD gene is between NdeI and XhoI. 2 µL of plasmid were added to a stock of *E. coli* competent cells (BL21(DE3)) in a 1.5 mL Eppendorf tube previously cooled on ice and mixed gently. A thermal shock was provided incubating the cells for 30'' at 42°C followed by a quick transfer on ice. After the addition of 250 µL of SOC medium (2% Trypton, 0,5% yeast extract, 10 mM *NaCl*, 2.5 mM *KCl*, 10 mM $MgCl_2$, 10 mM $MgSO_4$ and 20 mM glucose), the mixture was incubated for 1 h at 37°C and 225 rpm. The culture was transferred on agar plates containing LB medium, supplemented with 100 µg mL^{-1} ampicillin and incubated at 37°C overnight. The transformed cells were stores as cryostocks (Roti® Store Cryoröhrchen, Roth).

Cells fermentation and biocatalysts production. This protocol was used for all of the three (de)carboxylases used in this work. For pre-culturing, colonies from agar plates or a single bead from cryostocks, were added to 100 mL Erlenmeyer flasks

containing 20 mL Luria Bertani (LB) medium supplemented with 100 μg mL^{-1} ampicillin and incubated overnight at 37°C and 120 rpm. 1.5 L Erlenmeyer flasks were inoculated with the overnight culture (ONC) (3 mL ONC/500 mL LB medium) and the incubation was performed at 37°C and 120 rpm. When an OD_{600} between 0.6-1.5 was reached, the enzyme synthesis was induced with IPTG (2 mM for Ao_DHBD and 0.5 mM for the other enzymes) and the overexpression was continued overnight at 20°C, 120 rpm. The next day the cells were harvested by centrifugation and washed with 50 mM KP_i buffer pH 7.5. In case the biocatalysts were to be used as whole cells, aliquots of cell pellet were suspended in the minimal amount of 50 mM KP_i buffer pH 7.0, frozen at –80°C and then lyophilized.

Preparation of cell-free extracts. For the preparation of cell-free extracts (CFEs), wet cells were suspended in 50 mM KP_i buffer pH 7.0 (4 g mL^{-1} for Mc_PAD and 0.6 g mL^{-1} for the other enzymes) and the suspension sonicated (5 mm sonication tip, 70% power, 50% duty cycle, 3') on ice for three times and centrifuged at 24000 rpm (69673 rcf) for 20-30 min at 4°C. McPAD CFE were stored at –20°C, Rsp_ DHBD and Ao_DHBD CFE were stored at +4°C.

Enzyme purification via affinity chromatography. Enzyme purification was carried out using a Nickel-NTA-agarose packed column (9 cm high, conical 0.8 x 4 cm). After washing the column with an equilibration buffer (Tris 20 mM, NaCl 300 mM, imidazole 10 mM, pH 7.4) with 3 column volumes, the CFE was loaded by gravity using a ratio of 0.4 mL (10 mg of total proteins) of CFE per mL of chromatographic matrix for McPAD and of 0.5 mL (7.6 mg of total proteins) per mL of matrix. Unspecific adsorbed proteins were removed by washing with 5 column volumes of washing buffer (Tris 20 mM, NaCl 300 mM, imidazole 20 mM, pH 7.4) and the (de)carboxylase was eluted using 2.5 column volumes of elution buffer (Tris 20 mM, NaCl 300 mM, imidazole 250 mM, pH 7.4). Protein adsorption was carried out at +4°C, all the other steps were carried out at room temperature. Imidazole was removed by centrifugation (5000 rpm –3850 rcf– for 10' at +4°C) using tubes having a membrane with 10 KDa cut-off using an exchange buffer (KP_i buffer, 50 mM, pH 7.0) for storage.

Biotransformation of catechol to 2,3-DHBA. If not specified differently, carboxylation reactions were carried out in HPLC screw capped glass vials using an unbuffered $KHCO_3$ solution (pH 8.0, total volume 1 mL), shaking at 30°C and 500 rpm. After addition of $KHCO_3$, ascorbic acid and catechol in the desired

concentrations, the reactions were started by the addition of the (de)carboxylase in the appropriate amount. Data points were taken by diluting samples (50 µL) with a water/acetonitrile solution (20:80, 450 µL) supplemented with trifluoroacetic acid (3% v/v) to stop the reaction. The samples were centrifuged (5 min, 13000 rpm –15870 rcf–) and analyzed by HPLC.

Biotransformation of catechol to 2,3-DHBA under CO_2 pressure. The desired amounts of catechol, ascorbic acid and (de)carboxylase containing cell-free extracts were mixed in 0.2 M KP_i buffer pH 8.0, in a test tube, which was mounted to a Berghof RHS 295 high-pressure autoclave equipped with heating jacket, digital manometer and magnetic stirring; the temperature was directly controlled by a thermocouple. The autoclave was sealed and heated to 40 ± 1 °C and CO_2 preheated to 40 °C was slowly introduced to reach the target pressure. Once the desired pressure and temperature were reached, stirring was turned on at 500 rpm and the conditions were kept constant for 24 h. The pressure was then slowly released (5 bar min^{-1}) and the temperature was lowered to room conditions. Sampling were realized as over mentioned in the protocol at ambient conditions.

General procedures for carboxylation reactions catalyzed by Ao_DHBD. Carboxylation reactions were carried out in HPLC screw capped glass vials using an unbuffered 3 M $KHCO_3$ solution (pH 8.0, total volume 1 mL), shaking at 30°C and 500 rpm using 30 mg Ml^{-1} (2.1 U mL^{-1}) of *E. coli* whole lyophilized cells hosting the decarboxylase, 10 mM of phenolic substrate (supplemented either from a stock solution or neat in case of liquid phenolics). Data points were taken by diluting samples with a water:acetonitrile mixture (20:80) supplemented with trifluoroacetic acid (3% v/v). Samples were centrifuged (5', 13000 rpm, –15870 g–) and analyzed by RP-HPLC. The employed units in the reactions refer to the assay conducted using catechol as substrate.

General procedures for carboxylation reactions using CO_2/amines. In a 50 mL thermovessel, 8.98 mL 0.1 M KP_i buffer solution pH 8.0 containing 1 M amine (from Table 2.1.3) was saturated with carbon dioxide through bubbling aeration for 1 hour. After the addition of the phenolic substrate with a final concentration of 10 mM –and 10 mM ascorbic acid in the case of catechol–, 1 mL of *E. coli* lyophilized cells (final concentration 0.23 U mL^{-1} (3 mg mL^{-1})) containing the Ao_DHBD in 0.1 M KP_i buffer pH 8.0 was added to start the reaction. The lyophilized cells were pre-hydrated by shaking in the buffer for 10 min prior to the reaction. In case of strong

foam formation, a foam breaker was added on top of the set-up. Data points were taken by diluting samples with a water:acetonitrile mixture (20:80) supplemented with trifluoroacetic acid (3% v/v). Samples were centrifuged (5', 13000 rpm, –15870 g–) and analyzed by RP-HPLC. The employed units in the reactions refer to the assay conducted using 100 mM catechol as substrate in 2 M $KHCO_3$.

Monitoring bicarbonate formation using FT-IR spectroscopy. Bicarbonate formation was measured using an FT-IR probe connected to a Mettler Toledo ReactIR 45m equipped with a MCT detector, a silver halide optical fiber and a diamond crystal ATR probe. The apparatus was purged for 2 hours with nitrogen prior to utilization to remove the moisture and the detector was cooled with liquid nitrogen. A 50 mL thermovessel containing 1 M amine in 10 mL 0.1 M KP_i buffer, pH 8.0 was equipped with the IR probe, heated at 30°C and stirred at 500 rpm. Directly after start the bubbling aeration with CO_2, 64 scans per time point were recorded.

Hydrolytic assay for Rsp_DHBD. Assays were performed using a UVIKON XL spectrophotometer in 1 mL UV-transparent cuvettes. After the addition of the purified Rsp_DHBD (0.75-1.5 mg mL^{-1}) to a 1 mM *para*-nitrophenylacetate solution in 0.1 M KP_i buffer pH 7.0, the formation of *para*-nitrophenol was monitored at 402 nm.

Biotransformation of ferulic acid to 4-vinylguaiacol. Unless otherwise stated, for screening experiments and kinetic constants determination, assays were performed in 0.1 M KP_i buffer pH 7.0 in glass vials (1 mL volume) shaken at 700 rpm. After addition of the substrate, the reaction was started by addition of the enzyme. Samples (50 µL) were withdrawn and diluted with a water:acetonitrile solution (20:80 + 3% v/v trifluoroacetic acid) to stop the reaction. The samples were centrifuged (5', 13000 rpm –15700 rcf–) and analyzed by HPLC. Using the fermentation protocol and the CFE preparation method described in the previous section, 10-20 µL of extract (corresponding to 0.2-0.5 mg mL^{-1} total protein concentration in the assay) are appropriate to detect the linear range (less than 10 % conversion) in a 3 minutes time span. The U mL^{-1} values reported for each experiment refer to a reference assay performed in 1 mL volume in 0.1 M KP_i buffer pH 7.0, 5 mM FA, shaking at 37°C and 700 rpm. Apart from the kinetic measurements, reactions were performed using CFEs. Enzyme concentrations given in the text represent the target enzyme in the CFE.

Decarboxylation of FA in a 2LPS. The optimized reaction conditions at 100 mM FA concentration are described here as an example: 194 mg (1 mmol) of ferulic acid were added to a 50 mL thermostated vessel equipped with a magnetic stir bar. After the addition of 7 mL of an aqueous solution composed of 0.5 M KP_i buffer pH 7.0 and 70 mM KOH, the mixture was stirred vigorously at 37°C until FA was completely solubilized. After the addition of 20 mL of hexane, the reaction was started by the addition of the enzyme solution (3 mL, 90 µg mL^{-1} final concentration) into the aqueous layer and stirred at 37°C and 500 rpm. After the reaction, the organic layer was separated, dried over anhydrous magnesium sulfate, filtered and evaporated by rotary evaporator, yielding 118 mg (79% yield) of 4VG as transparent oil. The identity of the product was assayed comparing analytical data with the commercial reference material. TLC (R_f = 0.7 in hexane:EtOAc 2:1); GC-MS: m/z = 150 [M^+], 135 [$C_8H_7O_2^+$], 107 [$C_7H_7O^+$], 77 [$C_6H_5^+$]. For the experiments using 170 mM FA, the autotitration system Metrohm 848 Titrino plus was used. For the experiments using the integrated distillation set-up the tubings Fluran® (Ismatec IPC F-5500-A, 0.91 mm, Cole-Parmer) were used.

Synthesis of 4EG. 100 mM 4VG in hexane was transferred *via* syringe and under nitrogen flow into a two-neck reactor previously charged with Pd/C (2.5 mol%, 5% Pd basis) and connected to a hydrogen balloon. After three vacuum (2 mbar)-nitrogen cycles, the reaction was started by the establishment of a hydrogen atmosphere inside the reactor. The reaction was carried out for 1 h at room temperature under vigorous stirring. After the reaction, the mixture was filtered through Celite® under nitrogen gas to remove the catalyst and the solvent was evaporated to yield a transparent oil in 80% yield. In the synthesis starting from ferulic acid, the organic layer from the decarboxylation reactor was transferred into the hydrogenation reactor following the same steps as mentioned above. The identity of the product was assayed comparing analytical data with commercial reference material. TLC (R_f= 0.8 in hexane:EtOAc 2:1); GC-MS: m/z = 152 [M^+], 137 [$C_8H_9O_2^+$], 91 [$C_7H_7^+$], 77 [$C_6H_5^+$].

Determination of partition coefficients and extraction rates. Extraction parameters were calculated following extraction progress curves of 5 mM 4VG in buffer/organic solvents mixtures (1:1) in 1 mL volume in glass HPLC vials at 37°C and 700 rpm. The ratios of the concentration in organic/aqueous phase were calculated at equilibrium, which was reached under these conditions after

approximately 1 hour. Extraction rates were calculated by fitting the concentration increase in the organic phase to an exponential function.

Homology modelling and docking simulations. The structural model for the Ao_DHBD (2,3-dihydroxybenzoic acid (de)carboxylase from *Aspergillus oryzae*, sequence reference number: 5989458) was generated using Rsp_DHBD (2,6-duhydroxybenzoic acid (de)carboxylase from *Rhizobium* sp., PDB code: 2DVU) as the template. The homology model for McPAD (NCBI reference sequence: WP_007777524.1) was generated using PAD from *Bacillus subtilis* (PDB code: 2P8G) as the template. The models were obtained using the SWISS-MODEL server. Ao_DHBD and Rsp_DHBD showed a sequence identity of 45.6% and a GMQE (Global Model Quality Estimation) of 0.72. McPAD and PAD from *B. subtilis* showed a sequence identity of 54% and a GMQE (Global Model Quality Estimation) of 0.77. Substrates dockings were realized using Autodock 4.0 and Autodock Tools. For the *ortho*-(de)carboxylase: Ao_DHBD structure was cleaned, hydrogen atoms assigned and to the Zn ion a formal charge of +2 was assigned. The docking box was set to 60x60x60 around the active site. For the *para*-(de)carboxylase: McPAD structure was cleaned and hydrogen atoms assigned. The docking box was set to 20x20x20 around the active site. Results were clustered using the Lamarckian genetic algorithm (Morris *et al.* 1998). All visualizations were created using PyMOL.

Non-linear fitting protocols. Fitting of initial rates data to saturation kinetics equations and of reaction progress curves to exponential functions were performed with Microsoft Excel (Excel 2010, Microsoft) using the least squares method.

Estimation of the environmental factor (E-factor). E-factors were calculated with the aid of the free-ware software EATOS (Environmental Assessment Tool for Organic Syntheses). When not specified by the procedure, the following values were assumed: desiccant: 20 g L^{-1} of solution; Celite® for filtration: 0.1 g mL^{-1} of solution; silica gel for chromatography: 20 g g^{-1} of product; eluents for chromatography: 500 mL g^{-1} of product. Additional assumptions taken:

- Acetate/heat decarboxylation (Kunitsky *et al.*): the specific procedure refers to the decarboxylation of 4-hydroxycinnamic acid (the authors of the patent report this synthesis as general procedure); the final product was isolated as yellow powder, indicating that a further purification step is necessary (not included in the calculation); drying with anhydrous salt was assumed.

- Knovenagel condensation (Aldabalde 2011): neutralization and dilution with ice water; volumes were assumed to be equal to the volume of pyridine (values not reported in the original publication).

- Wittig olefination (Rein *et al.* 2005): the specific procedure refers to syringaldehyde; LiBr formed as coupled product of the ylide formation was also considered; the aqueous work-up mentioned in the original manuscript was assumed to proceed via extraction with ethyl acetate, washing with water and drying over sodium sulfate.
- Ionic liquid/microwave decarboxylation (Sharma *et al.* 2008): purification by column chromatography was assumed to be unnecessary, although this is not clear from the original manuscript.
- Stille coupling (Littke *et al.* 2002): the specific procedure refers to 4-hydroxybromophenol; "copious amounts of diethyl ether" described in the original manuscript was assumed as 10 times the volume of the diethyl ether (5 mL) added after the reaction.
- Wittig–Pd/C sequence (Broekhof 1986): the specific procedure refers to ethyl vanillin; LiBr formed as coupled product of the ylide formation was also considered; since the procedure requires the isolation of the intermediate, the global E-factor was considered as the sum of the E-factors for the individual steps.

- This work: reaction performed in distilled water as solvent and in the preparative scale of 100 mL volume using 100 mM ferulic acid; catalyst concentration refers to the concentration of active enzyme.

Matlab® scripts.

Kinetic model for the *ortho*-carboxylation:

Matlab function:

```
function dcdt = Kinetik_Lorenzo(~,c)
global cEnzyme vmax Km vmax2 Km2 Kmp Km2a
%c(1) = catechol
%c(2) = DHBA = 2,3-dihydroxybenzoic acid
%c(3) = KB = potassium bicarbonate
%Reaction equ.
vI=((vmax.*c(1).*c(3))./(Km*Km2)-
(vmax2*c(2)/Kmp))./(1+(c(1)/Km)+(c(3)/Km2a)+(c(2)/Kmp)+(c(1).*c(3)./(Km*Km2)));
cdot(1) = cEnzyme*(-vI);   %cat
cdot(2) = cEnzyme*vI;   %DHBA
cdot(3) = cEnzyme*(-vI); %KB
dcdt = [cdot(1), cdot(2), cdot(3)]';
end
```

Matlab script:

```
%constants
global cEnzyme vmax Km vmax2 Kmp Km2 Km2a
cEnzyme = ?;
vmax = 0.35;
Km = 30.2;
vmax2 = 1;
Kmp = 1.2;
Km2 = 87.6;
Km2a = 839.4;
c0_Catechol = ?;
c0_DHBA = ?;
c0_KB = ?;
%time vector
tspan = 0:.1:500;
%initial conditions
c0 = [c0_Catechol, c0_DHBA, c0_KB];
%solving diff. equ.
[t,c] = ode45(@Kinetik_Lorenzo,tspan,c0);
```

Kinetic model for the *beta*-decarboxylation in one phase:

Matlab function:

```
function dcdt = PAD_cEnz(t,c)
global  vmax Km  Ki E0
%Reaction equ.
tspan = 0:.1:1440;
vI = (vmax.*c(1))./(Km*(1+c(2)/Ki) +c(1));
E = E0 .* exp(-0.0008.*t);
cdot(1) = E.* (-vI);   %FA
cdot(2) = E.* vI;   %MVP
dcdt = [cdot(1), cdot(2)]';
end
```

Matlab script:

```
global  vmax Km  Ki E0
E0 = ?;
vmax = 89;
Km = 2.4;
Ki = 0.14;
E = E0 .* exp(-0.0006* t);
c0_FA = ?;
c0_MVP = 0;
%time vector
tspan = 0:.1:1;
% initial conditions
c0 = [c0_FA, c0_MVP];
%solving diff. equ.
[t,c] = ode45(@PAD_cEnz,tspan,c0);
```

Kinetic model for the *beta*-decarboxylation in 2LPS:

Matlab function:

```
function dcdt = LorenzoPAD_Tolrev(t,c)
global cEnzyme vmax Km Ki k
%c(1) = FA
%c(2) = MVP aq
%c(3) = MVP org
%Reaction equ.
vI = exp(-0.00018.*t).*(vmax.*c(1))./(Km.*(1+c(2)/Ki)+c(1));
vII = k.*c(2);
vIII = 0.009.*c(3);
cdot(1) = cEnzyme*(-vI);   %FA
cdot(2) = cEnzyme*vI - vII + vIII;   %MVP aq
cdot(3) = vII-vIII;   %MVP org
dcdt = [cdot(1), cdot(2), cdot(3)]';
end
```

Matlab script:

```
global cEnzyme vmax Km Ki k
cEnzyme = ?;
vmax = 80.2;
Km = 2.57;
Ki = 0.23;
k = 0.09;
c0_FA = ?;
c0_MVP = 0;
c0_MVPo = 0;
%time vector
tspan = 0:.1:240;
%initial conditions
c0 = [c0_FA, c0_MVP, c0_MVPo];
 %solving diff. equ.
[t,c] = ode45(@LorenzoPAD_Tolrev,tspan,c0);
```

Progress curve analysis for the determination of the kinetic constants (example for K_i determination in one phase):

Fitness function and ODE solver:

```
global  Data
Data=load('F:\LC2.txt', '-ascii'); %indicate the source and load Data
t=Data(:,1);
c_SUB=Data(:,2); % odesolv(:,1)
c_PRO=Data(:,3); % odesolv(:,2)
%%Fitness function
fitnessFunction = @lse_res_LC;
%%Number of Variables
nvars = 3;
```

```
%Linear inequality constraints
Aineq = [];
Bineq = [];
%Linear equality constraints
Aeq = [];
Beq = [];
%Bounds
% order: Vmax, KmSUB, KiPRO
LB= [88   2.3  0.1]; % lower boundary
UB= [89   2.5  0.3]; % upper boundary
%Nonlinear constraints
nonlconFunction = [];
%Start with default options
options = gaoptimset;
%%Modify some parameters
PopulationSize=1000;
%Nonlinear constraints
nonlconFunction = [];
%Start with default options
options = gaoptimset;
%%Modify some parameters
options = gaoptimset(options,'PopInitRange' ,[LB;UB]);
options = gaoptimset(options,'PopulationSize',PopulationSize);
options = gaoptimset(options,'Generations',10);
options = gaoptimset(options,'StallGenLimit' ,inf);
options = gaoptimset(options,'StallTimeLimit',inf);
options = gaoptimset(options,'MutationFcn' ,@mutationadaptfeasible);
options = gaoptimset(options,'TolCon',1e-6);
options = gaoptimset(options,'TolFun',1e-6);
options = gaoptimset(options,'Display' ,'iter');
options = gaoptimset(options,'EliteCount',PopulationSize/10);
options = gaoptimset(options,'CrossoverFraction' ,0.6);
%options = gaoptimset(options,'Vectorized' ,'on');
options_a=options;
%Run GA
[X,FVAL,REASON,OUTPUT_a,POPULATION,SCORES]
=ga(fitnessFunction,nvars,Aineq,Bineq,Aeq,Beq,LB,UB,nonlconFunction,options);
y_0=[c_SUB(1) c_PRO(1)];
t=[0:.1:150]; %#ok<*NBRAK>
[t,odesolv]=ode45(@ode_LC,t,y_0,[],X);
% figure(1)
% clf(1)
```

Residual function:

```
function [residual]=lse_res_LC(Parameter_Enzym)
global Data
t=Data(:,1);
c_SUB=Data(:,2); % odesolv(:,1)
c_PRO=Data(:,3); % odesolv(:,2)
y_0=[c_SUB(1) c_PRO(1)];
[t,odesolv]=ode45(@ode_LC,t,y_0,[],Parameter_Enzym);  %#ok<*ASGLU>
residual=[sum((odesolv(:,1)-c_SUB).^2) sum((odesolv(:,2)-c_PRO).^2)];
residual=sum(residual);
```

```
end
```

Kinetic equation:

```
function dy = ode_LC(t,y,Parameter_Enzym) %#ok<*INUSL>
dy = zeros(2,1);
%Enzymatic Reaction
vmax=Parameter_Enzym(1);
Km_SUB=Parameter_Enzym(2);
Ki_PRO=Parameter_Enzym(3);
c_SUB=y(1); %Substrate
c_PRO=y(2); %Product
% Rate equations
v_PAD=(vmax*c_SUB)/(Km_SUB*(1+(c_PRO/Ki_PRO))+c_SUB);
PAD=0.017; %mg/mL
% Diff Reactants
dy(1)= PAD* (-v_PAD); %DSUB
dy(2)= PAD* (v_PAD); %DPRO
```

Analytical methods. Starting materials and products concentrations were measured by an Agilent LC-1100 HPLC system equipped with a diode array detector using a RP Phenomenex Luna C18 column (150 x 4.60 mm, 5 µm) (for catechol/2,3-DHBA) or a LichroCART® 250-4 Lichrosphere® 100 RP-18 (5 µm) (for all the other compounds in this thesis), at 25°C. Water/TFA (0.1%) and acetonitrile/TFA (0.1%) with a flow rate of 1 mL min^{-1} were used as mobile phases, with the following gradients (% refers to the volume of acetonitrile/TFA): Method A: 0-2 min 15%; 2-10 min 15-100%; Method B: 0-2 min 15%; 2-10 min 15-100%; 10-12 min 100%; 12-16 min 100-15%; Method C: 0-2 min 0%; 2-15 min 0-100%; 15-17 min 100%; 17-20 min 100-0%; Method D: 0-2 min 15%; 2-15 min 15-100%; 15-17 min 100%; 17-20 min 100-15%; Method E: 0-2 min 15%; 2-17 min 15-100%; 15-17 min 100%; 17-18 min 100%; 18-22 min 100-15%.

Phenolic compounds	Method	Retention times (min)(substrate/product) Wavelenght detection (nm) (substrate/product)
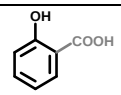	A	8.5/9 280/254
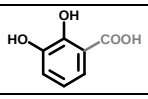	B	6.2/6.8 254/254
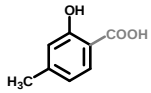	A	9.2/9.6 254/254
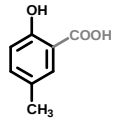	A	9.3/9.6 254/254
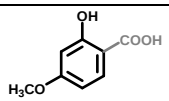	C	11.4/12.3 254/254
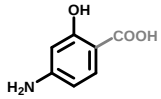	C	-/8.7 -/270
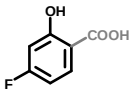	A	9.1/9.5 280/254
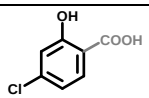	D	11.7/12.4 280/305
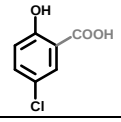	D	13.5/14.0 280/305
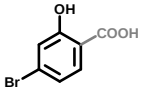	E	12.8/13.5 254/254
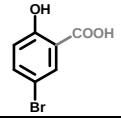	E	16.8/17.3 300/300
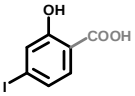	A	10.3/10.7 254/254
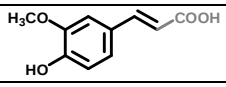	A	9.8/7.8 254/280

4VG and 4EG were analyzed by an Agilent 7890A GC system using a HP-5 (30 m x 320 µm x 0.25 µm) column coupled to an Agilent 5975C quadrupole mass spectrometer. The method required heating at 80°C for 1' followed by an increase of 5°C min^{-1} to 235°C for 34'. Helium was used as mobile phase with a 1.5 mL min^{-1} flow. Retention times for 4VG and 4EG were 6.75 and 7.78 min, respectively.

7 Appendix

Definitions

Conversion	%	$X = \left(\frac{n_{S0} - n_S}{n_{S0}}\right) x\ 100$
Yield	%	$Y = \frac{n_P - n_{P0}}{n_{S0}}\ x\ \left(\frac{\upsilon_S}{\upsilon_P}\right) x\ 100$
Turnover number	mol mol^{-1}	$TN = \frac{n_P - n_{P0}}{n_E}$
Enzyme consumption	Kg g^{-1}	$EC = \frac{m_P - m_{P0}}{m_E}$

Additional Figures and Schemes

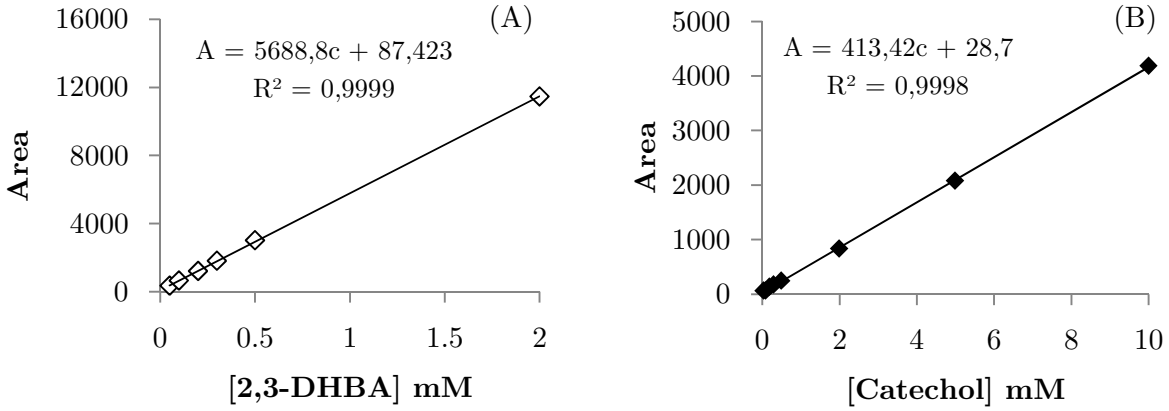

Figure A1: HPLC calibration curves for 2,3-DHBA (A) and catechol (B).

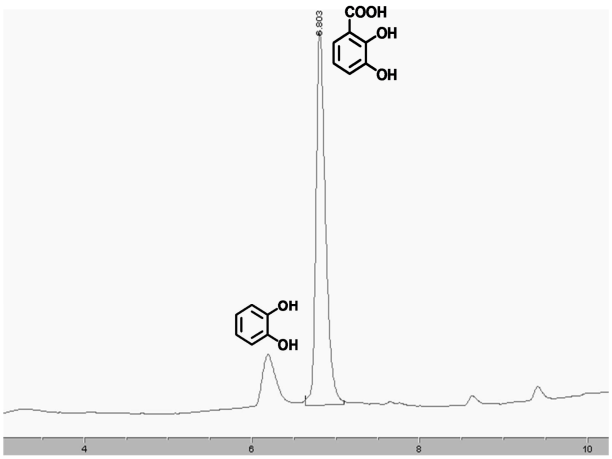

Figure A2: Typical chromatogram of a carboxylation reaction of catechol; 6.1 min catechol; 6.8 min 2,3-DHBA.

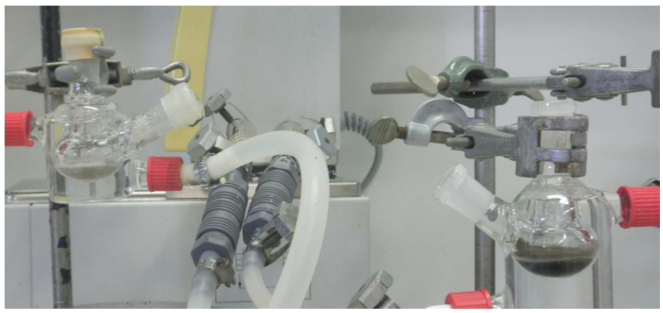

Figure A3: Reaction mixtures during catechol carboxylation in a closed (left) and open (right) reaction vessels after 4 h of reaction. Reaction conditions: 10 mM catechol, 4 mg mL^{-1} CFE in 2 M $KHCO_3$, at 30°C and 500 rpm.

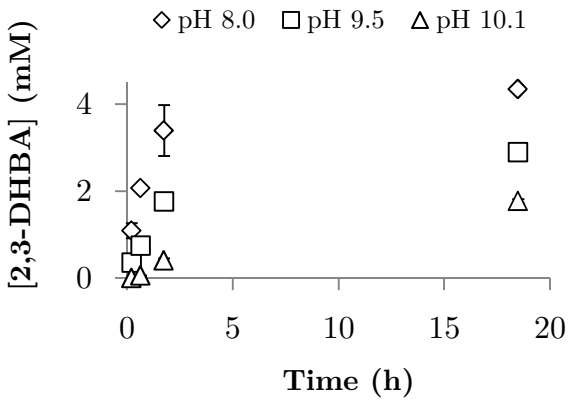

Figure A4: Catechol carboxylation course at different pH values. Reaction conditions: 20 mM catechol, 20 mM ascorbic acid, 2 M *KHCO₃*, 30 mg mL^{-1} whole cells containing Rsp_DHBD at 30°C and 500 rpm. The pH was adjusted by the addition of *KOH*.

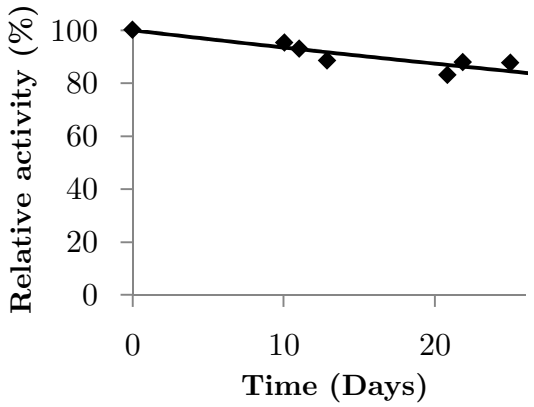

Figure A5: Enzyme stability in storing conditions (as CFE in a plastic test tube at 4°C). Reaction conditions: 80 mM catechol, 80 mM ascorbic acid, 2.3 mg mL^{-1} CFE in 2 M *KHCO₃*, at 30°C and 500 rpm.

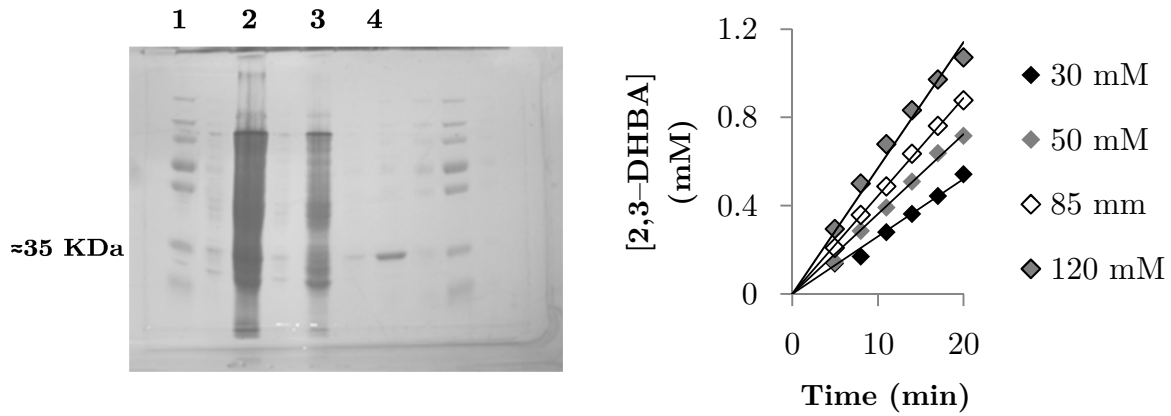

Figure A6: left: SDS-PAGE of the purified Rsp_DHBD; 1: PageRuler Plus Prestained Protein Ladder (Thermo scientific) ; 2-3 : CFE before and after adsorption into the column (1 µL); 4: eluted Rsp_DHBD (1 µL). Right: activity assays for carboxylation performed with the purified Rsp_DHBD; Reaction conditions: 30-120 mM catechol, 30-120 mM ascorbic acid, 0.25 mg mL^{-1} Rsp_DHBD in 2 M *KHCO₃*, at 30°C and 500 rpm.

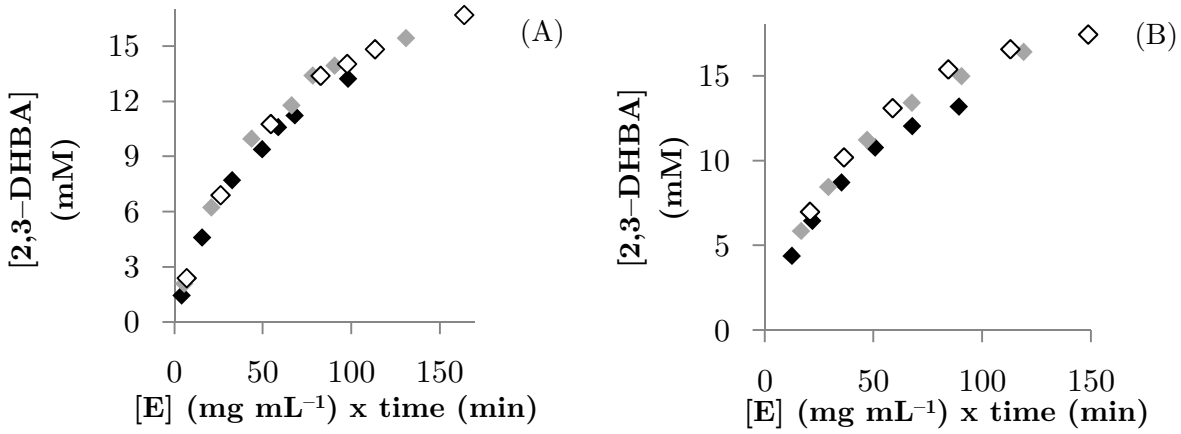

Figure A7: Deactivation assay using 80 mM (A) and 100 mM (B) catechol. black diamonds: 0.20 mg mL^{-1} CFE; grey diamonds: 0.27 mg mL^{-1} CFE; white diamonds: 0.35 mg mL^{-1} CFE. Reaction conditions: 30 or 200 mM catechol, 80 or 100 mM ascorbic acid, Rsp_DHBD in 2 M *KHCO₃*, at 30°C and 500 rpm.

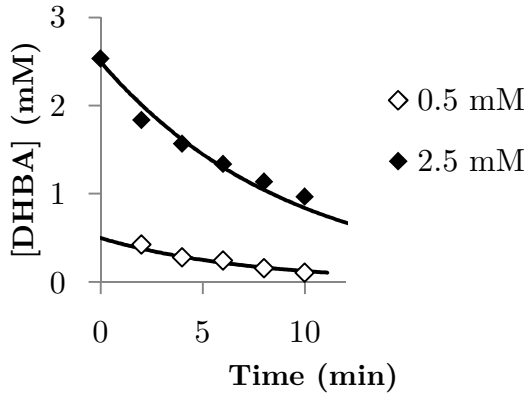

Figure A8: Activity assays for decarboxylation performed with the purified Rsp_DHBD; reaction conditions: 0.5-2.5 mM 2,3-DHBA, 0.22-0.38 mg mL^{-1} Rsp_DHBD in KP_i buffer 0.1 M pH 8.0, at 30°C and 500 rpm.

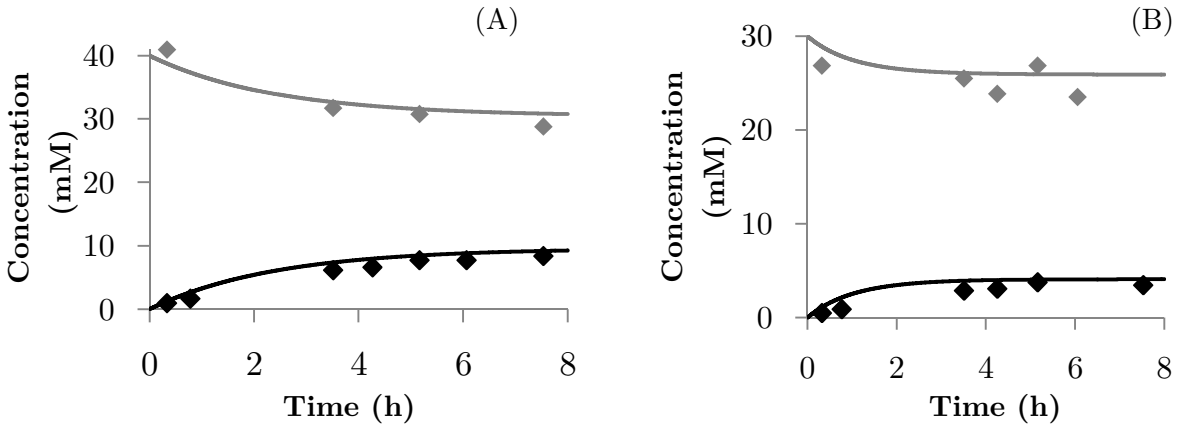

Figure A9: Comparison of experimental data with numerical simulations of Eq. 2.1.2; A: Reaction conditions: 40 mM catechol, 40 mM ascorbic acid, 0.22 mg mL^{-1} Rsp_DHBD in 2 M $KHCO_3$, at 30°C and 500 rpm; B: Reaction conditions: 30 mM catechol, 30 mM ascorbic acid, 0.25 mg mL^{-1} Rsp_DHBD. in 1 M $KHCO_3$, at 30°C and 500 rpm.

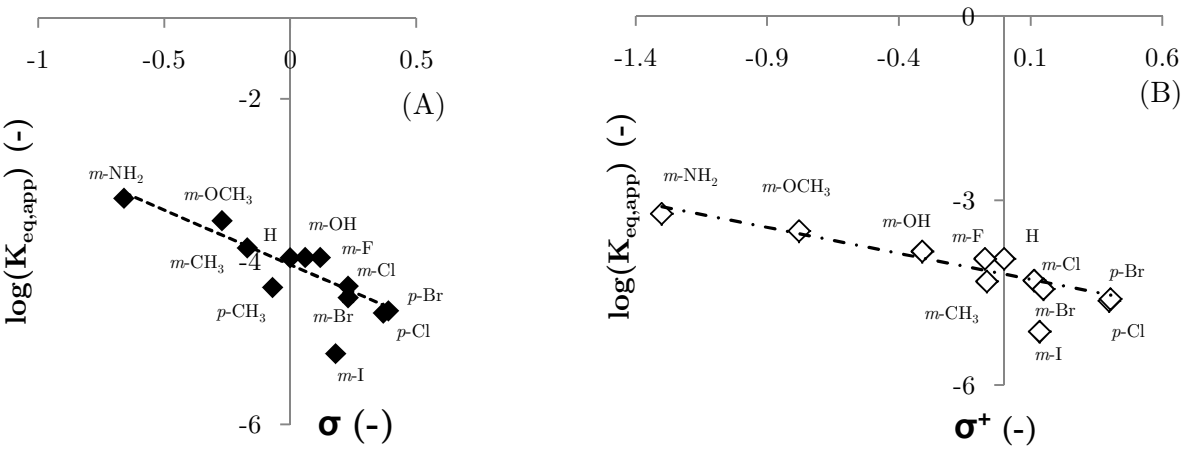

Figure A10: A: Correlation of the logarithm of the calculated $K_{eq,app}$ with respect to the Hammett constants σ ($R^2 = 0.87$); B: Correlation of the logarithm of the calculated $K_{eq,app}$ with respect to the electrophilic substitution constants σ^+ ($R^2 = 0.91$).

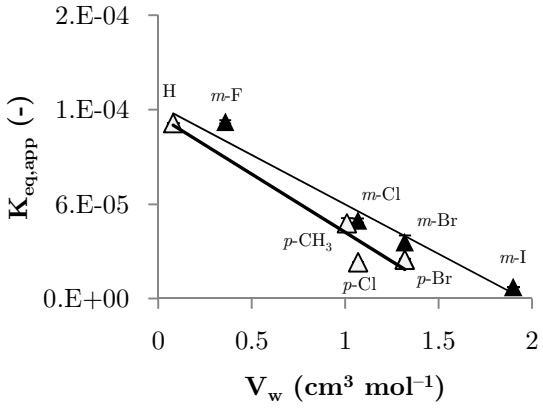

Figure A11: Correlation of the logarithm of the calculated $K_{eq,app}$ with respect to the Van der Waals volumes of the substituents V_w ($R^2 = 0.97$ for *meta*-substituents; $R^2 = 0.95$ for *para*-substituents).

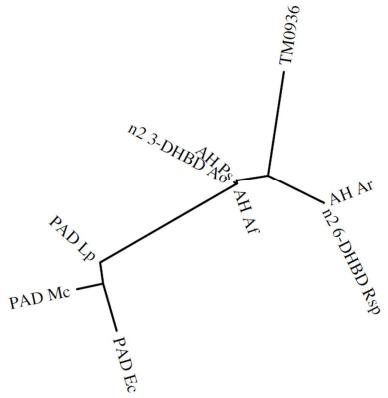

Figure A12: phylogenetic tree constructed using sequences of phenolic (de)carboxylases and amidohydrolases. PAD_Ec (Phenolic acid decarboxylase from *Enterobacter chloachae*); PAD_Ec (Phenolic acid decarboxylase from *Mycobacterium colombiense*); PAD_Ec (Phenolic acid decarboxylase from *Lactobacillus plantarum*); n2 3-DHBD_Ao (2,3-Dihydroxybenzoic acid decarboxylase from *Aspergillus oryzae*); AH_Af (Amidohydrolase from *Aspergillus fumigatus*); AH_Ps (Amidohydrolase from *Penicillum solitum*); TM0936 (*S*-adenosylhomocysteine deaminase from *Thermotoga maritima*); n2 6-DHBD_Rsp(2,6-Dihydroxybenzoic acid decarboxylase from *Rhizobium* sp.). Phylogenetic tree realized using the MUSCLE alignment implemented in Phylogeny.fr.

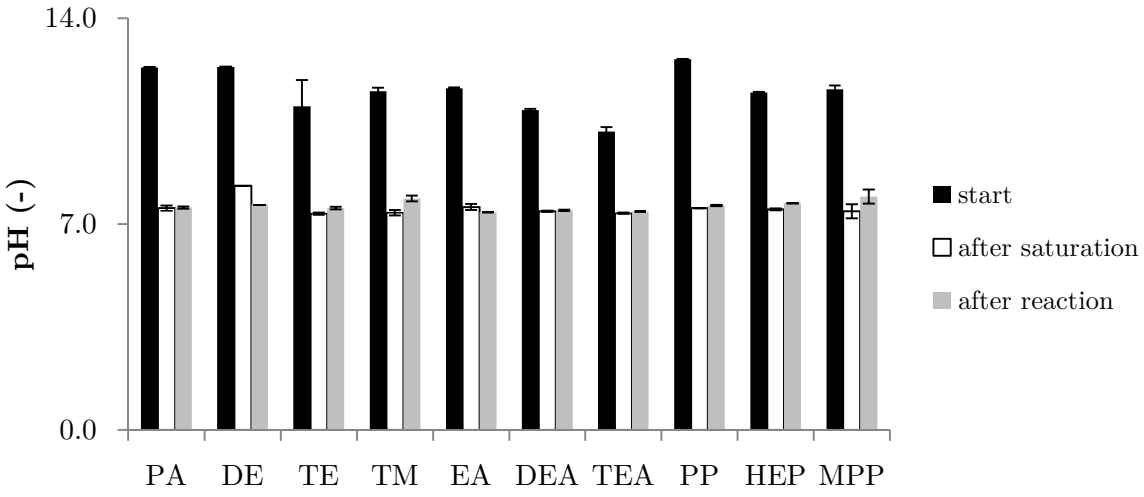

Figure A13: pH measurements in the biocatalytic carboxylation of catechol using CO_2/amines as co-substrate; black bars: pH of the amine solution; white bars: pH after 1 h bubbling aeration of CO_2; grey bars: pH after 24 h biotransformation. Reaction conditions: 10 mM catechol, 10 mM ascorbic acid, 3 mg mL^{-1} (2.3 U mL^{-1}) Ao_DHBD (whole cells) in KP_i buffer 0.1 M, pH 8.0, 1 M amine under CO_2 bubbling aeration 0.1 L min^{-1}, at 30°C and 500 rpm.

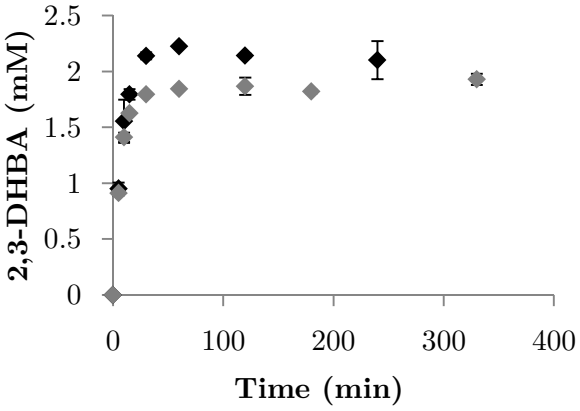

Figure A14: Biocatalytic carboxylation of catechol using a constant CO_2 supply (black diamonds) or CO_2/triethylamine (grey diamonds) as co-substrate; Reaction conditions: 10 mM catechol, 10 mM ascorbic acid, 3 mg mL^{-1} (2.3 U mL^{-1}) Ao_DHBD (whole cells) in KP_i buffer 0.1 M, pH 8.0, 1 M $KHCO_3$ or 1 M DE under CO_2 bubbling aeration, at 30°C and 500 rpm.

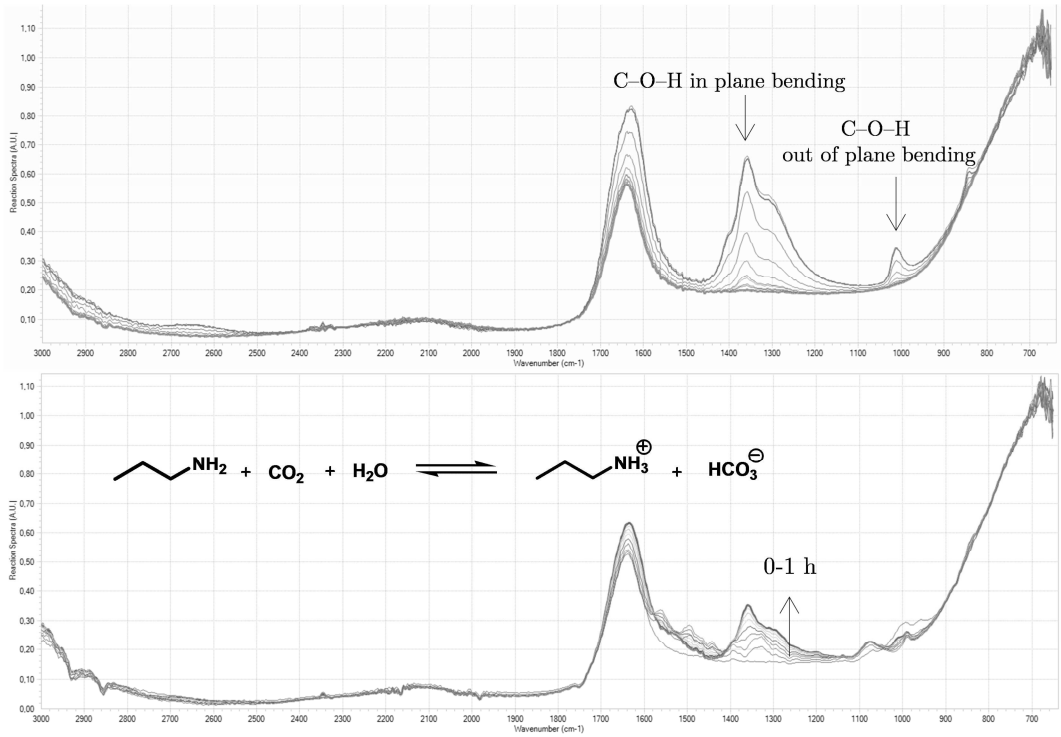

Figure A15: FT-IR spectra of bicarbonate from 10 mM to 3 M (upper) and inline monitoring of bicarbonate formation for the reaction of CO_2 with propylamine (below).

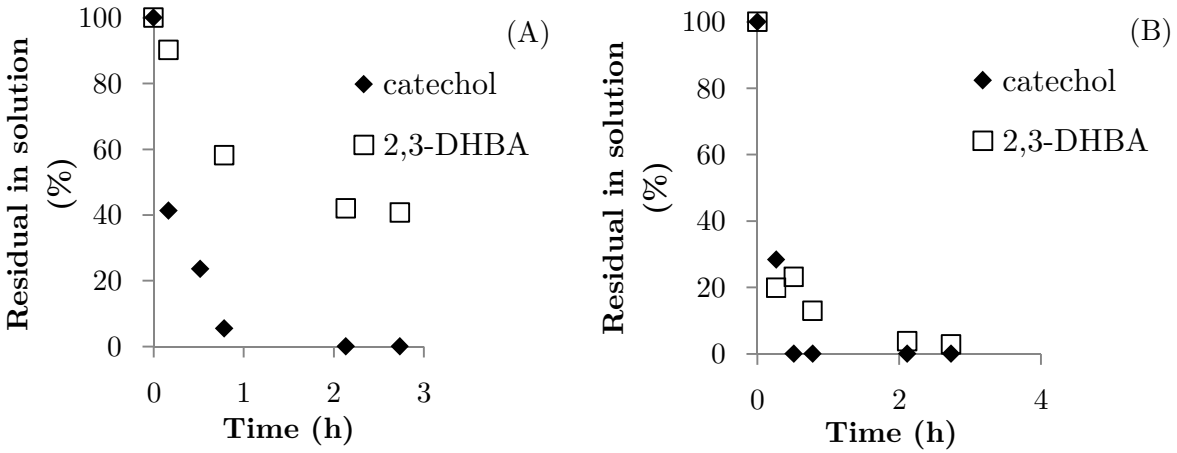

Figure A16: Adsorption of catechol and 2,3-DHBA on weak anion exchanger resin (Diaion WA30, styrene-divinylbenzene based); A: pH 8.0; B: pH 5.5; Reaction conditions: 5 mM catechol/2,3-DHBA, 5 mM ascorbic acid, 100 mg adsorber in 1 mL 0.1 M KP_i buffer, pH 8.0 or 5.5, at 30°C and 500 rpm.

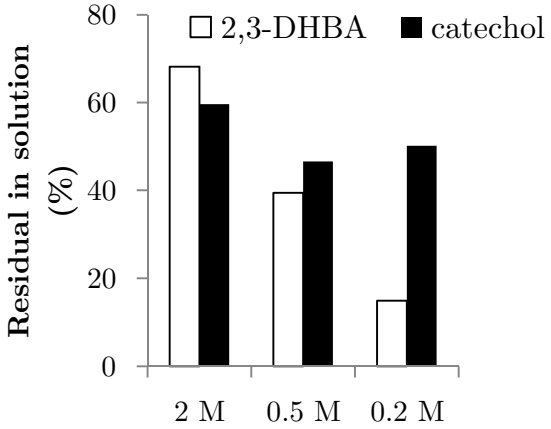

Figure A17: Adsorption of catechol and 2,3-DHBA on strong anion exchanger resin (Amberlite IRA958®, acrylate based) in various bicarbonate solutions; Reaction conditions: 10 mM catechol/2,3-DHBA, 10 mM ascorbic acid, 100 mg adsorber in 1 mL 0.2-2 M $KHCO_3$, at 30°C and 500 rpm.

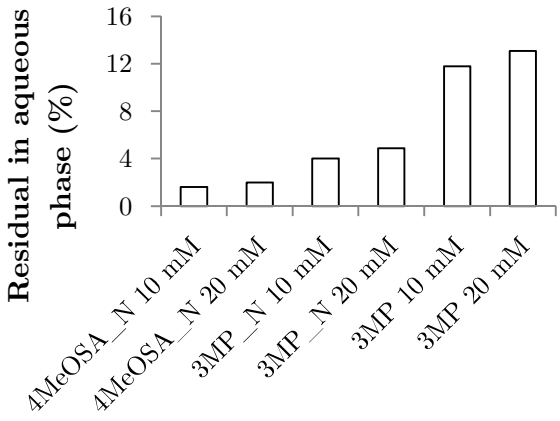

Figure A18: Extraction of *meta*-methoxyphenol (3MP) and 4-methoxysalicylic acid (4MeOSA) in 2LPS (buffer:DCM) in the presence of tetrabutylammonium chloride (TBACl, _N in the legend); Reaction conditions: 10-20 mM 3MP/4MeOSA, TBACl/phenolic 18:1 mol:mol, 0.1 M KP_i buffer pH 8, aqueous:organic 1:1 v/v, shaking for 10 minutes at 30°C and 500 rpm.

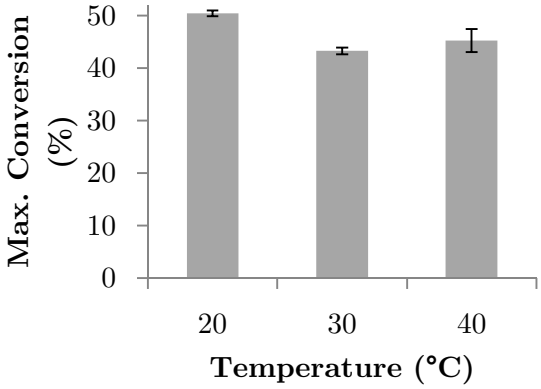

Figure A19: Temperature influence on the enzymatic carboxylation of catechol using 30% v/v GlC in aqueous bicarbonate; Reaction conditions: 10 mM catechol, 10 mM ascorbic acid, 30 mg mL^{-1} Rsp_DHBD (whole cells) in 2 M $KHCO_3$, 30% v/v GlC, at 30°C and 500 rpm.

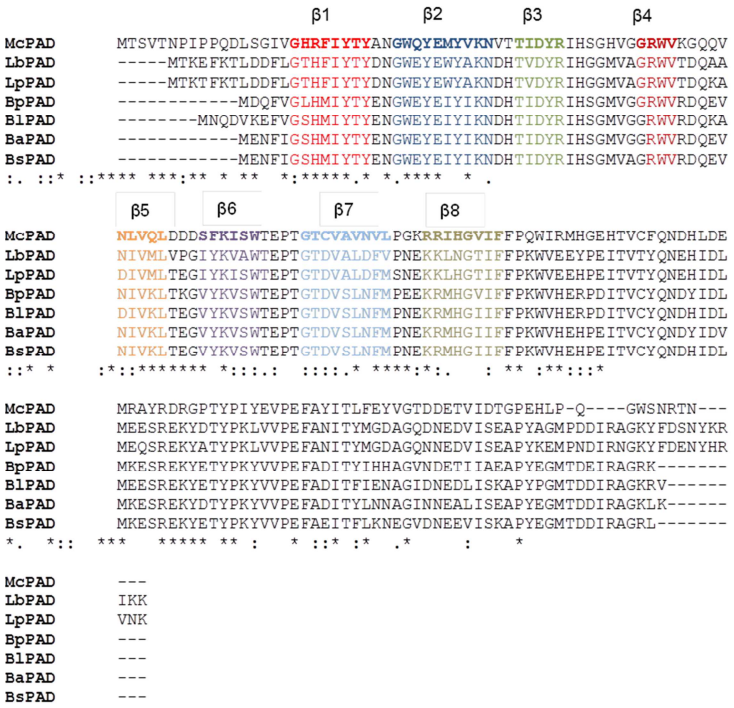

Figure A20: Sequence alignment of McPAD with other reported PADs: LbPAD (*Lactobacillus brevis*), LpPAD (*Lactobacillus plantarum*), BpPAD (*Bacillus pumilus*), BlPAD (*Bacillus licheniformis*), BaPAD (*Bacillus amiloliquefaciens*), BsPAD (*Bacillus subtilis*). Sequence alignment realized with the PRALINE multiple sequence alignment tool available from The Centre for Integrative Bioinformatics (VU Amsterdam, The Netherlands).

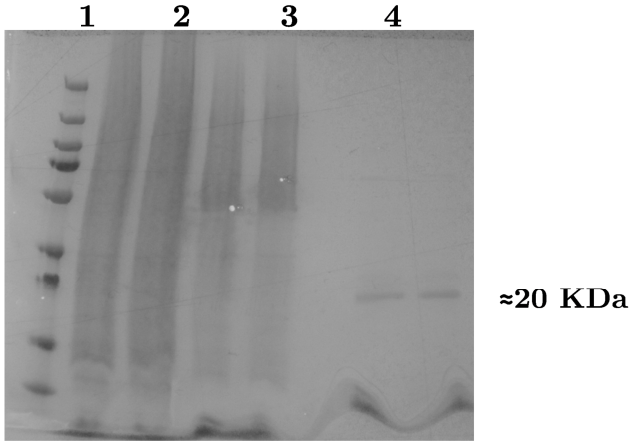

Figure A21: SDS-PAGE of the purified McPAD; 1: PageRuler Plus Prestained Protein Ladder (Thermo scientific); 2: CFE before adsorption into the column (1 µL); 3: CFE after adsorption into the column; 4: eluted McPAD (1 µL).

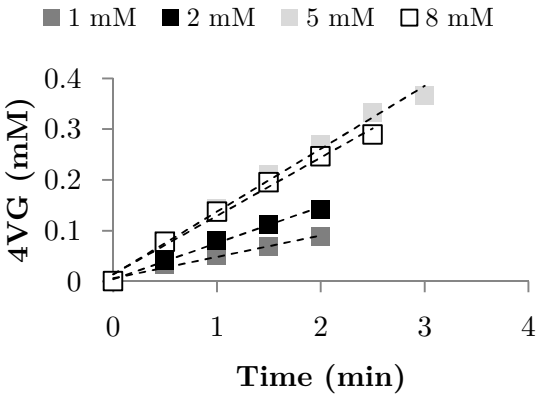

Figure A22: Initial rate measurements at 1, 2, 5 and 8 mM FA. Reaction conditions: 1–8 mM FA, 0.1 U mL^{-1} (1.7 µg mL^{-1}) McPAD, in 0.1 M KP_i buffer pH 7.0, at 37°C and 700 rpm.

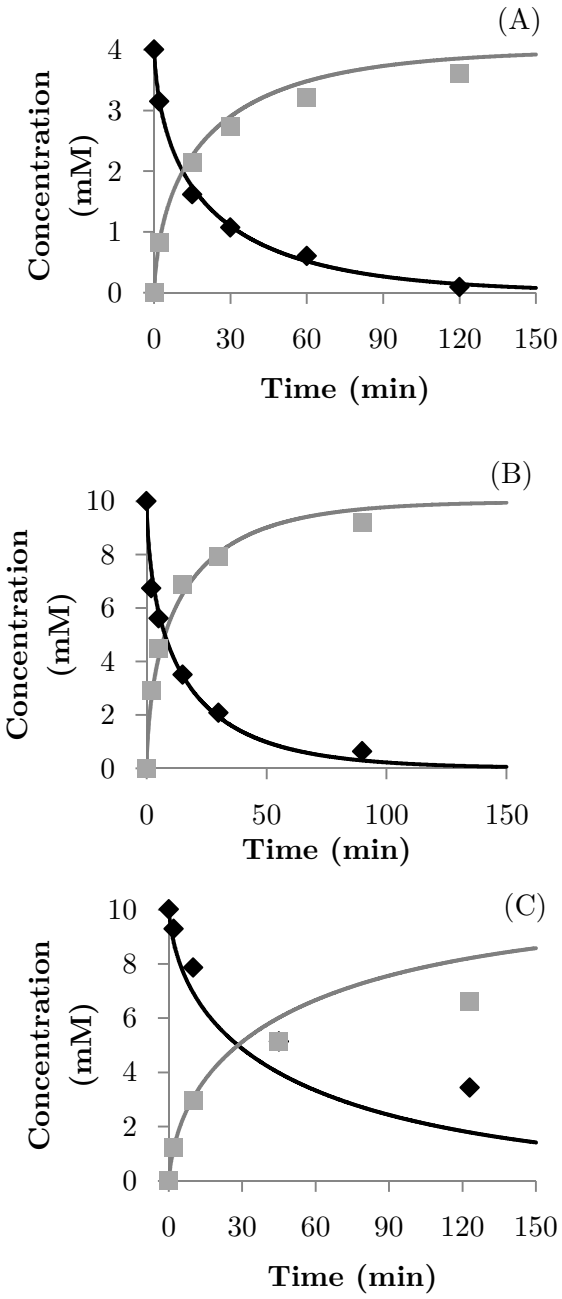

Figure A23: Comparison of the experimental batch data (white diamonds: FA; grey squares: 4VG) with the simulation of the kinetic model (solid lines) at different FA and McPAD concentrations. Reaction conditions: A: 5 mM FA 0.7 U mL^{-1} (10.8 µg mL^{-1}) McPAD; B: FA 10 mM, 3.8 U mL^{-1} (59 µg mL^{-1}) McPAD; C: FA 10 mM, 1.07 U mL^{-1} (16.5 µg mL^{-1}) McPAD, in 0.1 M KP_i buffer pH 7.0, at 37°C at 700 rpm.

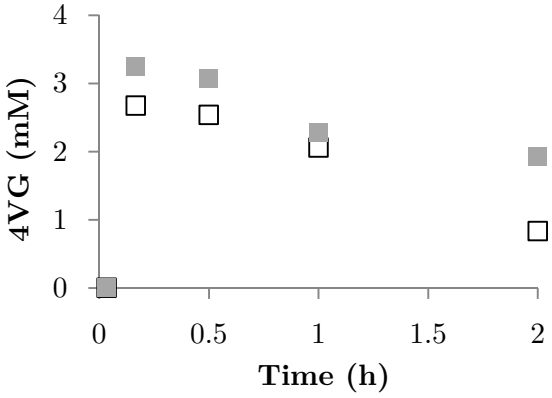

Figure A24: Extraction of 4VG during FA decarboxylation in hexane (grey squares) and toluene (white squares). 20 mM FA, 0.58 U mL^{-1} (9 µg mL^{-1}) McPAD, in a 2LPS (organic: aqueous, 1:2 (v/v)), aqueous medium 0.1 M KP_i buffer pH 7.0, at 37°C, 700 rpm.

Figure A25: 4VG isolated from the decarboxylation using toluene as second phase. 20 mM FA, 0.58 U mL^{-1} (9 µg mL^{-1}) McPAD, in a 2LPS (organic: aqueous, 1:2 (v/v)), aqueous medium 0.1 M KP_i buffer pH 7.0, at 37°C, 700 rpm.

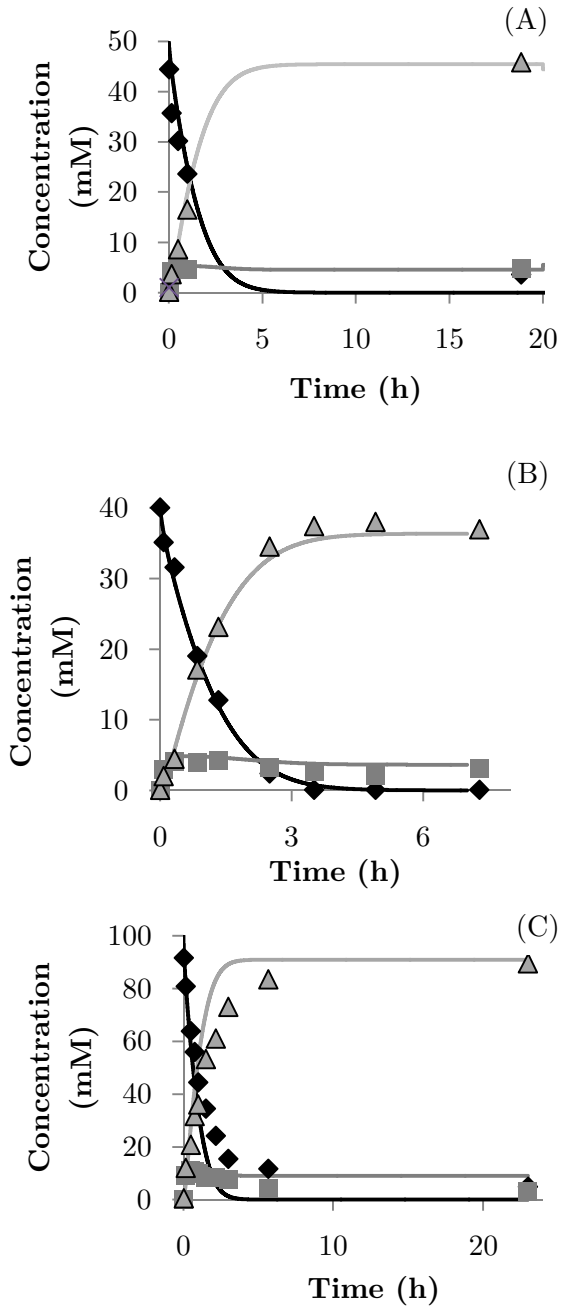

Figure A26: Experimental data versus simulated data in two-phase systems (buffer:hexane 1:2) at different FA/McPAD concentrations. Reaction conditions: A: 50 mM FA 0.84 U mL^{-1} (13 µg mL^{-1}) McPAD; B: FA 40 mM, 0.91 U mL^{-1} (14 µg mL^{-1}) McPAD; C: FA 100 mM, 5.85 U mL^{-1} (90 µg mL^{-1}) McPAD, in 2LPS (organic: aqueous, 1:2 (v/v)), aqueous medium 0.1 M KP_i buffer pH 7.0, at 37°C, 700 rpm.

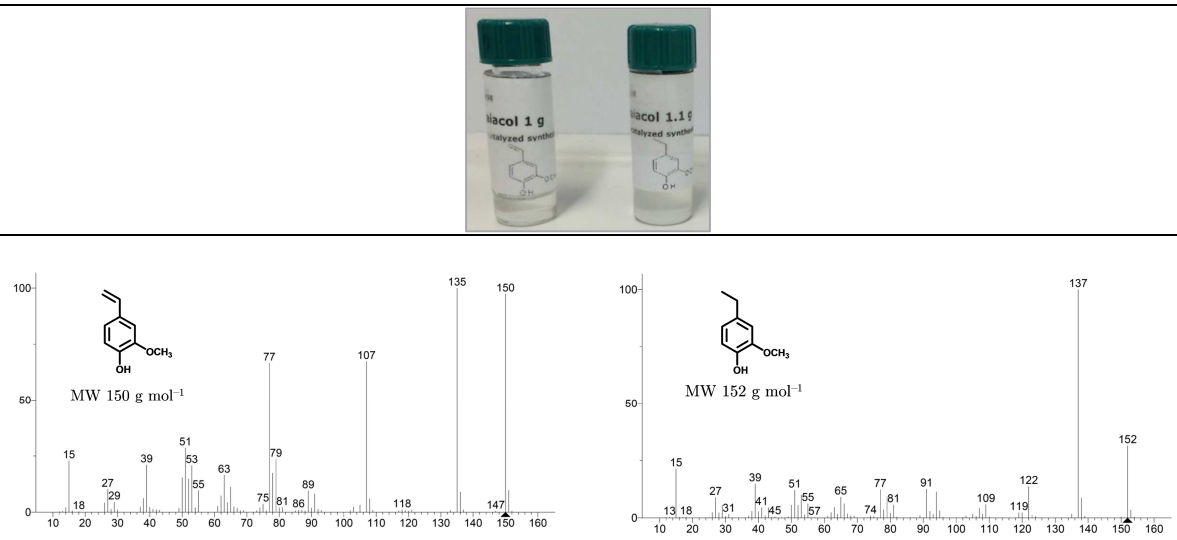

Figure A27: Synthesized 4VG and 4EG (top) and relative MS-spectra (4VG, left; 4EG, right).

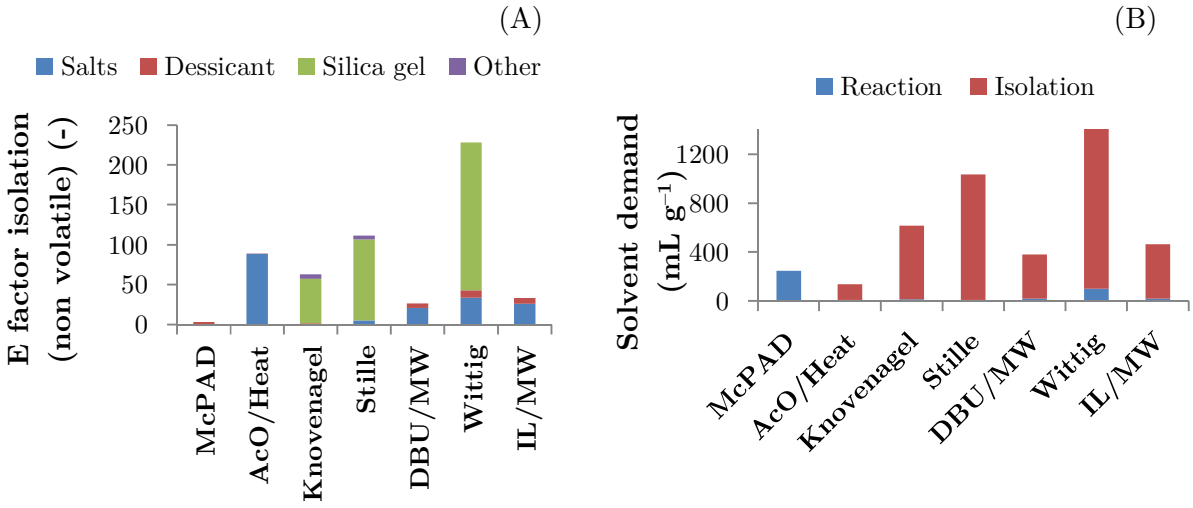

Figure A28: E-Factor analysis for isolation of 4VG (A) and corresponding solvent demand for reaction and isolation (B).

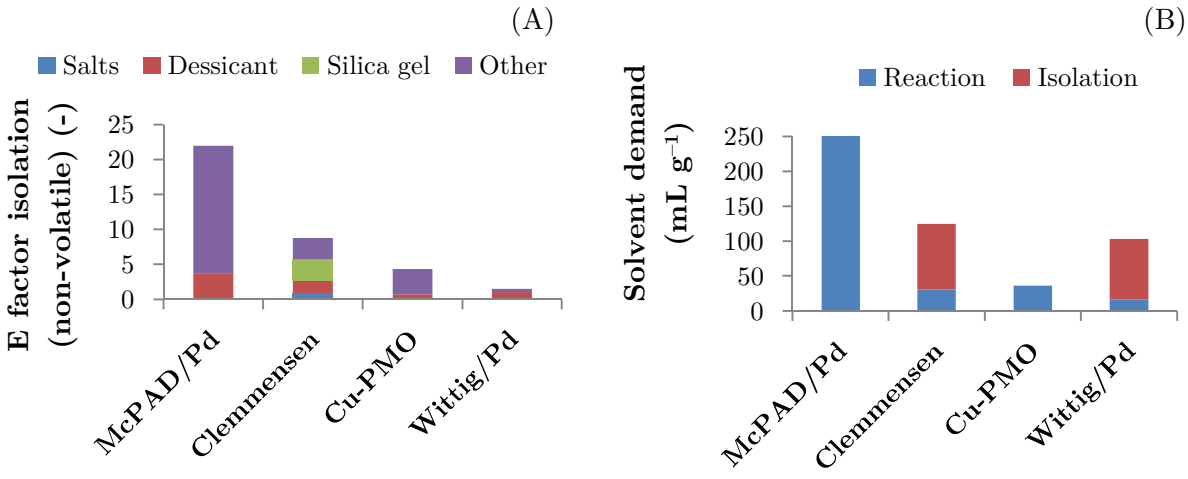

Figure A29: E-Factor analysis for isolation of 4EG (A) and corresponding solvent demand for reaction and isolation (B).

Bibliography

Aldabalde, V. 2011. Organocatalyzed Decarboxylation of Naturally Occurring Cinnamic Acids: Potential Role in Flavoring Chemicals Production. *Open J. Phys. Chem.* **1**, 85–93.

Andreini, C., Bertini, I., Cavallaro, G., Holliday, G.L. & Thornton, J.M. 2008. Metal ions in biological catalysis: from enzyme databases to general principles. *J. Biol. Inorg. Chem.* **13**, 1205–1218.

Aresta, M. 2006. Carbon Dioxide Reduction and Uses as a Chemical Feedstock. In: W.B. Tolman (ed) *Activation of Small Molecules: Organometallic and Bioinorganic Perspectives*, pp. 1–41. WILEY-VCH Verlag GmbH, Weinheim.

Aresta, M., Quaranta, E., Liberio, R., Dileo, C. & Tommasi, I. 1998. Enzymatic synthesis of 4-OH-benzoic acid from phenol and CO2: the first example of a biotechnological application of a Carboxylase enzyme. *Tetrahedron* **54**, 8841–8846.

Bamberger, A., Sieder, G. & Maurer, G. 2000. High pressure (vapor+liquid) equilibrium in binary mixtures of (carbon dioxide+water or acetic acid) at temperatures from 313 to 353 K. *J. Supercrit. Fluids* **17**, 97–110.

Baqueiro-Peña, I., Rodríguez-Serrano, G., González-Zamora, E., Augur, C., Loera, O. & Saucedo-Castañeda, G. 2010. Biotransformation of ferulic acid to 4-vinylguaiacol by a wild and a diploid strain of Aspergillus niger. *Bioresour. Technol.* **101**, 4721–4724.

Bathelt, C.M., Ridder, L., Mulholland, A.J. & Harvey, J.N. 2004. Mechanism and structure-reactivity relationships for aromatic hydroxylation by cytochrome P450. *Org. Biomol. Chem.* **2**, 2998–3005.

Bergman, R.I. & Frisch, N.W. 1966. Production of maleic anhydride by oxidation of n-butane. *US Patent 3293268*.

Bernini, R., Mincione, E., Barontini, M., Provenzano, G. & Setti, L. 2007. Obtaining 4-vinylphenols by decarboxylation of natural 4-hydroxycinnamic acids under microwave irradiation. *Tetrahedron* **63**, 9663–9667.

Bhuiya, M.W., Lee, S.G., Jez, J.M. & Yu, O. 2015. Structure and Mechanism of Ferulic Acid Decarboxylase (FDC1) from Saccharomyces cerevisiae. *Appl. Environ. Microbiol.* **81**, 4216–4223.

Borkar, V.T., Bonde, S.L. & Dangat, V.T. 2013. A Quantitative Structure-Reactivity Assessment of Phenols by Investigation of Rapid Iodination Kinetics Using Hydrodynamic Voltammetry: Applicability of the Hammett Equation in Aqueous Medium. *Int. J. Chem. Kinet.* **45**, 693–702.

Boullard, O., Leblanc, H. & Besson, B. 2000. Salicylic Acid. In: *Ullmann's Encyclopedia of Industrial Chemistry*. Wiley-VCH Verlag GmbH & Co. KGaA, Weinheim.

Brenneis, R. & Baeck, B. 2012. Esterification of fatty acids using Candida antarctica lipase A in water-abundant systems. *Biotechnol. Lett.* **34**, 1459–1463.

Broekhof, N. 1986. Perfume composition and perfumed products which contain one or more O-alkoxyphenols as perfume component. *European Patent EP0179523 A1.*

Brown, H.C. & Okamoto, Y. 1958. Electrophilic Substituent Constants. *JACS* **80**, 4979–4987.

Bumagin, N.A. & Luzikova, E.V. 1997. Palladium catalyzed cross-coupling reaction of Grignard reagents with halobenzoic acids, halophenols and haloanilines. *J. Organomet. Chem.* **532**, 271–273.

Burdock, G.A. 2010. Fenaroli´s Handbook of Flavor Ingredients. CRC Press, Boca Raton.

Bustamante, P., Peña, M.A. & Barra, J. 2000. The modified extended Hansen method to determine partial solubility parameters of drugs containing a single hydrogen bonding group and their sodium derivatives: benzoic acid/Na and ibuprofen/Na. *Int. J. Pharm.* **194**, 117–124.

Carrea, G. & Riva, S. 2000. Properties and Synthetic Applications of Enzymes in Organic Solvents. *Angew. Chem. Int. Ed.* **39**, 2226–2254.

Castillo, E., Casas-Godoy, L. & Sandoval, G. 2016. Medium-engineering: a useful tool for modulating lipase activity and selectivity. *Biocatalysis* **1**, 178–188.

Cavin, J., Dartois, V. & Diviès, C. 1998. Gene Cloning, Transcriptional Analysis, Purification, and Characterization of Phenolic Acid Decarboxylase from Bacillus subtilis. *Appl. Environ. Microbiol.* **64**, 1466–1471.

Centi, G. & Perathoner, S. 2003. Catalysis and sustainable (green) chemistry. *Catal. Today* **77**, 287–297.

Chapman, N.B. & Shorter, J. 1978. Correlation analysis in chemistry, Recent advances. Plenum Press, New York.

Chittimalla, S.K., Bandi, C., Putturu, S., Kuppusamy, R., Boellaard, K.C., Tan, David Chu Aan & Lum, Demi Ming Jie 2014. Access to 3-Arylindoles through a Tandem One-Pot Protocol Involving Dearomatization, a Regioselective Michael Addition Reaction, and Rearomatization. *Eur. J. Org. Chem.* **2014**, 2565–2575.

Crooks, J.E. & Donnellan, P. 1989. Kinetics and Mechanism of the Reaction between Carbon Dioxide and Amines in Aqueous Solution. *J. Chem. Soc., Perkin Trans.* **2**, 331–333.

Cuéllar-Franca, R.M. & Azapagic, A. 2015. Carbon capture, storage and utilisation technologies: A critical analysis and comparison of their life cycle environmental impacts. *J. CO2 Util.* **9**, 82–102.

da Silva, E.F. & Svendsen, H.F. 2004. Ab Initio Study of the Reaction of Carbamate Formation from CO 2 and Alkanolamines. *Ind. Eng. Chem. Res.* **43**, 3413–3418.

Danckwerts, P.V. 1979. The Reaction of CO2 with ethanolamines. *Chem. Eng. Sci.* **34**, 443–446.

Davin, L.B. & Lewis, N.G. 2005. Lignin primary structures and dirigent sites. *Curr. Opin. Biotechnol.* **16**, 407–415.

Dawes, G., Scott, E.L., Le Nôtre, J., Sanders, J. & Bitter, J.H. 2015. Deoxygenation of biobased molecules by decarboxylation and decarbonylation – a review on the role of heterogeneous, homogeneous and bio-catalysis. *Green Chem.* **17**, 3231–3250.

Dibenedetto, A., Lo Noce, R., Pastore, C., Aresta, M. & Fragale, C. 2006. First in vitro use of the phenylphosphate carboxylase enzyme in supercritical CO2 for the selective carboxylation of phenol to 4-hydroxybenzoic acid. *Environ. Chem. Lett.* **3**, 145–148.

Ding, B., Schmeling, S. & Fuchs, G. 2008. Anaerobic metabolism of catechol by the denitrifying bacterium Thauera aromatica--a result of promiscuous enzymes and regulators? *J. Bacteriol.* **190**, 1620–1630.

Dmuchovsky, B., Freerks, M.C., Pierron, E.D., Munch, R.H. & Zienty, F.B. 1965. A study of the catalytic oxidation of benzene to maleic anhydride. *J. Catal.* **4**, 291–300.

Dodds, W.S., Stutzman, L.F. & Sollami, B.J. 1956. Carbon dioxide solubility in water. *Ind. Eng. Chem. Chem. Eng.* **1**, 92–95.

Dutcher, B., Maohong, F. & Armistead, G.R. 2015. Amine-Based CO2 Capture Technology Development from the Beginning of 2013—A Review. *ACS Appl. Mater. Interfaces* **7**, 2137–2148.

EPA 2016 (WWW document). https://www3.epa.gov/climatechange/ghgemissions/sources/industry.html.

Erb, T.J. 2011. Carboxylases in natural and synthetic microbial pathways. *Appl. Environ. Microbiol.* **77**, 8466–8477.

Erb, T.J., Brecht, V., Fuchs, G., Müller, M. & Alber, B.E. 2009. Carboxylation mechanism and stereochemistry of crotonyl-CoA carboxylase/reductase, a carboxylating enoyl-thioester reductase. *PNAS* **106**, 8871–8876.

Everse, J. 1982. The Pyridine Nucleotide Coenzymes. Academic Press, New York.

Falorni, M., Porcheddu, A. & Taddei, M. 1999. Mild reduction of carboxylic acids to alcohols using cyanuric chloride and sodium borohydride. *Tetrahedron Lett.* **40**, 4395–4396.

Faulds, C.B. & Williamson, G. 1999. The role of hydroxycinnamates in the plant cell wall. *J. Sci. Food Agric.* **79**, 393–395.

Ferrentino, G., Schuster, J., Braeuer, A. & Spilimbergo, S. 2016. In situ Raman quantification of the dissolution kinetics of carbon dioxide in liquid solutions during a dense phase and ultrasound treatment for the inactivation of Saccharomyces cerevisiae. *J. Supercrit. Fluids* **111**, 104–111.

Fersht, A.R., Leatherbarrow, R.J. & Wells, T. 1986. Quantitative analysis of structure-activity relationships in engineered proteins by linear free-energy relationship. *Nature* **322**, 284–286.

Frank, A., Eborall, W., Hyde, R., Hart, S., Turkenburg, J.P. & Grogan, G. 2012. Mutational analysis of phenolic acid decarboxylase from Bacillus subtilis (BsPAD), which converts bio-derived phenolic acids to styrene derivatives. *Catal. Sci. Technol.* **2**, 1568–1574.

Freeman, A., Woodley, J.M. & Lilly, M.D. 1993. In Situ Product Removal as Tool for Bioprocessing. *Nat. Biotechnol.* **11**, 1007–1012.

Garcia-Gonzalez, L., Teichert, H., Geeraerd, A.H., Elst, K., van Ginneken, L., van Impe, J.F., Vogel, R.F. & Devlieghere, F. 2010. Mathematical modelling and in situ determination of pH in complex aqueous solutions during high-pressure carbon dioxide treatment. *J. Supercrit. Fluids* **55**, 77–85.

Gerhard, M. & Schomburg, D. 2013. Biochemical Pathways: An Atlas of Biochemistry and Molecular Biology. John Wiley and sons, Hoboken, NJ.

Glueck, S.M., Gümüs, S., Fabian, Walter M F & Faber, K. 2010. Biocatalytic carboxylation. *Chem. Soc. Rev.* **39**, 313–328.

Goto, M., Hayashi, H., Miyahara, I., Hirotsu, K., Yoshida, M. & Oikawa, T. 2006. Crystal structures of nonoxidative zinc-dependent 2,6-dihydroxybenzoate (gamma-resorcylate) decarboxylase from Rhizobium sp. strain MTP-10005. *J. Biol. Chem.* **281**, 34365–34373.

Gross, G.G. & Zenk, M.H. 1969. Reduktion aromatischer Säuren zu Aldehyden und Alkoholen im zellfreien System. *Eur. J. Biochem.* **8**, 413–419.

Gu, W., Yang, J., Lou, Z., Liang, L., Sun, Y., Huang, J., Li, X., Cao, Y., Meng, Z. & Zhang, K.-Q. 2011. Structural basis of enzymatic activity for the ferulic acid decarboxylase (FADase) from Enterobacter sp. Px6-4. *PloS one* **6**, e16262.

Guliants, V.V., Benziger, J.B. & Sundaresan, S. 1996. The Oxidation of C4 Molecules on Vanadyl Pyrophosphate Catalysts. In: J.W. Hightower, W.N. Delgass, E. Iglesia & A.T. Bell (eds) *11th International Congress on Catalysis-40th Anniversery. Studies in Surface Science and Catalysis*, pp. 991–1000. Elsevier Science B.V .

Hammett, L.P. 1937. The Effect of Structure upon the Reactions of Organic Compounds. Benzene Derivatives. *JACS* **59**, 96–103.

Hansch, C., Leo, A. & Taft, W. 1991. A Survey of Hammett Substituent Constants and Resonance and Field Parameters. *Chem. Rev.* **91**, 165–195.

Hansen, C.M. 2007. Hansen solubility parameters. A user's handbook. CRC Press, Boca Raton.

Hararah, M.A., Ibrahim, K.A., Al-Muhtaseb, A.H., Yousef, R.I., Abu-Surrah, A. & Qatatsheh, A. 2010. Removal of phenol from aqueous solutions by adsorption onto polymeric adsorbents. *J. Appl. Polym. Sci.* **117**, 1908–1913.

Hofland, G.W., Rijke, A. de, Thiering, R., van der Wielen, Luuk A.M & Witkamp, G.-J. 2000. Isoelectric precipitation of soybean protein using carbon dioxide as a volatile acid. *J. Chromatogr. B: Biomed. Sci. Appl.* **743**, 357–368.

Hong, Y.K., Hong, W.H. & Han, D. 2001. Application of Reactive Extraction to Recovery of Carboxylic Acids. *Biotechnol. Bioprocess Eng.* **6**, 386–394.

Höök, M. & Tang, X. 2013. Depletion of fossil fuels and anthropogenic climate change—A review. *Energy Policy* **52**, 797–809.

Hu, H., Li, L. & Ding, S. 2015. An organic solvent-tolerant phenolic acid decarboxylase from Bacillus licheniformis for the efficient bioconversion of hydroxycinnamic acids to vinyl phenol derivatives. *Appl. Microbiol. Biotechnol.* **99**, 5071–5081.

Huang, H., Chen, L., Tokashiki, M., Ozawa, T., Taira, T. & Ito, S. 2012. An endogenous factor enhances ferulic acid decarboxylation catalyzed by phenolic acid decarboxylase from Candida guilliermondii. *AMB Express* **2**, 1–10.

Ienaga, S., Kosaka, S., Honda, Y., Ishii, Y. & Kirimura, K. 2013. p-Aminosalicylic Acid Production by Enzymatic Kolbe–Schmitt Reaction Using Salicylic Acid Decarboxylases Improved through Site-Directed Mutagenesis. *Bull. Chem. Soc. Jpn.* **86**, 628–634.

Iwasaki, Y., Kino, K., Nishide, H. & Kirimura, K. 2007. Regioselective and enzymatic production of gamma-resorcylic acid from resorcinol using recombinant Escherichia coli cells expressing a novel decarboxylase gene. *Biotechnol. Lett.* **29**, 819–822.

Jung, D.-H., Choi, W., Choi, K.-Y., Jung, E., Yun, H., Kazlauskas, R.J. & Kim, B.-G. 2013. Bioconversion of p-coumaric acid to p-hydroxystyrene using phenolic acid decarboxylase from B. amyloliquefaciens in biphasic reaction system. *Appl. Microbiol. Biotechnol.* **97**, 1501–1511.

Kamath, A.V. & Vaidyanathan, C.S. 1990. Structural requirements for the induction and inhibition of 2,3-dihydroxybenzoic acid decarboxylase of Aspergillus niger. *Curr. Microbiol.* **20**, 111–114.

Kang, S.-Y., Choi, O., Lee, J.K., Ahn, J.-O., Ahn, J.S., Hwang, B.Y. & Hong, Y.-S. 2015. Artificial de novo biosynthesis of hydroxystyrene derivatives in a tyrosine overproducing Escherichia coli strain. *Microb. Cell Fact.* **14**, 78–88.

Kanth, J. & Periasamy, M. 1991. Selective Reduction of Carboxylic Acids into Alcohols Using NaBH, and I2. *J. Org. Chem.* **56**, 5964–5965.

Karlheinz D. & Waldmann, H. 2002. Enzyme Catalysis in Organic Synthesis. Wiley-VCH, Weinheim.

Kaufhold, D., Kopf, F., Wolff, C., Beutel, S., Hilterhaus, L., Hoffman, M., Scheper, T., Schluter, M. & Liese, A. 2013. Chemical Absorption of CO2 in Helically Wound Hollow Fiber Membrane Contactors. *Chem. Ing. Tech.* **85**, 476–483.

Khalili, F., Rayer, A.V., Henni, A., East, A.L.L. & Tontiwachwuthikul, P. 2012. Kinetics and Dissociation Constants (pKa) of Polyamines of Importance in Post-Combustion

Carbon Dioxide (CO2) Capture Studies. In: M.I. Attalla (ed) *Recent Advances in Post-Combustion CO2 Capture Chemistry*, pp. 43–70. American Chemical Society, Washington, DC.

Kirimura, K., Gunji, H., Wakayama, R., Hattori, T. & Ishii, Y. 2010. Enzymatic Kolbe-Schmitt reaction to form salicylic acid from phenol: enzymatic characterization and gene identification of a novel enzyme, Trichosporon moniliiforme salicylic acid decarboxylase. *Biochem. Biophys. Res. Commun.* **394**, 279–284.

Klibanov, A.M. 2001. Improving enzymes by using them in organic solvents. *Nature* **409**, 241–246.

Knoll, G. & Winter, J. 1989. Degradation of phenol via carboxylation to benzoate by a defined, obligate syntrophic consortium of anaerobic bacteria. *Appl. Microbiol. Biotechnol.* **30**, 318–324.

Kopec, J., Schnell, R. & Schneider, G. 2011. Structure of PA4019, a putative aromatic acid decarboxylase from Pseudomonas aeruginosa. *Acta Crystallogr., Sect. F: Struct. Biol. Cryst. Commun.* **67**, 1184–1188.

Krtschil, U., Hessel, V., Reinhard, D. & Stark, A. 2009. Flow Chemistry of the Kolbe-Schmitt Synthesis from Resorcinol: Process Intensification by Alternative Solvents, New Reagents and Advanced Reactor Engineering. *Chem. Eng. Technol.* **32**, 1774–1789.

Kubinyi, H. 1993. QSAR: Hansch analysis and related approaches. Wiley-VCH, Weinheim.

Kunal, R. 2015. Quantitative Structure-Activity Relationships in Drug Design, Predictive Toxicology and risk assessment. IGI GLOBAL.

Kunitsky, K., Shah, M.C., Shuey, S.W., Trost, B.M. & Wagman, M.E. Method for preparaing hydroxystyrenes and acetylated derivatives thereof. *US Patent WO2005097719 A1.*

Laane, C. 1987. Medium-Engineering For Bio-Organic Synthesis. *Biocatalysis* **1**, 17–22.

Laane, C., Boeren, S., Vos, K. & Veeger, C. 1987. Rules for optimization of biocatalysis in organic solvents. *Biotechnol. Bioeng.* **3**, 81–87.

Landete, J.M., Rodríguez, H., Curiel, J.A., de las Rivas, Blanca, Mancheño, J.M. & Muñoz, R. 2010. Gene cloning, expression, and characterization of phenolic acid decarboxylase from Lactobacillus brevis RM84. *J. Ind. Microbiol. Biotechnol.* **37**, 617–624.

Langone, J.J. 1991. Molecular Design and Modeling: Concepts and Applications. Part A: Proteins, Peptides and Enzymes. Academic Press, Inc.

Lee, L.G. & Whitesides, G.M. 1986. Preparation of Optically Active 1,2-Diols and &-Hydroxy Ketones Using Glycerol Dehydrogenase as Catalyst: Limits to Enzyme-Catalyzed Synthesis due to Noncompetitive and Mixed Inhibition by Product. *J. Org. Chem.* **51**, 25–36.

Leisch, H., Grosse, S., Morley, K., Abokitse, K., Perrin, F., Denault, J. & Lau, P.C. 2013. Chemicals from agricultural biomass: chemoenzymatic approach for production of vinylphenols and polyvinylphenols from phenolic acids. *Green Process. Synth.* **2**, 7–17.

Li, T. & Rosazza, J. 1997. Purification, Characterization, and Properties of an Aryl Aldehyde Oxidoreductase from Nocardia sp. Strain NRRL 5646. *J. Bacteriol.* **179**.

Lide, D.R. 1994. Handbook of Chemistry and Physics. CRC Press, Boca Raton, FL.

Liese, A., Karutz, M., Kamphuis, J., Wandrey, C. & Kragl, U. 1996. Enzymatic resolution of 1-phenyl-1,2-ethanediol by enantioselective oxidation: Overcoming product inhibition by continuous extraction. *Biotechnol. Bioeng.* **51**, 544–550.

Liese, A., Seelbach, K. & Wandrey, C. 2006. Industrial biotransformations. Wiley-VCH, Weinheim.

Lindsey A & Jeskey H 1957. The Kolbe-Schmitt reaction. *Chem. Rev.* **57**, 583–620.

Littke, A.F., Schwarz, L. & Fu, G.C. 2002. Pd/P(t -Bu)3. A Mild and General Catalyst for Stille Reactions of Aryl Chlorides and Aryl Bromides. *JACS* **124**, 6343–6348.

Liu, J., Zhang, X., Zhou, S. & Tao, P. 2007. Purification and characterization of a 4-hydroxybenzoate decarboxylase from Chlamydophila pneumoniae AR39. *Curr. Microbiol.* **54**, 102–107.

Lopez, M., Vu, H., Wang, C.K., Wolf, M.G., Groenhof, G., Innocenti, A., Supuran, C.T. & Poulsen, S.-A. 2011. Promiscuity of carbonic anhydrase II. Unexpected ester hydrolysis of carbohydrate-based sulfamate inhibitors. *JACS* **133**, 18452–18462.

Lye, G.J. & Woodley, J.M. 1999. Application of in situ product-removal techniques to biocatalytic processes. *Trends Biotechnol.* **17**, 395–402.

Manta, B., Raushel, F.M. & Himo, F. 2014. Reaction mechanism of zinc-dependent cytosine deaminase from Escherichia coli: a quantum-chemical study. *J. Phys. Chem. B* **118**, 5644–5652.

Markovic, Z., Engelbrecht, J.P. & Markovic, S. 2002. Theoretical Study of the Kolbe-Schmitt Reaction Mechanism. *Z. Naturforsch.* **57a**, 812–818.

Matsuda, T., Ohashi, Y., Harada, T., Yanagihara, R., Nagasawa, T. & Nakamura, K. 2001. Conversion of pyrrole to pyrrole-2-carboxylate by cells of Bacillus megaterium in supercritical CO2. *Chem. Commun.*, 2194–2195.

Matsui, T., Yoshida, T., Yoshimura, T. & Nagasawa, T. 2006. Regioselective carboxylation of 1,3-dihydroxybenzene by 2,6-dihydroxybenzoate decarboxylase of Pandoraea sp. 12B-2. *Appl. Microbiol. Biotechnol.* **73**, 95–102.

Morris, G.M., Goodsell, D.S., Halliday, R.S., Huey, R., Hart, W.E., Belew, R.K. & Olson, A.J. 1998. Automated docking using a Lamarckian genetic algorithm and an empirical binding free energy function. *J. Comput. Chem.* **19**, 1639–1662.

Murmann, J.P. 2002. Chemical Industries after 1850. Article for the Oxford Encyclopedia of Economic History. Oxford University Press.

Ni, Y., Holtmann, D. & Hollmann, F. 2014. How Green is Biocatalysis? To Calculate is To Know. *ChemCatChem* **6**, 930–943.

NOAA Research 2016. http://www.esrl.noaa.gov/gmd/ccgg/trends/ (WWW document). http://www.esrl.noaa.gov/gmd/ccgg/trends/.

O´Leary, M.H. 1992. Catalytic Strategies in Enzymic Carboxylation and Decarboxylation. In: D.S. Sigman (ed) *The Enzymes. Mechanism of Catalysis*, pp. 236–266. Academic Press, Inc., San Diego, California.

OECD 2001. OECD Environmental Outlook for the Chemicals Industry.

Ou, G., He, B., Li, X. & Lei, J. 2012. Glycerol Carbonate: A Novel Biosolvent with Strong Ionizing and Dissociating Powers. *Sci. World J.* **2012**, 1–6.

Ou, G., He, B. & Yuan, Y. 2011. Lipases are soluble and active in glycerol carbonate as a novel biosolvent. *Enzyme Microb. Technol.* **49**, 167–170.

Page, M.J. & Di Cera, E. 2006. Role of Na+ and K+ in enzyme function. *Physiol. Rev.* **86**, 1049–1092.

Petitjean, L., Gagne, R., Beach, E.S., Xiao, D. & Anastas, P.T. 2016. Highly selective hydrogenation and hydrogenolysis using a copper-doped porous metal oxide catalyst. *Green Chem.* **18**, 150–156.

Posner, G.H. & Canella, K.A. 1985. Phenoxide-Directed Ortho Lithiation. *JACS* **107**, 2571–2573.

Putz, M.V. 2013. QSAR and SPECTRAL-SAR in Computational Ecotoxicology. Apple academic press, Oakville.

Rangarajan, E.S., Li, Y., Iannuzzi, P., Tocilj, A., Hung, L.-W., Matte, A. & Cygler, M. 2004. Crystal structure of a dodecameric FMN-dependent UbiX-like decarboxylase (Pad1) from Escherichia coli O157: H7. *Protein Sci.* **13**, 3006–3016.

Rein, M.J., Ollilainen, V., Vahermo, M., Yli-Kauhaluoma, J. & Heinonen, M. 2005. Identification of novel pyranoanthocyanins in berry juices. *Eur. Food Res. Technol.* **220**, 239–244.

Ren, J., Yao, P., Yu, S., Dong, W., Chen, Q., Feng, J., Wu, Q. & Zhu, D. 2016. An Unprecedented Effective Enzymatic Carboxylation of Phenols. *ACS Catal.* **6**, 564–567.

Richard, P., Viljanen, K. & Penttilä, M. 2015. Overexpression of PAD1 and FDC1 results in significant cinnamic acid decarboxylase activity in Saccharomyces cerevisiae. *AMB Express* **5**, 1–5.

Riddick, J.A., Bunger, W.B. & Sakano, T.K. 1985. Techniques of Chemistry. Organic Solvents. John Wiley and sons, New York.

Ritzer, E. & Sundermann, R. 2000. Hydroxycarboxylic Acids, Aromatic. In: *Ullmann's Encyclopedia of Industrial Chemistry*. Wiley-VCH Verlag GmbH & Co. KGaA, Weinheim.

Rodríguez, H., Angulo, I., las Rivas, B. de, Campillo, N., Páez, J.A., Muñoz, R. & Mancheño, J.M. 2010. p-Coumaric acid decarboxylase from Lactobacillus plantarum:

structural insights into the active site and decarboxylation catalytic mechanism. *Proteins* **78**, 1662–1676.

Rodríguez, N. & Goossen, L.J. 2011. Decarboxylative coupling reactions: a modern strategy for C-C-bond formation. *Chem. Soc. Rev.* **40**, 5030–5048.

Rodríguez-Sanz, A.A., Carrazana-García, J., Cabaleiro-Lago, E.M. & Rodríguez-Otero, J. 2013. Effect of stepwise microhydration on the methylammonium-phenol and ammonium-phenol interaction. *J. Mol. Model.* **19**, 1985–1994.

Rosazza, J., Huang, Z., Dostal, L., Volm, T. & Rousseau, B. 1995. Review: Biocatalytic transformations of ferulic acid: An abundant aromatic natural product. *J. Ind. Microbiol.* **15**, 457–471.

Sangster, J. 1989. Octanol-Water Partition Coefficients of Simple Organic Compounds. *J. Phys. Chem. Ref. Data* **18**, 1111–1227.

Santha, R., Savithri, H.S., Rao, N.A. & Vaidyanathan, C.S. 1995. 2,3–Dihydroxybenzoic Acid Decarboxylase from Aspergillus niger. *Eur. J. Biochem.* **230**, 104–110.

Schada von Borzyskowski, L., Rosenthal, R.G. & Erb, T.J. 2013. Evolutionary history and biotechnological future of carboxylases. *J. Biotechnol.* **168**, 243–251.

Schmeling, S. & Fuchs, G. 2009. Anaerobic metabolism of phenol in proteobacteria and further studies of phenylphosphate carboxylase. *Arch. Microbiol.* **191**, 869–878.

Schmidt, N.D., Peschon, J.J. & Segel, I.H. 1983. Kinetics of enzymes subject to very strong product inhibition: analysis using simplified integrated rate equations and average velocities. *J. theor. Biol.* **100**, 597–611.

Schmitt, R. 1885. Beitrag zur Kenntnis der Kolbe´schen Salicylsäure Synthese. *J. Prakt. Chem.* **31**, 397–411.

Schühle, K. & Fuchs, G. 2004. Phenylphosphate carboxylase: a new C-C lyase involved in anaerobic phenol metabolism in Thauera aromatica. *J. Bacteriol.* **186**, 4556–4567.

Schweigert, N., Zehnder A. J. B. & Eggen R. I. L. 2001. Chemical properties of catechols and their molecular modes of toxic action in cells, from microorganisms to mammals. *Environ. Microbiol.* **3**, 81–91.

Seibert, C.M. & Raushel, F.M. 2005. Structural and catalytic diversity within the amidohydrolase superfamily. *Biochemistry* **44**, 6383–6391.

Selwyn, M.J. 1965. A simple test for inactivation of an enzyme during assay. *Biochim, Biophys. Acta* **105**, 193–195.

Shahidi, F. & Naczk, M. 2003. Phenolics in Food and Nutraceuticals. CRC Press, Boca Raton.

Sharma, A., Kumar, R., Sharma, N., Kumar, V. & Sinha, A.K. 2008. Unique Versatility of Ionic Liquids as Clean Decarboxylation Catalyst Cum Solvent: A Metal- and Quinoline-Free Paradigm towards Synthesis of Indoles, Styrenes, Stilbenes and Arene Derivatives under Microwave Irradiation in Aqueous Conditions. *Adv. Synth. Catal.* **350**, 2910–2920.

Sheldon, R.A. 2007. The E Factor: fifteen years on. *Green Chem.* **9**, 1273–1283.

Sheng, X., Lind, Maria E S & Himo, F. 2015. Theoretical study of the reaction mechanism of phenolic acid decarboxylase. *FEBS J.* **282**, 4703–4713.

Sigman, D.S. 1992. The Enzymes. Mechanism of Catalysis, San Diego, California. Academic Press, Inc.

Simpson, C.J., Fitzhenry, M.J. & Stamford, N.P. Preparation of vinylphenols from 2- and 4-hydroxybenzaldehydes. *Tetrahedron Lett.* **46**, 6893–6896.

Singh, P., Niederer, J.P. & Versteeg, G.F. 2007. Structure and activity relationships for amine based CO2 absorbents-I. *Int. J. Greenhouse Gas Control* **1**, 5–10.

Singh, P., Niederer, J.P. & Versteeg, G.F. 2009. Structure and activity relationships for amine-based CO2 absorbents-II. *Chem. Eng. Res. Des.* **87**, 135–144.

Smith, C.R. & Rajanbabu, T.V. 2010. Low Pressure Vinylation of Aryl and Vinyl Halides via Heck-Mizoroki Reactions Using Ethylene. *Tetrahedron* **66**, 1102–1110.

Sonnati, M.O., Amigoni, S., Taffin de Givenchy, E.P., Darmanin, T., Choulet, O. & Guittard, F. 2013. Glycerol carbonate as a versatile building block for tomorrow: synthesis, reactivity, properties and applications. *Green Chem.* **15**, 283–306.

Stark, A., Huebschmann, S., Sellin, M., Kralisch, D., Trotzki, R. & Ondruschka, B. 2009. Microwave-Assisted Kolbe-Schmitt Synthesis Using Ionic Liquids or Dimcarb as Reactive Solvents. *Chem. Eng. Technol.* **32**, 1730–1738.

Stepankova, V., Damborsky, J. & Chaloupkovaa, R. 2014. Hydrolases in Non-Conventional Media: Implications for Industrial Biocatalysis. In: P. Grunwald *Industrial Biocatalysis*, pp. 583–629. CRC Press.

Štěpánková, V., Paterová, J., Damborský, J., Jungwirth, P., Chaloupková, R. & Heyda, J. 2013. Cation-specific effects on enzymatic catalysis driven by interactions at the tunnel mouth. *J. Phys. Chem. B* **117**, 6394–6402.

Suezawa, Y. & Suzuki, M. 2007. Bioconversion of Ferulic Acid to 4-Vinylguaiacol and 4-Ethylguaiacol and of 4-Vinylguaiacol to 4-Ethylguaiacol by Halotolerant Yeasts Belonging to the Genus Candida. *Biosci. Biotechnol. Biochem.* **71**, 1058–1062.

Tchobanov, I., Gal, L., Guilloux-Benatier, M., Remize, F., Nardi, T., Guzzo, J., Serpaggi, V. & Alexandre, H. 2008. Partial vinylphenol reductase purification and characterization from Brettanomyces bruxellensis. *FEMS Microbiol. Lett.* **284**, 213–217.

Vaidya, P.D. & Kenig, E.Y. 2007. CO2-Alkanolamine Reaction Kinetics: A Review of Recent Studies. *Chem. Eng. Technol.* **30**, 1467–1474.

Vasic Racki, D., Kragl, U. & Liese, A. 2003. Benefits of Enzyme Kinetics Modelling. *Chem. Biochem. Eng. Q.* **17**, 7–18.

Voutsas, E.C., Stamatis, H., Kolisis, F.N. & Tassios, D. 2009. Solvent Effects on Equilibrium Position and Initial Rate of Lipase-catalyzed Esterification Reactions in Organic Solvents: Experimental Results and Prediction Capabilities. *Biocatal. Biotransform.* **20**, 101–109.

Wang, Y. & Gevorgyan, V. 2015. General method for the synthesis of salicylic acids from phenols through palladium-catalyzed silanol-directed C-H carboxylation. *Angew. Chem., Int. Ed.* **54**, 2255–2259.

Wasewar, K.L. 2012. Reactive Extraction: An Intensifying Approach for Carboxylic Acid Separation. *Int. J. Chem. Eng. Appl.* **3**, 249–255.

Wen, D. & Olesik, S.V. 2000. Characterization of pH in Liquid Mixtures of Methanol/H2O/CO2. *Anal. Chem.* **72**, 475–480.

Wieser, M., Fujii, N., Yoshida, T. & Nagasawa, T. 1998. Carbon dioxide fixation by reversible pyrrole-2-carboxylate decarboxylase from Bacillus megaterium PYR2910. *Eur. J. Biochem.* **257**, 495–499.

Williams, A. 2003. Free Energy Relationships in Organic and Bio-organic Chemistry. Royal Society of Chemistry, Cambridge.

Williams, D.L. & Kuklenz, K.D. 2009. A Determination of the Hansen Solubility Parameters of Hexanitrostilbene (HNS). *Prop., Explos., Pyrotech.* **34**, 452–457.

Willke, T., Prüße, U. & Vorlop, K.D. 2006. Biocatalytic and Catalytic Routes for the Production of Bulk and Fine Chemicals from Renewable Resources. In: B. Kamm, P.I. Gruber & M. Kamm (eds) *Biorefineries – Industrial Processes and Products*, pp. 385–406. WILEY-VCH Verlag GmbH & Co.

Wuensch, C., Glueck, S.M., Gross, J., Koszelewski, D., Schober, M. & Faber, K. 2012. Regioselective enzymatic carboxylation of phenols and hydroxystyrene derivatives. *Org. Lett.* **14**, 1974–1977.

Wuensch, C., Gross, J., Steinkellner, G., Gruber, K., Glueck, S.M. & Faber, K. 2013a. Asymmetric enzymatic hydration of hydroxystyrene derivatives. *Angew. Chem. Int. Ed.* **52**, 2293–2297.

Wuensch, C., Gross, J., Steinkellner, G., Lyskowski, A., Gruber, K., Glueck, S.M. & Faber, K. 2014. Regioselective ortho-carboxylation of phenols catalyzed by benzoic acid decarboxylases: a biocatalytic equivalent to the Kolbe–Schmitt reaction. *RSC Adv.* **4**, 9673–9679.

Wuensch, C., Pavkov-Keller, T., Steinkellner, G., Gross, J., Fuchs, M., Hromic, A., Lyskowski, A., Fauland, K., Gruber, K., Glueck, S.M. & Faber, K. 2015. Regioselective Enzymatic β-Carboxylation of para-Hydroxy- styrene Derivatives Catalyzed by Phenolic Acid Decarboxylases. *Adv. Synth. Catal.* **357**, 1909–1918.

Wuensch, C., Schmidt, N., Gross, J., Grischek, B., Glueck, S.M. & Faber, K. 2013b. Pushing the equilibrium of regio-complementary carboxylation of phenols and hydroxystyrene derivatives. *J. Biotechnol.* **168**, 264–270.

Xiang, D.F., Kumaran, D., Swaminathan, S. & Raushel, F.M. 2014. Structural characterization and function determination of a nonspecific carboxylate esterase from the

amidohydrolase superfamily with a promiscuous ability to hydrolyze methylphosphonate esters. *Biochemistry* **53**, 3476–3485.

Yadav, G.D. & Pathre, G.S. 2007. Selectivity Engineering of Cation-Exchange Resins over Inorganic Solid Acids in C-Alkylation of Guaiacol with Cyclohexene. *Ind. Eng. Chem. Res.* **46**, 3119–3127.

Yang, G., Lien, E.G. & Guo Z. 1986. Physical Factors Contributing to Hydrophobic Constant. *Quant. Struct.-Act. Relat.* **5**, 12–18.

Yoshida, M., Fukuhara, N. & Oikawa, T. 2004a. Thermophilic, reversible gamma-resorcylate decarboxylase from Rhizobium sp. strain MTP-10005: purification, molecular characterization, and expression. *J. Bacteriol.* **186**, 6855–6863.

Yoshida, T., Fujita, K. & Nagasawa, T. 2002. Novel reversible indole-3-carboxylate decarboxylase catalyzing nonoxidative decarboxylation. *Biosci. Biotechnol. Biochem.* **66**, 2388–2394.

Yoshida, T., Hayakawa, Y., Matsui, T. & Nagasawa, T. 2004b. Purification and characterization of 2,6-dihydroxybenzoate decarboxylase reversibly catalyzing nonoxidative decarboxylation. *Arch. Microbiol.* **181**, 391–397.

Yoshida, T. & Nagasawa, T. 2000. Enzymatic Functionalization of Aromatic N-Heterocycles: Hydroxylation and Carboxylation. *J. Biosci. Bioeng.* **89**, 111–118.

Yu, D., Teong, S.P. & Zhang, Y. 2015. Transition metal complex catalyzed carboxylation reactions with CO2. *Coord. Chem. Rev.* **293-294**, 279–291.

Zago, A., Degrassi, G. & Bruschi, C.V. 1995. Cloning, sequencing, and expression in E. coli of the Bacillus pumilus gene for ferulic acid decarboxylase. *Appl. Environ. Microbiol.* **61**, 4484–4486.

Zeida, M., Wieser, M., Yoshida, T., Sugio, T. & Nagasawa, T. 1998. Purification and Characterization of Gallic Acid Decarboxylase from Pantoea agglomerans T71. *Appl. Microbiol. Biotechnol.* **64**, 4743–4747.

Zhen-mao, J., Ai-min, L., Jian-guo, C., Chun, W. & Quan-xin, J. 2007. Adsorption of phenolic compounds from aqueous solutions by aminated hypercrosslinked polymers. *J. Environ. Sci.* **19**, 135–140.

Zhou, Z., Yao, Z., Wang, H.Q., Xu, H., Wei, P. & Ouyang, P.K. 2011. Improved enzymatic synthesis of N-carbamoyl-D-phenylalanine with in situ product recovery. *Biotechnol. Bioprocess Eng.* **16**, 611–616.

Zhu, W., Tan, X., Puah, C.M., Gu, J., Jiang, H., Chen, K., Felder, C.E., Silman, I. & Sussman, J.L. 2000. How does ammonium interact with aromatic groups? a density functional theory (DFT/B3LYP) investigation. *J. Phys. Chem. A* **104**, 9573–9580.

Curriculum vitae

Name	Lorenzo
Surname	Pesci
Nationality	Italian
Date of birth	29.11.1987
Place of Birth	Rome, Italy

09.2001-07.2006	Secondary school studies, "Liceo Scientifico Democrito" (Democritus Science High School), Rome, Italy
09.2006-12.2009	Bachelor degree in "Chemistry", Università "La Sapienza" di Roma (University "La Sapienza" of Rome), Rome, Italy
09.2010-02.2013	Master degree in "Agricultural and Industrial Biotechnology", Università della Tuscia di Viterbo (Tuscia University), Viterbo, Italy
04.2013-07.2016	Doctoral studies at the Institute of Technical Biocatalysis, Hamburg University of Technology, Hamburg, Germany
11.2016-present	Research assistant at the Tuscia University, Viterbo, Italy